Development and Characterization of Electrospun Wound Dressings Containing Birch Bark Extract

Dissertation

der Mathematisch-Naturwissenschaftlichen Fakultät

der Eberhard Karls Universität Tübingen

zur Erlangung des Grades eines

Doktors der Naturwissenschaften

(Dr. rer. nat.)

vorgelegt von

Francis Kamau Mwiiri

aus Kiambu

Kenia

Tübingen

2020

Gedruckt mit Genehmigung der Mathematisch-Naturwissenschaftlichen Fakultät der Eberhard Karls Universität Tübingen.

Tag der mündlichen Qualifikation:	29.10.2020
Stellvertretender Dekan:	Prof. Dr. József Fortágh
1. Berichterstatter:	Prof. Dr. Rolf Daniels
2. Berichterstatter:	Prof. Dr. Dominique J. Lunter

Acknowledgement

First and foremost, I would like to express my deepest gratitude to my main supervisor Prof. Dr. Rolf Daniels for giving me the opportunity to join his research group and to work on this exciting and interdisciplinary project. I would like to thank him for being always present, his excellent scientific support throughout this work and guidance, which also contributed to my personal development over the last four years. Furthermore, I thank him for giving me the opportunity to participate in an advanced training course in Pharmaceutical Technology.

Thanks to Prof. Dr. Martin A. Wahl for all the helpful and interesting discussion in the past years, as well as for being the second supervisor of this thesis.

I kindly thank Prof. Dr. Dominique J. Lunter for evaluating my thesis. Furthermore, I thank her for introducing me to Confocal Raman Microscopy and Profile Drop Analysis Tensiometer.

I am grateful to Phospholipid Research Center for funding this research, their financial support is really appreciated.

Meanwhile, I deeply thank Klaus Weyhing for capturing all the SEM images. I especially thank him for his time and patient with SEM imaging of many samples and for his kind introduction of lab instruments.

I also appreciate all personnel and group members in Pharmaceutical Technology for their grateful assistances at the lab.

I would like to thank my family and friends for your support during my time as a PhD student. Thanks to my cousin David Thuku for your advice and encouragement. I am happy to have you as my only cousin here in Germany, 3,874 miles away from Kenya.

Finally, special thanks to my mum Alice Waithira who have given unwavering support and love throughout my education. To you I dedicate this thesis.

Nĩ ũndũ ũcio tiga gwĩtigĩra, mĩgũkorwo ndĩ hamwe nawe; tiga kũmaka, mĩgũkorwo niĩ nĩ niĩ Ngai waku. Nĩndĩkuongagĩrĩra hinya na ngũteithagie; na ti-itherũ nĩndĩrĩgũtiiragĩrĩra na guoko gwakwa kwa ũrĩo kwa ũthingu.

(Isaia 41:10)

So do not fear, for I am with you; do not be dismayed, for I am your God. I will strengthen you and help you; I will uphold you with my righteous right hand.

(Isaiah 41:10)

Contents

Summary

Wound care is a challenging task in our daily lives. Therefore, it would be highly desirable to have simple, acceptable dressing materials that can be used directly to cover wounds and accelerate wound healing. Birch bark triterpene extract (TE) has the ability to accelerate the wound healing process. Thus, the main goal of this work was to develop novel electrospun wound dressings with TE as the active principal. The underlying concept was to blend colloidal dispersions of TE with polyvinyl alcohol (PVA) matrix and produce wound dressings by electrospinning. However, TE particles exhibit unique structures which cannot be crushed by common techniques to reach particles in the colloidal size range even when high energy dispersion techniques are used. This represents an obstacle for a simple incorporation of TE into the PVA matrix through electrospinning.

In the first part of this PhD thesis, the colloidal dispersions were designed to contain TE, sunflower oil, phospholipids (PL90H) and water. First, an interfacial tension analysis was performed to investigate and understand the potential influence of PL90H in the dispersion process and its interaction with TE. A synergistic interaction between PL90H and TE was also discussed. An optimized stepwise homogenization process made it feasible to produce colloidal dispersions with particle sizes below 1 µm.

In order to design and develop novel wound dressings as delivery devices capable of releasing TE, we focused on emulsion electrospinning technique for bioactive scaffold production. Electrospinning parameters to fabricate the dressings were investigated and optimized. In particular, the varying of concentration and molecular weight of the polymer had a significant effect on spinnability, rheological properties of polymer solution and the resulting fiber properties. We showed that bioactive wound dressings with smooth and uniform fibers can be produced.

Cumulative *in vitro* drug release and *ex vivo* permeation profiles showed that TE-loaded scaffolds can release Betulin in a sustained release manner. By adjusting components of the colloidal dispersions, namely PL90H and sunflower oil, the release of Betulin can be controlled. Amazingly, *ex-vivo* wound healing results indicated that treatment with nanofibrous wound dressings especially with low TE amounts achieved superlative and accelerated wound healing recovery.

In the last phase of this thesis, films containing colloidal dispersions were produced using the solvent casting method, for possible alternative formulations towards wound therapy. From the *in vitro* drug release and *ex vivo* wound healing studies, these films gave positive insights to serve as additional wound dressings. Nevertheless, TE-loaded electrospun wound dressings were superior to such cast films in wound healing. With the current developments in electrospinning technology, it is possible to manufacture electrospun dressings at industrial level within shorter times. On the other hand, fabrication of such cast films could also serve as efficient dressings for covering wounds.

In vivo studies could be essential for future translation of the developed TE dressings while utilizing the basis of this work.

This project clearly shows that through an innovative approach we have developed bioactive wound dressings that present an alternative pharmaceutical formulation potential for wound therapy in the near future.

Zusammenfassung

Ein effizientes und einfach zu handhabendes Wundmanagement ist immer noch eine große Herausforderung. In unserem täglichen Leben wäre es äußerst wünschenswert, einfache, akzeptable Verbandmaterialien zu haben, die einerseits direkt zur Abdeckung von Wunden und andererseits zur Beschleunigung der Wundheilung verwendet werden können. Ein Triterpentrockenextrakt (TE) aus der Birkenrinde kann nachgewiesenermaßen den Wundheilungsprozess beschleunigen. Daher war das Hauptziel dieser Arbeit die Entwicklung von elektrogesponnenen Wundauflagen mit TE als aktiver Komponente. Das Grundkonzept bestand darin, kolloidale Dispersionen von TE in eine Polyvinylalkohol (PVA)-Matrix einzuarbeiten und Wundauflagen durch Elektrospinnen herzustellen. Die TE-Partikel weisen jedoch einzigartige Strukturen auf, die mit herkömmlichen Verfahren nicht zerkleinert werden können. Selbst wenn hochenergetische Dispersionstechniken eingesetzt werden, lassen sich in öligen oder wässrigen Dispersionen keine Partikel im kolloidalen Größenbereich herstellen. Dies stellt ein Hindernis für eine einfache Verwendung des TE in die PVA-Matrix beim Elektrospinnen dar.

Im ersten Teil dieser Doktorarbeit wurden kolloidale Dispersionen konzipiert, die TE, Sonnenblumenöl, Phospholipide (PL90H) und Wasser enthalten. Zunächst wurde eine Bestimmung der Grenzflächenspannung durchgeführt, um den potenziellen Einfluss von PL90H im Dispersionsprozess und seine Wechselwirkung mit TE zu untersuchen und zu verstehen. Es wurde eine synergistische Wechselwirkung zwischen PL90H und TE beobachtet. Durch ein optimiertes stufenweises Homogenisierungsverfahren war es möglich, kolloidale Dispersionen mit Partikelgrößen unter 1 µm herzustellen.

Im zweiten Teil wurden bioaktive elektrogesponnene Wundauflagen entwickelt und charakterisiert, die TE kontrolliert freisetzen können. Elektrospinnparameter zur Herstellung von Wundauflagen wurden untersucht und optimiert. Insbesondere die Variation von Konzentration und Molekulargewicht des Polymers hatte einen signifikanten Einfluss auf die Spinnbarkeit, die rheologischen Eigenschaften der Polymerlösung und die resultierenden Fasereigenschaften. Wir konnten zeigen, dass bioaktive Wundauflagen mit glatten und gleichmäßigen Fasern hergestellt werden können.

In-vitro-Freisetzungs- und *Ex vivo*-Permeationsuntersuchungen ergaben, dass elektrogesponnene Wundauflagen Betulin über einen Zeitraum von 72 Stunden freisetzen können. Durch die Veränderung der Komponenten von kolloidalen Dispersionen, nämlich PL90H und Sonnenblumenöl, kann die Freisetzung von Betulin gesteuert werden. *Ex-vivo*-Wundheilungsergebnisse deuten darauf hin, dass die Behandlung mit nanofaserigen Wundauflagen, insbesondere mit niedrigen TE-Mengen, eine überragende und beschleunigte Wundheilung erzielte.

Als alternative Formulierung zur Wundtherapie wurden in der letzten Phase der Arbeit TE-haltige Filme mittels Solvent Casting Methode hergestellt. Aus den *in-vitro*-Freisetzungs- und *ex vivo*-Wundheilungsstudien ergaben diese Filme positive Erkenntnisse, sodass diese ebenfalls als Wundauflagen dienen können. Dennoch waren TE-basierte elektrogesponnene Wundauflagen im Vergleich zu den gegossenen Filmen bei der Wundheilung überlegen. Mit den aktuellen Entwicklungen in der Elektrospinntechnologie ist es möglich, elektrogesponnene Wundauflagen innerhalb kürzerer Zeit auf industrieller Ebene herzustellen. Andererseits könnte die Herstellung gegossener Filme auch als einfache Alternative zur Abdeckung von Wunden dienen.

In-vivo-Studien könnten für die zukünftige Umsetzung der entwickelten TE-Wundauflagen unter Nutzung der Grundlage dieser Arbeit von wesentlicher Bedeutung sein.

Dieses Projekt zeigt deutlich, dass wir durch einen innovativen Ansatz bioaktive Wundauflagen entwickelt haben, die ein alternatives pharmazeutisches Formulierungspotenzial für die Wundtherapie in naher Zukunft darstellen.

Patent

EP 3 583 954 A1: Nanodispersions of birch bark extract, electrospun fibers containing such nanodispersions and their use for the treatment of wounds. Francis Kamau Mwiiri, Rolf Daniels.

List of publications

Publication 1

Francis Kamau Mwiiri and Rolf Daniels, Chapter 3 - Electrospun nanofibers for biomedical applications, in Delivery of Drugs, R. Shegokar, Editor. 2020, Elsevier. p. 53-74. DOI: 10.1016/B978-0-12-817776-1.00003-1.

Publication 2

Francis Kamau Mwiiri and Rolf Daniels, Optimized Birch Bark Extract loaded Colloidal Dispersion using Hydrogenated Phospholipids as stabilizer. Pharmaceutics, 2020. 12(9): p. 832. DOI: 10.3390/pharmaceutics12090832.

Publication 3

Francis Kamau Mwiiri, Johanna M. Brandner and Rolf Daniels, Electrospun Bioactive Wound Dressing Containing Colloidal dispersions of Birch Bark Dry Extract. Pharmaceutics, 2020. 12(8): p. 770. DOI: 10.3390/pharmaceutics12080770.

Publication 4

Francis Kamau Mwiiri and Rolf Daniels, Influence of PVA Molecular Weight and Concentration on Electrospinnability of Birch Bark Extract Loaded Nanofibrous Scaffolds Intended for Enhanced Wound Healing. Molecules, 2020. 25(20): p. 4799. DOI:10.3390/molecules25204799.

Personal contribution

Publication 1

Chapter 3 - Electrospun nanofibers for biomedical applications, in Delivery of Drugs, R. Shegokar, Editor. 2020, Elsevier. p. 53-74. DOI: 10.1016/B978-0-12-817776-1.00003-1.

Francis Kamau Mwiiri and Rolf Daniels

Francis Kamau Mwiiri

Main writing of the manuscript

Rolf Daniels

Idea generation and coordination

Partial writing, editing, proofreading and final approval of the manuscript

Corresponding Author

Publication 2

Optimized Birch Bark Extract loaded Colloidal Dispersion using Hydrogenated Phospholipids as stabilizer. Pharmaceutics, 2020. 12(9): p. 832. DOI: 10.3390/pharmaceutics12090832.

Francis Kamau Mwiiri and Rolf Daniels

Francis Kamau Mwiiri

General idea generation

Designed and conducted experiments

Main writing of the manuscript

Rolf Daniels

Idea generation and coordination

Discussion of the results

Partial writing, editing, proofreading and final approval of the manuscript

Corresponding Author

Publication 3

Electrospun Bioactive Wound Dressing Containing Colloidal dispersions of Birch Bark Dry Extract. DOI: 10.3390/pharmaceutics12080770.

Francis Kamau Mwiiri, Johanna M. Brandner and Rolf Daniels

Francis Kamau Mwiiri

General idea generation

Designed and conducted experiments

Main writing of the manuscript

Johanna M. Brandner

Designed and conducted *ex-vivo* wound healing assay

Editing of the manuscript

Rolf Daniels

Idea generation and coordination

Discussion and interpretation of the results

Partial writing, editing, proofreading and final approval of the manuscript

Corresponding Author

Publication 4

Influence of PVA Molecular Weight and Concentration on Electrospinnability of Birch Bark Extract Loaded Nanofibrous Scaffolds Intended for Enhanced Wound Healing. Molecules, 2020. 25(20): p. 4799. DOI:10.3390/molecules25204799.

Francis Kamau Mwiiri and Rolf Daniels

Francis Kamau Mwiiri

General idea generation

Designed and conducted experiments

Main writing of the manuscript

Rolf Daniels

Idea generation and coordination

Discussion and interpretation of the results

Partial writing, editing, proofreading and final approval of the manuscript

Corresponding Author

List of oral and poster presentations

Oral presentations

F.K. Mwiiri, R. Daniels; Electrospun bioactive wound dressing. Researcher's Day, organized by Phospholipid Research Centre, Mannheim, Germany, July 2018

F.K. Mwiiri, R. Daniels, Electrospun Bioactive Wound Dressing containing Nanodispersions of Birch Bark Extract. DPhG (German Pharmaceutical Society) Annual Meeting, Hamburg, Germany, October 2018

F.K. Mwiiri, R. Daniels, Electrospun Bioactive Wound Dressing containing Nanodispersions of Birch Bark Extract, Doktorandenkolleg, July 2018, Wala Heilmittel GmbH, Bad Boll, Germany

Poster presentations

F.K. Mwiiri, R. Daniels, Electrospun Bioactive Wound Dressing containing Nanodispersions of Birch Bark Extract, 6th International Symposium "Phospholipids in Pharmaceutical Research", Heidelberg, Germany, September 2019

List of Abbreviations

%	Percent
°C	Celsius Degree
µg	Microgram
µm	Micrometre
µS/cm	Microsiemens per centimeter
approx.	Approximately
CCD	Charge Coupled Device
Cm^2	Square centimeter
CP	Cone plate
CRM	Confocal Raman Microscopy
DLS	dynamic light scattering
DoE	Design of Experiments
DSC	Differential scanning calorimetry
ECM	Extracellular matrix
Eq.	Equation
FDA	US Food and Drug Administration
g	Grams
g/mL	Gram per millilitre
g/mol	Gram per mole
h	Hour
HPH	High pressure homogenizer
HPLC	High performance liquid chromatography
HSPC	Hydrogenated soybean phosphatidylcholine
Hz	frequency
kV	kilovolts
mg	Milligram
min	Minute
mL	Millilitre
mN/m	Millinewtons per meter
MPa	Megapascal
mS/cm	Millisiemens per centimeter
Mv	Millivolt
Mw	Molecular weight

nm	Nanometer
O/W	Oil in water
Pas	Pascal-second
PAT	Profile drop analysis tensiometer
PCL	Poly(ε-caprolactone)
PDI	Polydispersity index
PEG	Poly (ethylene glycol)
PL	Phospholipid
PL 90H	Phospholipon 90 H
PVA	Polyvinyl alcohol
PVP	Poly (vinyl pyrrolidone)
R^2	Coefficient of determination
RO	Reverse osmosis
rpm	Revolutions per minute
SD	Standard deviation
SEM	Scanning electron microscope
SO	Sunflower oil
TE	Dry triterpene extract
USP	United States Pharmacopeia
UV	Ultraviolet
Wt.%	Weight percent

Chapter 1: General introduction

1.1 Motivation

The human skin serves as a barrier to protect the body from the outside environment. Therefore, it is vulnerable to microbial, thermal, mechanical and chemical threats which can cause acute or chronic wounds. Acute wounds include, mechanical injuries caused by knives, gun shots and surgical wounds including burns and chemical injuries. Acute wounds usually take short period (8-12 weeks) to heal completely whereas chronic wounds such as from diabetic foot ulcers, decubitis ulcers heal slowly and take beyond 12 weeks to recover [1]. Wound healing is a complex process and several biological pathways are involved in three major phases-inflammation, proliferation, and maturation to restore damaged tissues. Globally, the management of wounds is a serious problem and a huge burden to the healthcare where in each year high costs are invested in. For instance, in Germany alone, the number of wound patients in 2012 was around 2.7 million patients whereas in USA chronic wounds were reported to affect 6.5 million patients and an excess of US$25 billion spent on treatment [2, 3]. Therefore, various materials have been widely used as wound dressings to assist the wound healing process. Traditionally, honey, plant extracts, animal products were used as dressing materials for covering wounds [4, 5]. An ideal wound dressing material should maintain a moist environment, allow removal of exudates, gaseous exchange, protect the wound from bacterial infection, non-toxic and need less frequent dressing changes at an affordable cost [6]. In wound care management, wound dressing materials for covering wounds have been manufactured in form of nanofibrous meshes. Techniques such as 3D printing, phase separation, self-assembly, melt blowing, drawing, electrospinning and centrifugal spinning are used to fabricate nanofibers. Among these fabrication techniques, electrospinning is the most widely used for production of nanofibrous materials [7-9]. Electrospinning as the name suggests, is a process by which nanofibers are generated from a polymer solution or melt in the presence of an electric field. It was known back in 1934 when A. Formhals patented this process describing the production of cellulose acetate based fibers using an acetone/alcohol solution as the solvent [10]. Thereafter, many researchers like Reneker and others especially in the 1990s stepped up further in using electrospinning technology to produce nanofibers and now we know that a wide range of polymers can be electrospun into nanofibers [11-17]. Since then, the technology has gained a lot of

momentum and interest in the recent years and nowadays it is widely used to generate nanofibers for various applications from tissue engineering to wound healing [18]. Besides, considerable publications have recently emerged based on electrospinning technology. Electrospinning technique is a simple, cost-effective and versatile process for preparing fibers having a diameter from few micrometers down to several nanometers [19, 20]. Beyond that, the obtained nanofiber mats possess not only good mechanical properties but also exhibit unique properties, such as high porosity, high encapsulation efficiency and high surface area to volume ratio thus high drug loading. These features make electrospun mats perfect materials for wound dressing. Besides mimicking the native extracellular matrix in human tissues, their high surface area and high porosity allow efficient gaseous exchange including removal of exudate, facilitate cell proliferation, act as a physical barrier against entry of microorganisms while preventing dehydration during wound healing [5, 21-23].

1.2 Significance of research

Polymeric nanofibers made from biodegradable and biocompatible synthetic or natural polymers have been utilized to develop drug delivery systems to treat various ailments and one of the potential areas to use them is medicated wound dressing [5, 21]. Many wound dressings based on electrospun fibrous mats have been developed and loaded with diverse active ingredients [1, 24, 25]. In particular, the incorporation of active ingredients with antibacterial properties in the electrospun wound dressing would prevent infection of the wound and accelerates the healing process. However, some wound dressings in the market containing active agents like hydrocolloids or silver dressings often used on wound healing have been reported to shown negative effects like allergic contact dermatitis [26] and use of dressings loaded with antibiotics has risk of developing antimicrobial resistance [27]. Therefore, it is crucial to develop bioactive wound dressings for not only covering wounds but at the same time accelerate the wound healing process with effective therapy even after long term usage.

Triterpenes from the outer bark of birch are known for various pharmacological effects including enhanced wound healing [28]. However, the low solubility of these triterpenes in polar and non-polar solvents makes formulation a challenging task which might limit their therapeutic application [29, 30]. For topical application only few formulation concepts are known. These include cosmetic water-in-oil creams, water-in-oil foams [31, 32] and an oleogel consisting of birch bark triterpene extract (TE) and sunflower

oil which received the European marketing authorization in January 2016 [33]. Hence, this research focuses on design and development of novel dressing materials that can provide alternative formulations of birch bark extract which are suitable for wound healing applications. In addition, we ensured that all the components used in this study are biocompatible and biodegradable when the dressing is applied to the human body, such that an invasive and / or traumatic intervention for dressing removal like in deep wounds is unnecessary resulting to a better patient compliance. Furthermore, water was used as the common solvent for the processing of the wound dressing which is non-toxic and affordable. This is eco-friendly and such type of electrospinning can also be regarded as green electrospinning.

In electrospinning, different strategies like coaxial method and the most commonly used principle, the blending, have been used for incorporation of therapeutic agents into the electrospun scaffolds [34]. By using the coaxial electrospinning principle, it is possible to electrospin two immiscible solutions using arranged nozzles. However, in most cases, where blend electrospinning is necessary, this may pose a challenge to produce fibers as a proper stabilizing agent is needed to stabilize the interface between immiscible phases. With the help of two types of dispersions systems oil-in-water (O/W) and water-in-oil (W/O), it is possible to manufacture nanofibers containing small drug enriched compartments and to modulate drug release rate by regulating the oil and water phase of the dispersions. For instance, the use of W/O dispersion electrospinning could improve the release of hydrophilic drugs whereas with O/W dispersions encapsulation of lipophilic components to electrospun fibers can be useful [35]. In this case, colloidal dispersions can be utilized in dispersion electrospinning to create core shell fibers even in blend electrospinning without further modification of the nozzle. However, encapsulation of birch bark dry extract into nanofibers by blend electrospinning may present a challenge. For instance, earlier studies showed that due to their unique structure the particle sizes of the dry triterpene extract cannot be grinded by common techniques to reach sufficiently small particles even when high energy dispersion techniques, e.g. sonication or high-pressure homogenization were used with aqueous and organic suspensions of the material [36]. This could be solved through processing of colloidal dispersions with birch bark dry extract as the active substance through homogenization and use of phospholipids as stabilizer. This phenomenon presumably seems to be directly linked to the use of phospholipids as

stabilizers. In this context, it was found by chance that the interfacial tension of mixtures of the triterpene extract and the phospholipids reveal cooperative effects [21, 22]. However, this interaction has not been studied systematically so far. There are first hints from previous PhD theses, that processing mixtures of triterpene extract, phospholipid, and oil with a high-pressure homogenizer yielded submicron-sized dispersions [36, 37]. Therefore, in the initial phase of this research, was to develop a suitable workflow for production of aqueous (O/W) colloidal dispersions consisting four constituents, the active substance (TE), sunflower oil, phospholipids (PL) as a stabilizer and water phase. Composition and processing conditions are expected to have a significant impact on the characteristics of these colloidal dispersions. Also, an interaction between PL and TE was studied systematically with the main goal to produce colloidal dispersions (particle sizes <1 µm) for better encapsulation into nanofibers. Consequently, the colloidal dispersions were blended with a polyvinyl alcohol polymer and electrospun to produce wound dressings. PVA was used because it's a biocompatible and biodegradable hydrophilic polymer with good chemical and mechanical properties, and has been approved by the FDA for different biomedical and pharmaceutical applications [38, 39]. Possibilities of electrospinning TE-loaded / PVA nanofibers from their solutions was explored together with effects of variables associated with the polymer and electrospinning process. Various electrospinning parameters such as- molecular weight, solution concentration, applied voltage, tip-to-collector distance and flow rate are expected to influence overall fiber morphology and diameter [40, 41]. Besides, a controlled drug release can be gained through variation of the dispersion constituents and polymer associated properties. After electrospinning, fiber morphologies as well as the presence of TE was assessed using a combination of scanning electron microscopy and confocal laser scanning microscopy. *Ex-vivo* permeation and in vitro drug release studies were performed, and the efficacy of the developed wound dressings evaluated through *ex-vivo* wound healing assay.

To our knowledge, there are no reports focusing on the development of this kind of wound dressing so this will be the first polymer based wound dressing containing birch bark dry extract aimed for future potential use in wound therapy. Apart from that, electrospinning of dispersions containing phospholipids has not been commonly

practiced so this study covers innovative aspects in all three fields, namely use of phospholipids, electrospinning and wound care.

1.3 General basics

1.3.1 The structure and function of human skin

The skin as the outermost organ of the human body, is the primary protective barrier against the external environment. It offers protection against physical, chemical and thermal injuries, micro-organisms invasion and dehydration. The skin is composed of two recognisable layers: epidermis and dermis (Figure 1). Together with the subcutaneous fat tissue it builds the outer integument. The epidermis is the outermost layer and act as a barrier to micro-organism invasion. The epidermal barrier attached to the underlying dermis, has a thickness of 50-100 µm in depth and comprises of stratum corneum (SC), stratum lucidum, stratum granulosum, stratum spinosum and stratum basale. Keratinocytes are the most common cell type in the epidermis and full of keratin filaments. In addition, keratinocytes produce cytokines in case of an injury. Melanocytes are part of the lower epidermis and are involved in skin pigmentation. The dermis has a thickness ranging from 1 to 2 mm which varies depending on the body site. It is made up of tough, supportive cell matrix which mainly consist collagen and fibrous proteins embedded in a proteoglycan-rich matrix. Collagen fibers secreted by fibroblasts, makes up to 70% of the dermis, providing the skin its flexibility and strength. It also contains nerve endings, hair follicles, and sebaceous and sweat glands. Beyond that, dermis is a highly vascularized tissue which provides nutrition to the epidermis. The subcutaneous layer (hypodermis) (1-2 mm) is the innermost layer of the outer integument located underneath the dermis. It consists of loose connective tissue and fat tissue, larger blood vessels and nerve cells which helps insulate the body from heat and cold and thus serves as energy reserve [42-44].

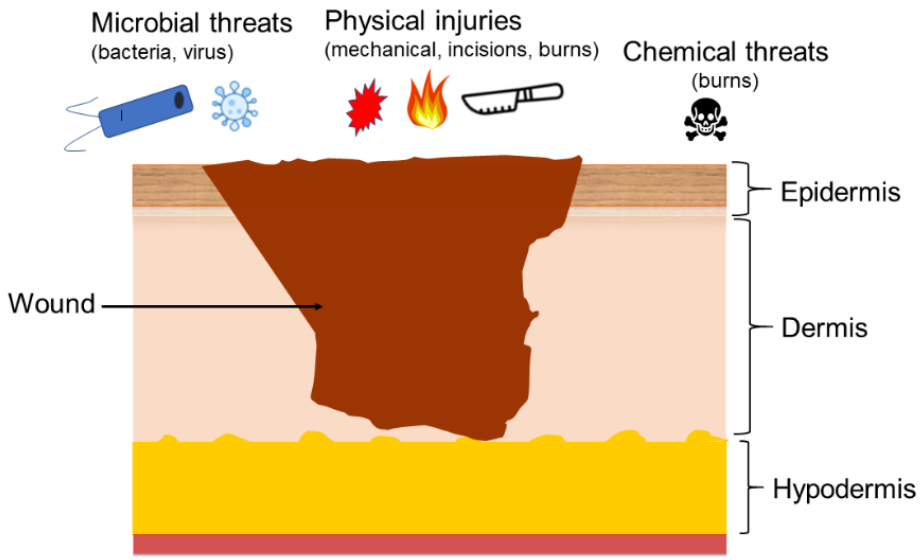

Figure 1. Schematic showing the three layers of the skin: epidermis, dermis, hypodermis and potential causes of skin wounds.

1.3.2 Wound healing

The main goal of the wound healing process is to restore the integrity of the damaged skin. This occurs through several sequential stages such as haemostasis, inflammation, cell proliferation and tissue remodelling. Haemostasis occurs immediately after tissue damage which leads to fibrin clot formation (initiated by platelets) to stop bleeding. Platelets release other mediators to recruit other functional cells to the injured area. Haemostasis is simultaneous to inflammation stage. During inflammation stage, blood neutrophils followed by phagocyte immune cells enter the injury site to remove dead cells and prevent invasive infection. In the proliferation phase, new blood vessels are formed (angiogenesis). Also, it is during proliferation phase where synthesis of extracellular matrix (ECM) and re-epithelialization is accomplished. In the remodelling stage as the final stage of wound healing, the development of new epithelium with eventual scar formation occurs. This brief description of wound healing phases clearly illustrate that the wound healing process is a very complex process cascaded by a series of biological processes and has been discussed extensively [45-50].

1.3.3 Triterpene composition of birch bark extracts and their characteristics

Birch bark is widely available in wood-processing industry as a low-value waste product which is generated in huge amounts. Therefore, birch bark extract is easily available at low costs. Purified triterpene-rich dry extract can be derived from the bark

of *Betula pendula and Betula pubescens*, or hybrids of both tree species [33]. Outer birch bark extracts have a high content of triterpenes which are known for various pharmacological properties such as anti-inflammatory, anti-viral, anti-cancer activity and wound healing effects [28, 29, 31, 51-55]. Triterpenes are widely found in plants but only the outer bark of the white barked birches contains up to 34 % (w/w) Betulin. A well characterized triterpene dry extract from the outer bark of birch contains about 80 % (w/w) Betulin. This TE is obtained by accelerated solvent extraction with n-heptane. It is also possible to use other extraction fluids or to use supercritical CO_2 for extraction [56]. Other minor constituents of the dry extract are lupeol (LU), erythrodiol (ER), Betulinic acid (BA), oleanolic acid (OA) and Betulinic acid methyl ester (BA-ME) as shown in Table 1 [57]. Meanwhile, the other substances present in the dry triterpene extract have now been characterised but are still undisclosed. The birch bark triterpenes are pentacyclic triterpenes and can be divided into the two basic Lupan and Oleanol backbones (Figure 2).

Table 1. Triterpene composition of birch bark extract.

Triterpene	**Triterpene extract [% (W/W)]**
Betulin (BE)	81.60
Lupeol (LU)	2.08
Betulinic acid (BA)	3.84
Erythrodiol (ER)	1.05
Oleanolic acid (OA)	0.97
Betulinic acid methyl ester (BA-ME)	0.52
Other (undisclosed) substances	9.94

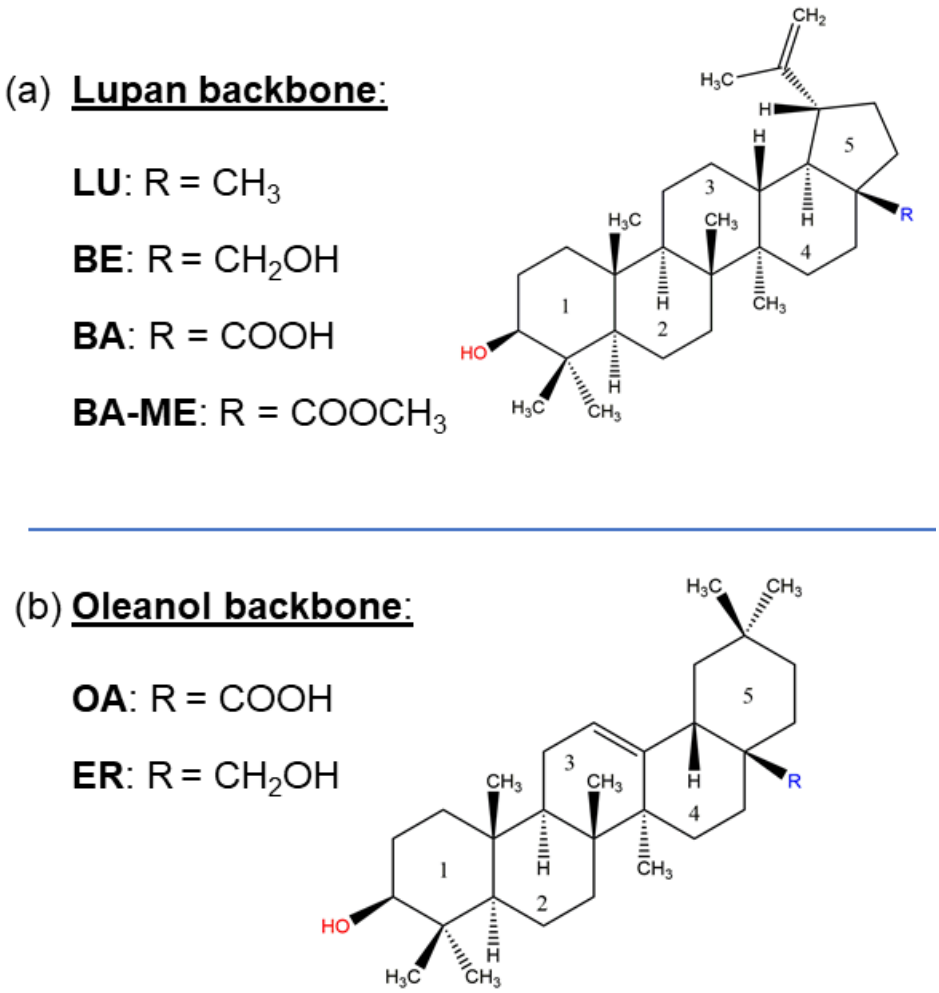

Figure 2. (a) Lupan and (b) Oleanol backbones of pentacyclic triterpenes from birch bark extract.

1.3.4 Galenical properties of birch bark extract

The triterpene extract consists of small particles and agglomerates with a d50 value of about 2-3 µm and a large rough hydrophobic surface resembling to that of cauliflower. The extract is in water practically insoluble (0.1 µg/mL) whereas in oils it is slightly soluble (0.15-0.3% (m/m)) [58]. Hence, the low solubility of these triterpenes in polar and non-polar solvents may hinder development of suitable pharmaceutical formulations or lead to a poor bioavailability which might limit their therapeutic application [29, 30]. TE forms semi-solid gels when suspended in oils through hydrogen bonds [32, 59]. Further, TE act as Pickering stabilizer to form water in oil emulsions [32, 60]. It has also been used to produce water-in-oil foams [31, 61].

1.3.5 Birch bark extract in wound healing

Ex-vivo and *in vivo* studies have been successfully undertaken to evaluate the wound healing properties of the birch bark extract. *Ex-vivo* studies have demonstrated the positive effects of TE on wound healing for example on diabetic wounds [62]. Additionally, the effects of TE-based formulations have been already investigated *in vivo* on different types of wounds such as superficial partial thickness burn wounds, surgical skin lesions including dystrophic epidermolysis bullosa where TE treatments promote or accelerate wound healing [63-65]. Beyond that, TE has been used to treat actinic keratoses and in the treatment of necrotizing herpes zoster after unsuccessful conventional therapy [66, 67]. A study conducted by Ebeling et al. showed the molecular mechanism of the effects of birch bark extract on wound healing properties in human primary keratinocytes and porcine *ex-vivo* wound healing models. They showed that TE and Betulin mainly accelerated re-epithelialization by enhancing migration of keratinocytes and their differentiation. Beyond that, they found that TE led to upregulation of proinflammatory mediators such as COX-2 and IL-6 which play a key role in wound healing und epidermal barrier repair [28, 68]. TE positive effects have been observed in all three phases of wound healing [33]. Porcine *ex-vivo* wound healing assays were performed with TE-oleogel (10% TE, 90% sunflower oil). It is worthwhile to note that TE together with sunflower oil support more wound healing than in combination with other oils as examined by Steinbrenner et al. [29]. An oleogel (Episalvan) consisting of TE and sunflower oil received the European marketing authorization in January 2016 for the treatment of superficial skin wounds [33].

1.3.6 Colloidal dispersions

A colloidal dispersion is defined by the IUPAC gold book as a system in which particles of colloidal size of any nature (e.g. solid, liquid or gas) are dispersed in a continuous phase of a different composition (or state) [69]. Colloidal dispersions have been widely used to create good colloidal drug carriers for various potential therapeutic applications i.e. oral, ocular, dermal and parenteral [70-74]. They have been used to incorporate poorly water soluble drugs, increase their bioavailability and can be used to minimise the side effects of potent drugs [75-78]. Several methods have been utilized to manufacture colloidal dispersions. Mostly they can be formed by first forming a primary coarse dispersion with large particle sizes in the micron range (1-5 µm) and subsequently subjecting them to e.g. high-pressure homogenization they can be

reduced to colloidal range (<1 µm) down to several hundred nanometers (100 – 500 nm). The pre-dispersion formed in the first step using a rotor-stator high shear mixer have high variable particle sizes whereas the subsequent high-pressure homogenization produces dispersions with more uniform particle sizes (Figure 3). Surface active substances such as proteins, polysaccharides and phospholipids play a key role in production and stabilization of colloidal dispersions [71, 79-81].

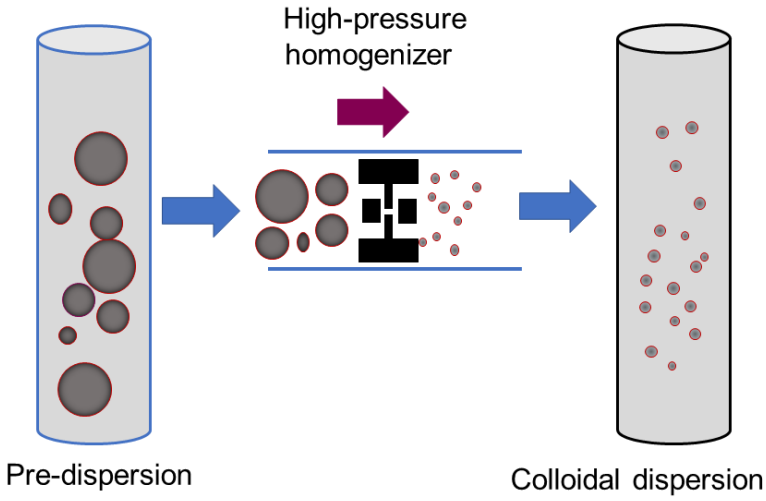

Figure 3. Schematic diagram of a typical two-step procedure used to produce colloidal dispersion.

1.3.7 Properties of phospholipids

Phospholipids (PL) are commonly found in all cell membranes and therefore exist in all living organisms where they serve both structural and functional purposes. Lecithin is the most common form of phospholipids where phosphatidylcholine (PC) is the major component [82, 83]. United States Pharmacopeia (USP) explains “lecithin as a complex mixture of acetone-insoluble phosphatides, which consist chiefly of phosphatidylcholine, phosphatidylethanolamine, phosphatidylserine, and phosphatidylinositol, combined with various amounts of other substances such as triglycerides, fatty acids, and carbohydrates, as separated from the crude vegetable oil source. It contains not less than 50.0 percent of acetone-insoluble matter”. This definition is lost where lecithin grades contain > 80% PC (arbitrarily PC) and those with < 80% PC are arbitrarily known as lecithin. Nowadays, food and cosmetic industry uses “lecithin” as a trade name for the mixture of phosphatides [82, 84]. Phospholipids are amphiphilic in nature having a polar head group and two lipophilic tails (Figure 4). The polar head unit containing a phosphate group can be esterified with an alcohol to an

organic molecule such as phosphatidylcholine (PC) with choline, in phosphatidylethanolamine (PE) with ethanolamine, phosphatidylglycerol (PG) with glycerol etc. Ionization status of phospholipids is controlled by their structure of the polar region and pH of the medium, where PE and PC are zwitterionic with a neutral charge at pH of about 7 whereas PG is negatively charged. PL can be derived from various sources such as eggs, meats, fish, shellfish, cereal grains and oilseeds hence differences in PLs content. The properties and composition of various PL classes with their origin are well described in the literature [82, 85, 86].

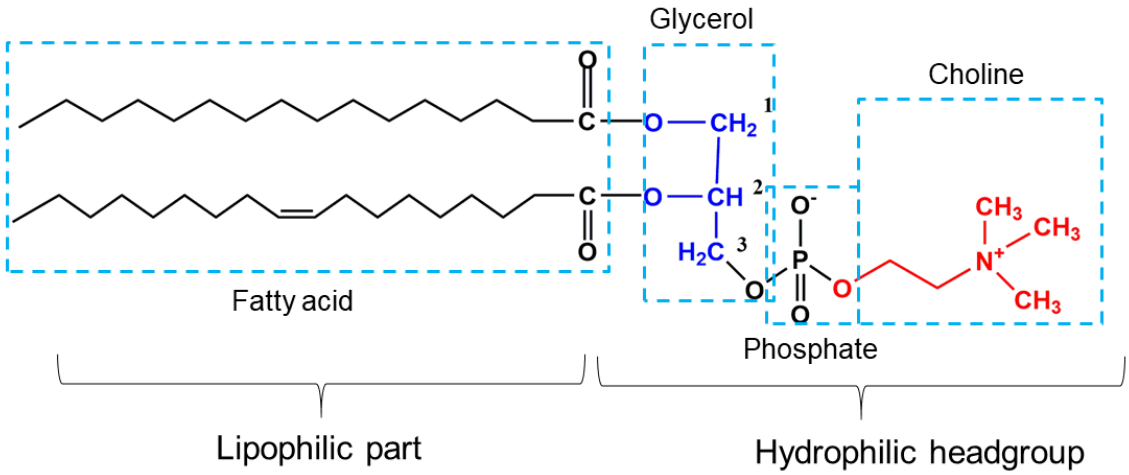

Figure 4. Chemical structure of a typical phospholipid, phosphatidylcholine.

Due to their amphiphilic character, PL shows various lyotropic and thermotropic phase structures. Depending on the solvent, the lipid composition and the temperature used, phospholipids can form self-assembled structures such as micelles, liposomes, hexagonal, lamellar, cylindrical structures and aggregates when they become hydrated. Hence, transitions between the phases can be induced for example, through temperature or lipid concentration variation. For instance, a lipid bilayer can take a solid gel phase state at lower temperature but undergo phase transition to a liquid crystalline state at higher temperature. This highly depends on the PL type and physicochemical properties, as PL chain length increases, phase transitions occur at higher temperatures. In liquid phase, PL is likely to form bilayer structures when swollen in water but tend to separate into two monolayers when swollen in oil. It has been reported that phase transition temperature of unsaturated PL is below 0 °C whereas that of saturated PL is between 40-55 °C after being hydrated [83, 87]. Fully hydrated phospholipids and glycolipids have been reported to undergo the following generalized sequence of thermotropic phase transitions:

$L_c \rightarrow L_\beta \rightarrow P_\beta \rightarrow L_\alpha \rightarrow Q_{II} \rightarrow H_{II} \rightarrow M_{II}$

Upon heating from low to high temperatures, a sub-transition begins where crystalline (L_c) phase transforms into a hydrated lamellar gel phase (L_β) with ordered lipid chains which may either be tilted or not tilted. Thereafter, a pretransition from the low temperature gel phase to an intermediate (rippled) gel phase (P_β) occurs. After that, main or chain melting from the gel phase with ordered chains to the fluid lamellar phase (L_α) phase with disordered lipid chains. In the fluid phase, further transitions may take place with increasing temperature form the lamellar phase to non-lamellar phases of the inverted (water-in-oil) type. The sequence of non-lamellar phases would be first inverted cubic (Q_{II}) and then inverted hexagonal (H_{II}). Finally, an isotropic melt would take place close to capillary melting point, presumably to an inverted micellar phase (M_{II}) which would be present as an immiscible oil in excess water. Some lipids can form two or more modifications of a given phase [88, 89].

1.3.8 Phospholipids interactions with triterpenes

Bioactive triterpenes such as Betulin, Betulinic acid and Lupeol can cause alterations of erythrocyte membrane through their hydrogen bonding properties [90]. Additionally, triterpenes like Betulin affect the lipidome of keratinocytes where it contributes to upregulation of glycerolphospholipids, sphingolipids and diacylglycerides, whereas those of cholesteryl esters and triacylglycerides were downregulated. It was concluded that Betulin is incorporated in the membrane and metabolized in keratinocytes [91]. It has been reported that phospholipid molecules can interact with triterpenes forming monolayers [92]. Further, triterpenes interact with phospholipids, being amphiphilic, through the choline head group and alkyl chains of PL. This depends on the structural properties of triterpenes. Specifically, triterpenes interact with PL and fluidize lipid membranes controlled by their free polar groups where tetracyclic triterpenes (e.g. cortisol) tend to be located at the head group, whereas pentacyclic ones (e.g. erythrodiol) being more hydrophobic are incorporated deeply in the lipid bilayers [93]. Cyclic triterpenes share similar structural properties with cholesterol, and it has been reported that such a monolayer containing cholesterol and PL is highly ordered. On the other hand, binary films of triterpenes and PLs are amorphous [92].

1.3.9 Phospholipids as a stabilizer

Natural phospholipid mixtures have high amounts of unsaturated fatty acids. The acyl chains being unsaturated, phase transition temperature from liquid crystalline to gel phase is below 0 °C. However, where stable formulations with increased stability are the target, PL with higher phase transition temperatures are favorable. The solution is to hydrogenate the unsaturated fatty acids natural PL. As a result, saturated PL are produced which are chemically more susceptible to oxidation and can be used to form stable formulations. Under certain conditions, PL when dispersed in water forms vesicles or liposomal structures which include multilamellar vesicles (> 500 nm), small unilamellar vesicles (< 100 nm) and large unilamellar vesicles (> 100 nm). These vesicles can be designed and loaded with bioactive compounds to create drug delivery systems [94, 95]. Stabilizing properties of PL have been well investigated making them suitable as perfect excipients to be used in pharmaceutical, cosmetic and food industry [82, 96-98]. On the other hand, since phospholipids contain both hydrophilic and hydrophobic groups they can form a monolayer at the oil/water interface which possess a thickness in the range of 1–3 nm [99-101]. Due to diffusion-controlled monolayer adsorption, the interfaces become viscoelastic [102]. Stabilizers adsorbed at oil–water interfaces play a key role in determining the stability and other physicochemical characteristics of dispersions [103]. Beyond that, this mechanism can also affect their production process which may include high shear mixing and homogenization [104]. Stabilizers have proved their efficiency in particle size reduction enhanced by their complex behaviour in the interface. The adsorption of PL at the oil-water interface results to a decrease of the interfacial tension between the two phases and reduces the pressure gradients required to disrupt the particles during emulsification process. The dispersion particle size depends on the stabilizer concentration whereby the particles significantly decrease in size as the stabilizer content was increased [103, 105-107]. These unique features make phospholipids most suitable to be used as excipients for poorly water-soluble drugs [108]. More exclusively, they can be used to increase their solubility and thereby leading to a better bioavailability [82].

1.3.10 Profile drop analysis

The measurement of dynamic interfacial tension can be performed using the Profile Analysis Tensiometer (PAT) through methods such as pendant drop and buoyant drop method (Figure 5). These methods involve the determination of the profile of a drop of

one liquid immersed in another immiscible liquid. By analysing the drop shape, conclusions can be drawn on the interfacial tension. Additionally, dynamic surface tension can also be analysed through these methods, if measurements are made in air as the bulk phase [109]. As mentioned in sub-section 1.3.9, the disruption of the particles depends on the oil-water interfacial tension; particle break-up is facilitated when the interfacial tension is low. The presence of stabilizer in the system may help to decrease the interfacial tension and then to minimise the effects of interfacial forces. The time taken by the stabilizer to adsorb at the interface is also important; for example, during emulsification process, a stabilizer must adsorb quickly at the particles which facilitates the particle disruption. The underlying concept to the measurement with PAT is the Young-Laplace equation (Equation 1). It represents the relationship between the curvature and the drop shape of a liquid in another immiscible liquid as follows:

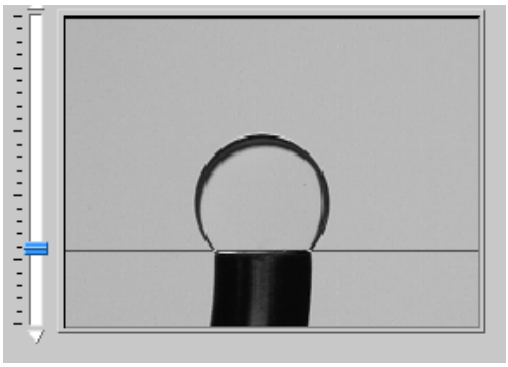

Figure 5. Buoyant drop method.

$$\gamma\left(\frac{1}{R_1}+\frac{1}{R_2}\right)=\Delta P_0+(\Delta\rho)gz \qquad \text{(Equation 1)}$$

Where R_1 and R_2 are main radii of interface curvature, γ is the interfacial tension, ΔP_0 is the pressure difference at a reference plane, $\Delta\rho$ is the density difference, g is the gravitational constant and z is the vertical height measured from the reference plane [110, 111].

1.3.11 Interfacial rheology

Interface refers to the contact surface between two phases (liquid/liquid, gas/liquid or solid/liquid) and the forces acting in the interfaces are known as interfacial tension. If forces are acting where one of the two phases is gaseous, it is known as surface tension [112]. Interfacial rheology serves as a powerful tool to investigate events

happening when molecules are adsorbed at fluid/fluid interfaces and both interfacial shear and dilatational deformation can be used. For instance, interfacial tension between the immiscible liquid phases, which usually consist of oil and water can be lowered by adding amphiphilic surface-active substances such as surfactants, polymers and phospholipids to enhance better stabilization [110]. These surface-active molecules lower the free energy at the phase boundary. Therefore, interfacial activity of these amphiphilic compounds plays an important role in the characteristics and stability of various formulations such as foams and dispersions. For example, they can hinder instabilities occurring in dispersions such as coalescence, flocculation, sedimentation and creaming [102, 113]. For instance, in this work, oscillating drop method using the buoyant drop technique (Figure 5) was employed to study dynamic dilatational rheology of interfacial layers. The principle of oscillating drop method involves changes of the size of the interface, where surface-active molecules are located, by continuously altering the drop volume. In a sinusoidal change (expansions and compressions) of drop volume and thus the interface, several observations can be made: as the interface narrows, stabilizer molecules desorb from the interface (interfacial tension increases temporarily) and during the subsequent enlargement adsorb the molecules again (interfacial tension decreases temporarily) [110, 114]. Hence, the rheological properties of adsorption layers are expressed by the relationship between the variation of the interfacial tension, from its initial value, and the expansion of the surface area. The interfacial elastic *(E)* and viscosity modulus can be expressed as [115]:

$$E = \frac{\mathrm{d}\gamma}{\mathrm{d}\ \ln(A)} \qquad \text{(Equation 2)}$$

$$\eta_d = \frac{\mathrm{d}\gamma}{(\mathrm{d}A/dt)/A} \qquad \text{(Equation 3)}$$

Where *E*: interfacial elasticity, γ is the interfacial tension and A is the area of the interface and η_d is interfacial dilational viscosity.

1.3.12 Polyvinyl alcohol (PVA)

PVA is a hydrophilic polymer which is water soluble with excellent chemical resistance, physical characteristics, non-toxic, biodegradable and biocompatible. This makes it one of the most frequently used synthetic polymer in the textile and paper industry, and

due to its good biodegradability and biocompatibility has found its use in biomedical applications such as drug delivery systems, tissue engineering and wound dressings [116, 117]. A Commercially available PVA polymer is usually made by the polymerization of vinyl acetate to first produce polyvinyl acetate, followed by the hydrolysis of polyvinyl acetate through saponification whereby the ester group is replaced by a hydroxyl group. Impurities from the production process such as sodium acetate, methanol and methyl acetate could be present in the final product. The percentage of acetate groups converted to hydroxyl groups determines the hydrolysis degree of PVA, thus affecting the degree of polymer crystallinity and solubility. Hence, PVA can be partially (84.2%-89%), moderately (92.2%-96.5%) or fully hydrolyzed (98%-99%) where fully hydrolyzed PVA exhibit high crystallinity and low solubility. The presence of acetyl groups in partially hydrolyzed PVA as spacers makes it semi-crystalline (18-60%). It has also been reported that the melting point for partially hydrolyzed PVA is between 180°C-190°C and 230°C for fully hydrolyzed whereas the boiling point of pure PVA is at 228°C. The glass transition temperature of pure PVA is in the range of 75°C-85°C. In addition, PVA has a wide range of molecular weights, varying between 20,000-400,000 g/mol. The degree of hydrolysis together with molecular weight highly affects the overall polymer behavior in aqueous solutions [38, 39, 118-120].

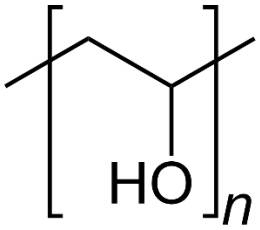

Figure 6. Structure of PVA.

An increase in molecular weight of PVA results to an increase in tensile strength, crystallinity, adhesion, resistance to solvents, film-formation and viscosity [121]. Moreover, adding PVA to water reduces the surface tension of water [122]. Notably, all these physicochemical properties are expected to have a significant impact in electrospinning. Studies have been carried out by use of different PVA molecular weights to investigate their behavior and the structures that may be formed through electrospinning [123, 124]. Researchers have also utilized PVA polymer where it has either been used alone or blended with other polymers and incorporated active

ingredients to produce electropsun nanofibrous meshes for wound healing applications. Some of these incorporated substances have antibacterial effects which would prevent the wound from infection during healing [5, 125, 126].

Table 2. PVA-based electrospun scaffolds as wound dressings.

Electrospun Scaffold	References
Chitosan/silver nanoparticles/PVA	[126]
PVA/Chitosan/Tetracycline hydrochloride	[127]
PVA/Soursop Leaves Extract (SLE)	[128]
PCL/PVA/curcumin (CU)	[129]
PVA/zein nanoparticles (NPs)/diclofenac (DLF)	[130]
PVA/PVP/PEG/Aloe vera	[131]
PVA/Gum tragacanth	[132]
PVA/chitosan/starch	[133]
PVA/silver nanoparticles	[134]
PVA/Tranexamic acid	[135]
PVA/hyaluronic acid/L-arginine	[136]
PVA/propolis	[137]

1.3.13 Phospholipids in electrospinning

As highlighted above, PL can form self-assembled structures such as lamellar phases or liposomes into various types of colloidal particles which can be further used to develop drug delivery systems [138]. The use of phospholipids in electrospinning has not been commonly practised but recently electrospun fibers with phospholipids have been prepared as drug delivery systems for bioactive substances as shown in Table 3. The use of PL alone in electrospinning has been performed to form electrospun fibers. However high concentrations of PL are needed >35% in order to form electrospun solutions. Further, electrospinning was possible at concentrations above the onset of entanglements of the micelles [139]. Asolectin, a mixture comprising roughly equal proportions of lecithin, cephalin and phosphatidylinositol, has also proved to provide antioxidant effect in electrospun fibers with increased encapsulation of drugs [140]. Surprisingly, there are very few studies on electrospinning with

hydrogenated phospholipids. De Freitas Zômpero et al. loaded β-carotene liposomes in PVA/PEO fibers and proposed that, strong interactions existed between the hydroxyl groups along the PVA polymer chain and the phospholipid head groups [141]. Beyond that, PL have been successfully used to develop core-sheath structured fibers through emulsion electrospinning. The principle here is to first load the compounds into dispersion systems such as O/W or W/O dispersions using PL as a stabilizer to produce colloidal dispersions to allow good encapsulation as well as miscibility with a polymer prior to electrospinning. As a result, the release of the incorporated substances can be modulated in the process. Furthermore, sensitive compounds can be protected against adverse conditions such as acidity and temperature [35, 142].

Table 3. Applications of phospholipids in electrospinning.

Application	**Electrospun material**	**References**
Nonwoven fibrous membranes	Lecithin	[139]
Fibrous scaffolds	1-palmitoyl-2-oleoyl-sn-glycero-3-phosphoethanolamine (POPE)	[143]
Novel biomedical materials and drug delivery systems	Polyvinylpyrrolidone (PVP) / soybean lecithin	[144]
Encapsulation and antioxidant systems	Asolectin / curcumin/vanillin	[140]
Transdermal drug delivery system	Chitosan / Phospholipids (asolectin) / curcumin, diclofenac and vitamin B12	[145]
UV photostability	β-carotene/PVA / polyethylene oxide (PEO)	[141]
Protection	Conjugated linoleic acids (CLA) / PVA / gelatin / cellulose acetate (CA)	[146]

1.4 References

1. Boateng, J.S., et al., *Wound Healing Dressings and Drug Delivery Systems: A Review.* Journal of Pharmaceutical Sciences, 2008. **97**(8): p. 2892-2923.
2. Köln., P.F.P.n.V., *Epidemiologie und Versorgung von Patienten mit chro-nischen Wunden – Eine Analyse auf der Basis der Versichertenstichprobe AOK Hessen/KV Hessen.* https://www.bvmed.de/download/pmv-zusammen-fassung-der-ergebnisse, 2015.
3. Sen, C.K., et al., *Human skin wounds: a major and snowballing threat to public health and the economy.* Wound repair and regeneration : official publication of the Wound Healing Society [and] the European Tissue Repair Society, 2009. **17**(6): p. 763-771.
4. Pereira, R.F. and P.J. Bártolo, *Traditional Therapies for Skin Wound Healing.* Advances in wound care, 2016. **5**(5): p. 208-229.
5. Zahedi, P., et al., *A review on wound dressings with an emphasis on electrospun nanofibrous polymeric bandages.* Polymers for Advanced Technologies, 2010. **21**(2): p. 77-95.
6. Jones, V., J.E. Grey, and K.G. Harding, *Wound dressings.* BMJ (Clinical research ed.), 2006. **332**(7544): p. 777-780.
7. Yilmaz, F., G. Celep, and G.J.N.R. Tetik, *Nanofibers in Cosmetics.* 2016: p. 127.
8. Vasita, R. and D.S. Katti, *Nanofibers and their applications in tissue engineering.* International journal of nanomedicine, 2006. **1**(1): p. 15-30.
9. Mendoza-Buenrostro, C., H. Lara, and C. Rodriguez, *Hybrid Fabrication of a 3D Printed Geometry Embedded with PCL Nanofibers for Tissue Engineering Applications.* Procedia Engineering, 2015. **110**: p. 128-134.
10. Formhals, A., *Process and apparatus for preparing artificial threads.* US Patent No. 1,975,504, 1934.
11. Jaeger, R., et al., *Electrospinning of ultra-thin polymer fibers.* Macromolecular Symposia, 1998. **127**(1): p. 141-150.
12. Panda, P. and B. Sahoo, *Synthesis and applications of electrospun nanofibers—A review.* Nanotechnology, 1990. **1**: p. 399-416.
13. Dzenis, Y.A. and D. Reneker, *Polymer hybrid nano/micro composites*. 1994, Technomic Publishing Co., Inc., Lancaster, PA (United States).
14. Doshi, J. and D.H. Reneker, *Electrospinning process and applications of electrospun fibers.* Journal of Electrostatics, 1995. **35**(2): p. 151-160.
15. Fang, X. and D. Reneker, *DNA fibers by electrospinning.* Journal of Macromolecular Science, Part B: Physics, 1997. **36**(2): p. 169-173.
16. Kim, J.s. and D.H. Reneker, *Mechanical properties of composites using ultrafine electrospun fibers.* Polymer composites, 1999. **20**(1): p. 124-131.
17. Huang, Z.-M., et al., *A review on polymer nanofibers by electrospinning and their applications in nanocomposites.* Composites Science and Technology, 2003. **63**(15): p. 2223-2253.
18. Thenmozhi, S., et al., *Electrospun nanofibers: New generation materials for advanced applications.* Materials Science and Engineering: B, 2017. **217**: p. 36-48.
19. El-hadi, A.M. and F.Y. Al-Jabri, *Influence of Electrospinning Parameters on Fiber Diameter and Mechanical Properties of Poly(3-Hydroxybutyrate) (PHB) and Polyanilines (PANI) Blends.* Polymers, 2016. **8**(3): p. 97.
20. Reneker, D.H. and I. Chun, *Nanometre diameter fibres of polymer, produced by electrospinning.* Nanotechnology, 1996. **7**(3): p. 216-223.
21. Kai, D., S.S. Liow, and X.J. Loh, *Biodegradable polymers for electrospinning: Towards biomedical applications.* Materials Science and Engineering: C, 2014. **45**: p. 659-670.
22. Zhong, S.P., Y.Z. Zhang, and C.T. Lim, *Tissue scaffolds for skin wound healing and dermal reconstruction.* Wiley Interdisciplinary Reviews: Nanomedicine and Nanobiotechnology, 2010. **2**(5): p. 510-525.
23. *Drug-loaded electrospun materials in wound-dressing applications and in local cancer treatment.* Expert Opinion on Drug Delivery, 2013. **10**(4): p. 469-483.

24. Garcia-Orue, I., et al., *Novel nanofibrous dressings containing rhEGF and Aloe vera for wound healing applications.* International Journal of Pharmaceutics, 2017. **523**(2): p. 556-566.
25. Wang, J. and M. Windbergs, *Functional electrospun fibers for the treatment of human skin wounds.* European Journal of Pharmaceutics and Biopharmaceutics, 2017. **119**: p. 283-299.
26. Alavi, A., et al., *Wound-Related Allergic/Irritant Contact Dermatitis.* Advances in skin & wound care, 2016. **29**(6): p. 278-286.
27. Boateng, J. and O. Catanzano, *Advanced Therapeutic Dressings for Effective Wound Healing—A Review.* Journal of Pharmaceutical Sciences, 2015. **104**(11): p. 3653-3680.
28. Ebeling, S., et al., *From a Traditional Medicinal Plant to a Rational Drug: Understanding the Clinically Proven Wound Healing Efficacy of Birch Bark Extract.* PLoS ONE, 2014. **9**(1): p. e86147.
29. Steinbrenner, I., et al., *Influence of the Oil Phase and Topical Formulation on the Wound Healing Ability of a Birch Bark Dry Extract.* PLoS ONE, 2016. **11**(5): p. e0155582.
30. Jäger, S., M.N. Laszczyk, and A. Scheffler, *A preliminary pharmacokinetic study of betulin, the main pentacyclic triterpene from extract of outer bark of birch (Betulae alba cortex).* Molecules, 2008. **13**(12): p. 3224-3235.
31. Färber, A. and R. Daniels, *Ex vivo Skin Permeation of Betulin from Water-in-Oil Foams.* Skin Pharmacology and Physiology, 2016. **29**(5): p. 250-256.
32. Grysko, M., *Herstellung und Charakterisierung von halbfesten Systemen auf der Basis von Triterpentrockenextrakt aus Birkenkork*. 2011.
33. Scheffler, A., *The Wound Healing Properties of Betulin from Birch Bark from Bench to Bedside.* Planta Med, 2019. **85**(07): p. 524-527.
34. Mohammadian, F. and A. Eatemadi, *Drug loading and delivery using nanofibers scaffolds.* Artificial Cells, Nanomedicine, and Biotechnology, 2017. **45**(5): p. 881-888.
35. Nikmaram, N., et al., *Emulsion-based systems for fabrication of electrospun nanofibers: Food, pharmaceutical and biomedical applications.* RSC Advances, 2017. **7**(46): p. 28951-28964.
36. Rott, C., *Thesis:Herstellung und Charakterisierung betulinhaltiger Zubereitungen für berührungsempfindliche Haut.* University of Tuebingen, 2016.
37. Dangelmayer, A., *Thesis: Entwicklung und Charakterisierung von triterpenhaltigen Schäumen zur Anwendung der Wundheilung.* University of Tuebingen, 2016.
38. Gajra*, B., et al., *Poly vinyl alcohol hydrogel and its pharmaceutical and biomedical applications: A review.* 2012. **4**(2): p. 20-26.
39. Gaaz, T.S., et al., *Properties and Applications of Polyvinyl Alcohol, Halloysite Nanotubes and Their Nanocomposites.* Molecules (Basel, Switzerland), 2015. **20**(12): p. 22833-22847.
40. Motamedi, A.S., et al., *Effect of electrospinning parameters on morphological properties of PVDF nanofibrous scaffolds.* Progress in Biomaterials, 2017. **6**(3): p. 113-123.
41. Haider, A., S. Haider, and I.-K. Kang, *A comprehensive review summarizing the effect of electrospinning parameters and potential applications of nanofibers in biomedical and biotechnology.* Arabian Journal of Chemistry, 2018. **11**(8): p. 1165-1188.
42. Venus, M., J. Waterman, and I. McNab, *Basic physiology of the skin.* Surgery (Oxford), 2011. **29**(10): p. 471-474.
43. Lai-Cheong, J.E. and J.A. McGrath, *Structure and function of skin, hair and nails.* Medicine, 2017. **45**(6): p. 347-351.
44. Boyce, J., et al., *WHO guidelines on hand hygiene in health care.* 2009.
45. Young, A. and C.-E. McNaught, *The physiology of wound healing.* Surgery (Oxford), 2011. **29**(10): p. 475-479.
46. Grubbs, H. and B. Manna, *Wound physiology*, in *StatPearls [Internet]*. 2018, StatPearls Publishing.

47. Gurtner, G.C., et al., *Wound repair and regeneration.* Nature, 2008. **453**(7193): p. 314-321.
48. Kondo, T. and Y. Ishida, *Molecular pathology of wound healing.* Forensic science international, 2010. **203**(1-3): p. 93-98.
49. Schreml, S., et al., *Wound healing in the 21st century.* Journal of the American Academy of Dermatology, 2010. **63**(5): p. 866-881.
50. Velnar, T., T. Bailey, and V. Smrkolj, *The wound healing process: an overview of the cellular and molecular mechanisms.* Journal of International Medical Research, 2009. **37**(5): p. 1528-1542.
51. Aiken, C. and C.H. Chen, *Betulinic acid derivatives as HIV-1 antivirals.* Trends in Molecular Medicine, 2005. **11**(1): p. 31-36.
52. Haque, S., et al., *Screening and Characterisation of Antimicrobial Properties of Semisynthetic Betulin Derivatives.* PLoS ONE, 2014. **9**(7): p. e102696.
53. Dehelean, C.A., et al., *Antitumoral activity of betulin, a compound present in birch tree, in formulations with cyclodextrin.* Studia Univ. VG, Seria St. Vietii, 2010. **20**: p. 55-58.
54. Dehelean, C.A., et al., *Study of the betulin enriched birch bark extracts effects on human carcinoma cells and ear inflammation.* Chemistry Central Journal, 2012. **6**: p. 137-137.
55. Metelmann, H.-R., F. Podmelle, and P.D. Waite, *Long-term cosmetic benefit of wound healing by betuline.* The American Journal of Cosmetic Surgery, 2012. **29**(1): p. 19-24.
56. Armbruster, M., et al., *Birch Bark Dry Extract by Supercritical Fluid Technology: Extract Characterisation and Use for Stabilisation of Semisolid Systems.* Applied Sciences, 2017. **7**(3): p. 292.
57. SCHEFFLER, A., *Triterpene-containing oleogel-forming agent, triterpene-containing oleogel and method for producing a triterpene-containing oleogel*. 2014, US20140050790 A1.
58. R. Daniels und M. Laszczyk, *Betulin für tensidfreie Emulsionen. Pharmazeutische Zeitung 153, Nr. 11. 862-863.* 2008.
59. Ghaffar, K.A. and R.J.P. Daniels, *Oleogels with Birch Bark Dry Extract: Extract Saving Formulations through Gelation Enhancing Additives.* 2020. **12**(2): p. 184.
60. Scheffler, A., *Emulsion containing a plant extract, method for producing said emulsion and for obtaining a plant extract*. 2003, Google Patents.
61. Daniels, R. and T. Zahn, *Betulin-containing water-in-oil foams and compositions thereof*. 2019, Google Patents.
62. Ueck, C., et al., *Comparison of In-Vitro and Ex-Vivo Wound Healing Assays for the Investigation of Diabetic Wound Healing and Demonstration of a Beneficial Effect of a Triterpene Extract.* PLOS ONE, 2017. **12**(1): p. e0169028.
63. Schwieger-Briel, A., et al., *Betulin-based oleogel to improve wound healing in dystrophic epidermolysis bullosa: a prospective controlled proof-of-concept study.* 2017. **2017**.
64. Frew, Q., et al., *Betulin wound gel accelerated healing of superficial partial thickness burns: Results of a randomized, intra-individually controlled, phase III trial with 12-months follow-up.* Burns, 2019. **45**(4): p. 876-890.
65. Metelmann, H.-R., et al., *Accelerated reepithelialization by triterpenes: proof of concept in the healing of surgical skin lesions.* 2015. **28**(1): p. 1-11.
66. Weckesser, S., et al., *Topical Treatment of Necrotising Herpes Zoster with Betulin from Birch Bark.* Complementary Medicine Research, 2010. **17**(5): p. 271-273.
67. Huyke, C., et al., *Treatment of actinic keratoses with birch bark extract: a pilot study.* 2006. **4**(2): p. 132-136.
68. Reinke, J.M. and H. Sorg, *Wound Repair and Regeneration.* European Surgical Research, 2012. **49**(1): p. 35-43.
69. Book, I.G., *colloidal dispersion (C01174) - IUPAC Gold Book.* https://doi.org/10.1351/goldbook.C01174 *,2014.*

70. Sznitowska, M., et al., *Submicron emulsions as drug carriers: Studies on destabilization potential of various drugs.* European Journal of Pharmaceutical Sciences, 2001. **12**(3): p. 175-179.
71. Benita, S. and M.Y. Levy, *Submicron emulsions as colloidal drug carriers for intravenous administration: Comprehensive physicochemical characterization.* Journal of Pharmaceutical Sciences, 1993. **82**(11): p. 1069-1079.
72. Fang, J.-Y., et al., *Lipid Nano/Submicron Emulsions as Vehicles for Topical Flurbiprofen Delivery.* Drug Delivery, 2004. **11**(2): p. 97-105.
73. Klang, S.H., A. Baszkin, and S. Benita, *The stability of piroxicam incorporated in a positively-charged submicron emulsion for ocular administration.* International Journal of Pharmaceutics, 1996. **132**(1): p. 33-44.
74. Aviv, H., et al., *Submicron emulsions as ocular drug delivery vehicles*. 1996, Google Patents.
75. Youenang Piemi, M.P., et al., *Positively and negatively charged submicron emulsions for enhanced topical delivery of antifungal drugs.* Journal of Controlled Release, 1999. **58**(2): p. 177-187.
76. Rubinstein, A., et al., *In Vitro Release and Intestinal Absorption of Physostigmine Salicylate from Submicron Emulsions.* Journal of Pharmaceutical Sciences, 1991. **80**(7): p. 643-647.
77. Schwarz, J.S., M.R. Weisspapir, and D.I. Friedman, *Enhanced Transdermal Delivery of Diazepam by Submicron Emulsion (SME) Creams.* Pharmaceutical Research, 1995. **12**(5): p. 687-692.
78. Sznitowska, M., E.A. Dabrowska, and S. Janicki, *Solubilizing potential of submicron emulsions and aqueous dispersions of lecithin.* International Journal of Pharmaceutics, 2002. **246**(1): p. 203-206.
79. Cortés-Muñoz, M., D. Chevalier-Lucia, and E. Dumay, *Characteristics of submicron emulsions prepared by ultra-high pressure homogenisation: Effect of chilled or frozen storage.* Food Hydrocolloids, 2009. **23**(3): p. 640-654.
80. Sjöström, B., B. Bergenståhl, and B. Kronberg, *A method for the preparation of submicron particles of sparingly water-soluble drugs by precipitation in oil-in-water emulsions. II: Influence of the emulsifier, the solvent, and the drug substance.* Journal of Pharmaceutical Sciences, 1993. **82**(6): p. 584-589.
81. McClements, D.J. and C.E. Gumus, *Natural emulsifiers — Biosurfactants, phospholipids, biopolymers, and colloidal particles: Molecular and physicochemical basis of functional performance.* Advances in Colloid and Interface Science, 2016. **234**: p. 3-26.
82. van Hoogevest, P. and A. Wendel, *The use of natural and synthetic phospholipids as pharmaceutical excipients.* European Journal of Lipid Science and Technology, 2014. **116**(9): p. 1088-1107.
83. Pichot, R., R.L. Watson, and I.T. Norton, *Phospholipids at the interface: current trends and challenges.* International journal of molecular sciences, 2013. **14**(6): p. 11767-11794.
84. Pharmacopeia, U.S., *Excipient Monographs 2, USP29-NF24 Page 3359; http://www.pharmacopeia.cn/v29240/usp29nf24s0_m44420.html.*
85. Weihrauch, J.L. and Y.-S. Son, *Phospholipid content of foods.* Journal of the American Oil Chemists' Society, 1983. **60**(12): p. 1971-1978.
86. Singh, R.P., H.V. Gangadharappa, and K. Mruthunjaya, *Phospholipids: Unique carriers for drug delivery systems.* Journal of Drug Delivery Science and Technology, 2017. **39**: p. 166-179.
87. van Hoogevest, P., *Review – An update on the use of oral phospholipid excipients.* European Journal of Pharmaceutical Sciences, 2017. **108**: p. 1-12.
88. Koynova, R. and B.J.O.B. Tenchov, *Transitions between lamellar and non-lamellar phases in membrane lipids and their physiological roles.* 2013. **1**(1): p. 1-9.
89. Marsh, D., *General features of phospholipid phase transitions.* Chemistry and Physics of Lipids, 1991. **57**(2): p. 109-120.

90. Ziegler, H.L., et al., *Erythrocyte membrane modifying agents and the inhibition of Plasmodium falciparum growth: structure–activity relationships for betulinic acid analogues.* Bioorganic & Medicinal Chemistry, 2004. **12**(1): p. 119-127.
91. Calderón, C., et al., *Lipid Atlas of Keratinocytes and Betulin Effects on its Lipidome Profiled by Comprehensive UHPLC–MS/MS with Data Independent Acquisition Using Targeted Data Processing.* **n/a**(n/a): p. 1900113.
92. Broniatowski, M., M. Flasiński, and P. Wydro, *Investigation of the interactions of lupane type pentacyclic triterpenes with outer leaflet membrane phospholipids – Langmuir monolayer and synchrotron X-ray scattering study.* Journal of Colloid and Interface Science, 2012. **381**(1): p. 116-124.
93. Abboud, R., C. Charcosset, and H. Greige-Gerges, *Tetra- and Penta-Cyclic Triterpenes Interaction with Lipid Bilayer Membrane: A Structural Comparative Study.* The Journal of Membrane Biology, 2016. **249**(3): p. 327-338.
94. Fiandaca, M. and K. Bankiewicz, *Micelles and Liposomes*. 2013. p. 51-64.
95. Himeno, T., Y. Konno, and N. Naito, *Chapter 31 - Liposomes for Cosmetics*, in *Cosmetic Science and Technology*, K. Sakamoto, et al., Editors. 2017, Elsevier: Amsterdam. p. 539-549.
96. Van Nieuwenhuyzen, W., *The industrial uses of special lecithins: A review.* Journal of the American Oil Chemists' Society, 1981. **58**(10): p. 886-888.
97. Hasenhuettl, G.L., *Overview of Food Emulsifiers*, in *Food Emulsifiers and Their Applications: Second Edition*, G.L. Hasenhuettl and R.W. Hartel, Editors. 2008, Springer New York: New York, NY. p. 1-9.
98. Cabezas, D.M., et al., *Emulsifying Properties of Different Modified Sunflower Lecithins.* Journal of the American Oil Chemists' Society, 2012. **89**(2): p. 355-361.
99. Hildebrandt, E., et al., *Adsorption of phospholipids at oil/water interfaces during emulsification is controlled by stress relaxation and diffusion.* Soft Matter, 2018. **14**(19): p. 3730-3737.
100. Grandell, D. and L. Murtomäki, *Surface Pressure Control of Phospholipid Monolayers at the Water/1,2-Dichloroethane Interface.* Langmuir, 1998. **14**(2): p. 556-559.
101. Shchipunov, Y.A. and P. Schmiedel, *Phase Behavior of Lecithin at the Oil/Water Interface.* Langmuir, 1996. **12**(26): p. 6443-6445.
102. Langevin, D., *Influence of interfacial rheology on foam and emulsion properties.* Advances in Colloid and Interface Science, 2000. **88**(1): p. 209-222.
103. Amine, C., et al., *Investigation of emulsifying properties and emulsion stability of plant and milk proteins using interfacial tension and interfacial elasticity.* Food Hydrocolloids, 2014. **39**: p. 180-186.
104. Yang, R., et al., *Role of phospholipids and copolymers in enhancing stability and controlling degradation of intravenous lipid emulsions.* Colloids and Surfaces A: Physicochemical and Engineering Aspects, 2013. **436**: p. 434-442.
105. Güell, C., et al., *Apparent Interfacial Tension Effects in Protein Stabilized Emulsions Prepared with Microstructured Systems.* Membranes, 2017. **7**(2): p. 19.
106. Pan, L.G., M.C. Tomás, and M.C. Añón, *Oil-in-water emulsions formulated with sunflower lecithins: Vesicle formation and stability.* Journal of the American Oil Chemists' Society, 2004. **81**(3): p. 241-244.
107. Henry, J.V.L., et al., *The influence of phospholipids and food proteins on the size and stability of model sub-micron emulsions.* Food Hydrocolloids, 2010. **24**(1): p. 66-71.
108. van Hoogevest, P., X. Liu, and A. Fahr, *Drug delivery strategies for poorly water-soluble drugs: the industrial perspective.* Expert opinion on drug delivery, 2011. **8**(11): p. 1481-1500.
109. Berry, J.D., et al., *Measurement of surface and interfacial tension using pendant drop tensiometry.* Journal of Colloid and Interface Science, 2015. **454**: p. 226-237.
110. Miller, R., et al., *Rheology of interfacial layers.* Colloid and Polymer Science, 2010. **288**(9): p. 937-950.

111. Zholob, S.A., et al., *Optimisation of calculation methods for determination of surface tensions by drop profile analysis tensiometry.* Advances in Colloid and Interface Science, 2007. **134-135**: p. 322-329.
112. *Surface and Interfacial Tension*, in *Surface Chemistry of Surfactants and Polymers*. p. 231-249.
113. Opawale, F.O. and D.J. Burgess, *Influence of Interfacial Rheological Properties of Mixed Emulsifier Films on the Stability of Water-in-Oil-in-Water Emulsions.* Journal of Pharmacy and Pharmacology, 1998. **50**(9): p. 965-973.
114. Javadi, A., et al., *Characterization methods for liquid interfacial layers.* The European Physical Journal Special Topics, 2013. **222**(1): p. 7-29.
115. Miller, R., et al., *Dilational and shear rheology of adsorption layers at liquid interfaces.* Colloids and Surfaces A: Physicochemical and Engineering Aspects, 1996. **111**(1): p. 75-118.
116. Aslam, M., et al., *Polyvinyl alcohol: a review of research status and use of polyvinyl alcohol based nanocomposites.* 2018. **58**(12): p. 2119-2132.
117. Wu, H., et al., *Biodegradation of polyvinyl alcohol by different dominant degrading bacterial strains in a baffled anaerobic bioreactor.* 2019. **79**(10): p. 2005-2012.
118. Feng, J.-H. and F. Dogan, *Aqueous processing and mechanical properties of PLZT green tapes.* Materials Science and Engineering: A, 2000. **283**(1): p. 56-64.
119. Tretinnikov, O.N. and S.A. Zagorskaya, *Determination of the degree of crystallinity of poly(vinyl alcohol) by FTIR spectroscopy.* Journal of Applied Spectroscopy, 2012. **79**(4): p. 521-526.
120. Ben Halima, N., *Poly(vinyl alcohol): review of its promising applications and insights into biodegradation.* RSC Advances, 2016. **6**(46): p. 39823-39832.
121. Muppalaneni, S. and H.J.J.D.D. Omidian, *Polyvinyl alcohol in medicine and pharmacy: a perspective.* 2013. **2**(3): p. 1-5.
122. Bhattacharya, A. and P. Ray, *Studies on surface tension of poly(vinyl alcohol): Effect of concentration, temperature, and addition of chaotropic agents.* 2004. **93**(1): p. 122-130.
123. Koski, A., K. Yim, and S. Shivkumar, *Effect of molecular weight on fibrous PVA produced by electrospinning.* Materials Letters, 2004. **58**(3-4): p. 493-497.
124. Ngadiman, N.H.A., et al., *Influence of polyvinyl alcohol molecular weight on the electrospun nanofiber mechanical properties.* Procedia Manufacturing, 2015. **2**: p. 568-572.
125. Ranjbar-Mohammadi, M., S.H. Bahrami, and M.T. Joghataei, *Fabrication of novel nanofiber scaffolds from gum tragacanth/poly(vinyl alcohol) for wound dressing application: In vitro evaluation and antibacterial properties.* Materials Science and Engineering: C, 2013. **33**(8): p. 4935-4943.
126. Abdelgawad, A.M., S.M. Hudson, and O.J. Rojas, *Antimicrobial wound dressing nanofiber mats from multicomponent (chitosan/silver-NPs/polyvinyl alcohol) systems.* Carbohydrate Polymers, 2014. **100**: p. 166-178.
127. Alavarse, A.C., et al., *Tetracycline hydrochloride-loaded electrospun nanofibers mats based on PVA and chitosan for wound dressing.* Materials Science and Engineering: C, 2017. **77**: p. 271-281.
128. Aruan, N.M., et al., *Polyvinyl Alcohol/Soursop Leaves Extract Composite Nanofibers Synthesized Using Electrospinning Technique and their Potential as Antibacterial Wound Dressing.* Procedia Engineering, 2017. **170**: p. 31-35.
129. Saeed, S.M., et al., *Designing and fabrication of curcumin loaded PCL/PVA multi-layer nanofibrous electrospun structures as active wound dressing.* Progress in Biomaterials, 2017. **6**(1): p. 39-48.
130. Ghalei, S., H. Asadi, and B. Ghalei, *Zein nanoparticle-embedded electrospun PVA nanofibers as wound dressing for topical delivery of anti-inflammatory diclofenac.* Journal of Applied Polymer Science, 2018. **135**(33): p. 46643.

131. Uslu, I., et al., *Preparation and properties of electrospun poly (vinyl alcohol) blended hybrid polymer with aloe vera and HPMC as wound dressing.* Hacettepe J. Biol. Chem, 2010. **38**(1): p. 19-25.
132. Ranjbar-Mohammadi, M., S.H. Bahrami, and M. Joghataei, *Fabrication of novel nanofiber scaffolds from gum tragacanth/poly (vinyl alcohol) for wound dressing application: In vitro evaluation and antibacterial properties.* Materials Science and Engineering: C, 2013. **33**(8): p. 4935-4943.
133. Adeli, H., M.T. Khorasani, and M. Parvazinia, *Wound dressing based on electrospun PVA/chitosan/starch nanofibrous mats: Fabrication, antibacterial and cytocompatibility evaluation and in vitro healing assay.* International Journal of Biological Macromolecules, 2019. **122**: p. 238-254.
134. Augustine, R., et al., *Electrospun polyvinyl alcohol membranes incorporated with green synthesized silver nanoparticles for wound dressing applications.* Journal of Materials Science: Materials in Medicine, 2018. **29**(11): p. 163.
135. Fatahian, R., et al., *Fabrication of antibacterial and hemostatic electrospun PVA nanofibers for wound healing.* SN Applied Sciences, 2020. **2**(7): p. 1-7.
136. Hussein, Y., et al., *Electrospun PVA/hyaluronic acid/L-arginine nanofibers for wound healing applications: Nanofibers optimization and in vitro bioevaluation.* International Journal of Biological Macromolecules, 2020. **164**: p. 667-676.
137. Alberti, T.B., et al., *Electrospun PVA nanoscaffolds associated with propolis nanoparticles with wound healing activity.* Journal of Materials Science, 2020: p. 1-16.
138. Akbarzadeh, A., et al., *Liposome: classification, preparation, and applications.* Nanoscale research letters, 2013. **8**(1): p. 102-102.
139. McKee, M.G., et al., *Phospholipid Nonwoven Electrospun Membranes.* Science, 2006. **311**(5759): p. 353.
140. Shekarforoush, E., et al., *Electrospun Phospholipid Fibers as Micro-Encapsulation and Antioxidant Matrices.* Molecules (Basel, Switzerland), 2017. **22**(10): p. 1708.
141. de Freitas Zômpero, R.H., et al., *Hybrid encapsulation structures based on β-carotene-loaded nanoliposomes within electrospun fibers.* Colloids and Surfaces B: Biointerfaces, 2015. **134**: p. 475-482.
142. Yang, C., et al., *Electrospun pH-sensitive core–shell polymer nanocomposites fabricated using a tri-axial process.* Acta Biomaterialia, 2016. **35**: p. 77-86.
143. Hunley, M.T., et al., *Taking Advantage of Tailored Electrostatics and Complementary Hydrogen Bonding in the Design of Nanostructures for Biomedical Applications.* 2008. **270**(1): p. 1-7.
144. Yu, D.-G., et al., *Self-assembled liposomes from amphiphilic electrospun nanofibers.* Soft Matter, 2011. **7**(18): p. 8239-8247.
145. Mendes, A.C., et al., *Hybrid electrospun chitosan-phospholipids nanofibers for transdermal drug delivery.* International Journal of Pharmaceutics, 2016. **510**(1): p. 48-56.
146. Nada, A.A., et al., *Protection of conjugated linoleic acid into hydrophobic/hydrophilic electrospun fibers.* Journal of Drug Delivery Science and Technology, 2018. **44**: p. 482-490.

1.5 Research objectives

The overall aim of this project was to design, fabricate and examine PVA-based electrospun wound dressings containing birch bark extract with an additional potential to improve the wound healing process. The aims and objectives set at the beginning of this work can be summarised as:

- To study the interaction of the birch bark extract with hydrogenated phospholipids
- To develop a suitable workflow to produce o/w-colloidal dispersions containing the active substance birch bark dry extract stabilized using hydrogenated phospholipids.
- To develop a suitable processing methodology to produce TE-loaded/PVA structures by electrospinning
- To study the influence of the addition of colloidal dispersions into polymeric PVA matrix
- To study the combined effects of polymer and electrospinning associated variables on the structure of the electrospun fibers. Parameters such as-solution concentration, molecular weight, applied voltage, tip-to-collector distance and flow rate will be investigated.
- To evaluate betulin release from TE-loaded dressings through *ex-vivo* permeation and in vitro drug release studies. Investigation on the effect of adjusting constituents of colloidal dispersions and polymer molecular weight on drug release will also be included.
- To examine the efficacy of TE-loaded PVA electrospun wound dressings through *ex-vivo* wound healing assay

1.6 Thesis layout

This thesis is composed of 5 chapters:

1. Chapter 1 is an introduction underlining the motivation, significance, general basics and objectives of this work

2. Chapter 2 of this thesis represents a comprehensive literature review on electrospinning technology in biomedical applications. It introduces electrospinning technology and parameters affecting the electrospinning process. It also gives an overview of the recent advances in electrospinning design for areas like tissue engineering and drug delivery applications. Further, such a review will allow identification of potential polymeric biomaterials with properties such as biocompatibility, biodegradability and non-toxicity which are suitable for development of wound dressing materials. The review concludes with an illustration of possible challenges and future directions of electrospinning.

3. Chapter 3 of this thesis describes production of colloidal dispersions. Initially, a study on interfacial interaction of phospholipids together with the lipophilic components; triterpene extract and sunflower oil, was investigated through dynamic interfacial tension measurements using Profile Analysis Tensiometer. These interfacial rheological experiments might reveal the possible key role played by phospholipids at the interface. This chapter concludes with production of TE-loaded colloidal dispersions through a step-wise homogenization procedure using hydrogenated phospholipids as a stabilizer. Here, a full factorial design of experiment (DOE) was used to generate combinations of formulations. In particular, the influence of phospholipid composition and phospholipid-to-oil ratio towards the reduction of particle size was evaluated and optimized.

4. Chapter 4 of this thesis focuses on *ex-vivo* wound healing efficacy of electrospun wound dressings. It also provides a comparative analysis between low and high loaded TE-dressings, TE-oleogel, control and placebo. Further, a detailed analysis towards *ex-vivo* permeation and in vitro drug release was also undertaken.

5. Chapter 5 is where a novel methodology was established to produce nanofibrous mats containing TE-loaded colloidal dispersions optimized in chapter 3. Further work in this chapter involved influence of the three different PVA molecular weights (Mw 67,000, Mw 130,000 and Mw 146-186,000) in fabrication and characterization of TE-loaded electrospun fibers. The influence of PVA molecular weight towards the resulting rheological properties of polymer solutions and fiber morphologies was explored. In addition, physicochemical properties as well as in vitro drug release and *ex-vivo* permeation experiments were also assessed.

2 Chapter 2: Electrospun nanofibers for biomedical applications

Francis Kamau Mwiiri, Rolf Daniels

Department of Pharmacy, Eberhard Karls Universität Tübingen,

Tübingen, Germany

Reprinted with permission from Elsevier, Book Chapter 3, Pages 53-74, Delivery of Drugs, Volume 2: Expectations and Realities of Multifunctional Drug Delivery Systems, 2020

DOI: 10.1016/B978-0-12-817776-1.00003-1

2.1 Abstract

Electrospinning has been revolutionized as an efficient process to prepare nanofibers from polymer solutions. It is a highly scalable process with a range of parameters which can be tuned to affect the outcome of the fiber properties. Therefore, proper control of these parameters is necessary to achieve desired fiber morphologies and diameters. The resulting nanofibers have special features, such as high surface area to volume ratio and can form mats/fleeces with high porosity which makes them attractive for many applications, such as in air filtration, textile industry, drug delivery, tissue engineering, and wound healing. In this chapter, we will present a concise introduction of the electrospinning technique and its application in drug delivery, tissue engineering and wound healing. Other issues such as technology challenges, limitations, regulatory aspect and possible future trends are also discussed.

Keywords:

Electrospinning, Nanofibers, Drug delivery, Extracellular Matrix (ECM), Tissue engineering

2.2 Introduction

Electrospinning, as the name suggests, is a process by which nanofibers are generated from a polymer solution or melt in the presence of an electric field. It was known back in 1934 when A. Formhals patented this process describing the production of cellulose acetate based fibers using an acetone / alcohol solution as the solvent [1]. Thereafter, many researchers like Reneker and others especially in the 1990s stepped up further in using electrospinning technology to produce nanofibers and now we know that a wide range of polymers can be electrospun into nanofibers [2-8]. Since then, the technology has gained a lot of momentum and interest in the recent years and nowadays it is widely used to generate nanofibers for various applications from drug delivery to tissue engineering [9]. The electrospinning technique is a simple and versatile process for preparing fibers having a diameter from few micrometers down to several nanometers [10, 11]. Even preparing nanofibers below 1 nm seems to be possible [12]. Beyond that, the obtained nanofibers possess not only good mechanical properties but also exhibit unique properties, such as high surface area to volume ratio and are able to form mats with small pore sizes and high porosity [8]. Porous fibers can allow large drug loading, free drug diffusion, outstanding cell attachment, sufficient nutrients transport, and quick waste removal [13, 14]. These outstanding characteristics together with the structural similarity of electrospun fibers to native extracellular matrix (ECM) makes electrospun scaffolds perfect biomaterials to be used in tissue engineering, wound healing and other biomedical applications [15, 16]. The composition of ECM varies with the nature of tissues. The two most common constituents involve structural proteins e.g., collagens, elastins, fibronectins, and proteoglycans [17].

Polymers required to fabricate nanofibers intended for various biomedical applications including controlled drug release and tissue engineering should be biocompatible and biodegradable [18]. Such polymers are highly desired as biomaterials, since they are broken down, excreted, or are absorbed from the body after serving their intended purpose; therefore, a second surgery intervention for implant removal can be avoided. Generally, they should not be only biocompatible and biodegradable but also non-immunogenic, non-toxic, and non-mutagenic. In addition, these polymers undergo biodegradation by hydrolytic or enzymatic route [19, 20]. These polymers may be synthetic, (esters, amides, ethers, urethanes) or of natural kind (polysaccharides and proteins) [21]. The most popular natural polymers are such as collagen, gelatin, silk fibroin, chitosan and alginate whereas synthetic polymers include polyvinyl alcohol (PVA), poly(ε-caprolactone) (PCL). Polyglycolide (PGA), and polylactide (PLA) together with their copolymers, namely poly (lactic-co-glycolic acid) (PLGA) and Poly(l-lactide-co-ε-caprolactone) (P(LLA-CL)), have been already approved for clinical use by the FDA. These polymers allow to tailor the degradation kinetic by using either the homopolymers or copolymers with a distinct molar ratio of the monomers [19].

A wide variety of these polymers can also be used for 3D printing. Unlike in electrospinning, the polymers are not dissolved in a suitable solvent but are processed

by hot-melt extrusion technique, e.g., in fused in fused deposition modelling (FDM). This enables 3D printing to precisely produce scaffolds according to user-defined specifications of the overall geometric structures. In electrospinning, this is still a challenge to produce scaffolds with an exact shape and complex geometries [22]. However, through 3D printing it is only possible to produce fibers of micrometer range which does not mimic the ECM with low cell adhesion properties as compared to electrospun nanofibers. Three-dimensional-printed scaffolds exhibit good mechanical properties and hence can be combined with electrospun nanofibers to produce structures with an improved biological and mechanical function [23].

Different strategies have been used for incorporation of therapeutic agents into the electrospun scaffolds namely; blending, coaxial, emulsion, surface modification and electrospraying can be performed. These techniques enable successful integration of any drug, DNA, growth factors, cells and other bioactive molecules [24].

The selection of solvent used to dissolve a polymer in electrospinning is important since solvents interact differently with polymers. Here, the Hansen parameters can be utilized while searching for an appropriate solvent in electrospinning that could produce good quality fibers. These parameters which are related to the Hildebrand solubility, essentially divide the solubility into three components including polar interactions (δ_P), hydrogen bonding (δ_H), and dispersive or van der Waals interactions (δ_D) in a three-dimensional sphere system [25]. Furthermore, Hansen solubility parameters are widely used to predict material properties such as their affinity, encapsulation efficiency of drugs and in selection of good or poor solvents for polymers [26-28]. The dissolution of a polymer depends not only on the type of the solvent used but also the temperature and degree of polymerization [29]. It is good to note that, the issue of molecular weight is a major concern when it comes to polymer and active ingredient selection. Many physicochemical properties of polymers are influenced by the length of the polymer chain like viscosity, glass transition temperature, and mechanical strength. Higher molecular weight is generally preferred as there will be greater chain entanglement to facilitate the formation of fibers during spinning. However, at higher polymer concentrations, an excessive viscosity increase may cause difficulty in the electrospinning process. In contrast, lower molecular weight polymer solutions tend to break up into droplets or form beads. In this case, increasing the concentration may facilitate the formation of fibers without running into problems due to a too high viscosity. However, the spinnability of a polymer with the resulting fiber morphology should always be tested [30-32].

Machotova et al. investigated through electrospinning of styrene-ethyl acrylate copolymers the influence of polymer polarity and glass transition temperature (T_G) on fiber formation and hydrophobicity. They concluded that, by performing the electrospinning process at the temperatures above the polymer glass transition temperature, sticking of fibers may occur resulting to non-uniform fibers with increased diameters. The hydrophobic / hydrophilic character of the electrospun mats was also influenced by changing the polarity of the polymer and T_G [33]. On the other hand, the

molecular weight of the active ingredient and its acidity/basicity should also be taken into consideration in controlling release [34]. Hence, depending on the intended purpose of use and the active agent to be loaded, a careful polymer selection is needed as the final product will also be affected [16].

The objective of this chapter is to give a reader a quick overview of the recent advances in electrospinning design for tissue engineering, drug delivery, and other biomedical applications (Fig. 3.1). An overview of the processing variables and setups used to modulate scaffold architecture in the electrospinning process is provided. A summary of available electrospun products together with scaling up opportunities and regulatory aspects is also covered.

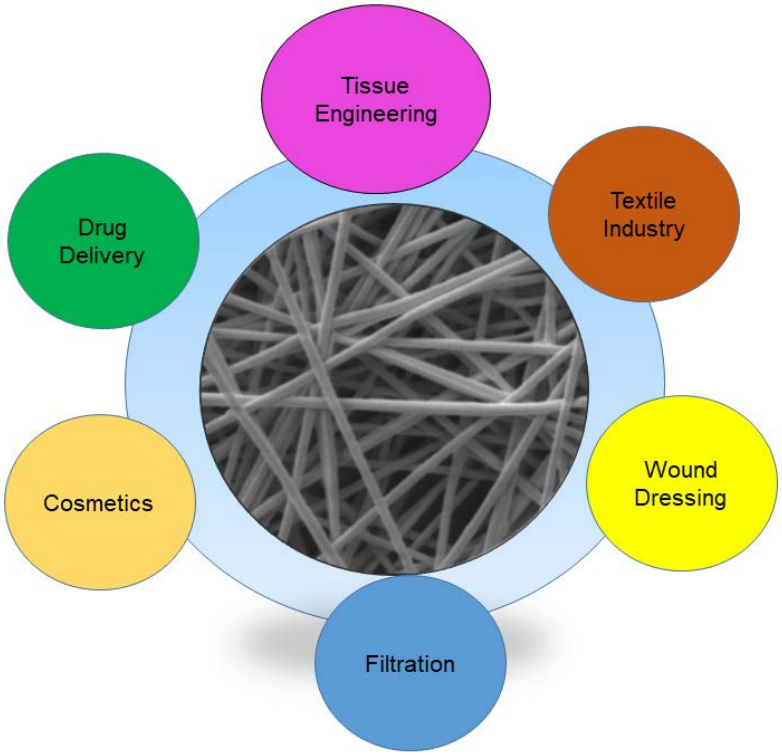

FIGURE 3.1. Diverse applications of electrospun nanofibers.

2.3 Electrospinning process and set up

Electrospinning occurs when high electric potential is applied to a pendant droplet of a starting polymer solution or melt to form a thin fiber. Precisely, the liquid is forced through a nozzle by a constant flow pump or pressurized gas, which initially forms a pendant drop at the nozzle tip. The drop is held there by its surface tension. An electrode from the high voltage supply is then directly attached to the nozzle of which blunt needles are most commonly used. The voltage supply is then turned on charging the polymer solution. The resulting electrical repulsion forces acting on the polymer solution causes the pendant droplet to deform into a conical shape which is also known as Taylor cone [35, 36]. When the voltage is increased, and a certain threshold is

reached, surface tension of the polymer solution is overcome, and a charged jet emerges from the Taylor cone migrating towards the collector. During its migration from the needle tip to the collector, the solvent from the jet evaporates quickly and the fibers are deposited over the grounded collector. As the jet travels towards the collector, it experiences stretching, bending and whipping favoured by repulsive charges existing along the jet [37, 38]. The resulting nanofiber mats are either in a nonwoven or aligned form depending on the type of the collector used.

The process of electrospinning is closely related to electrospraying although there is a marked difference in the morphology of the final product. The difference between the two processes is based on the concentration of the polymer solution. In electrospinning process, when the concentration of polymer concentration is high, provided that the resulting viscosity is optimal, there is elongation of a jet from the Taylor cone leading to fiber formation. On the other hand, if the polymer concentration is low, the jet is destabilized without elongation, and only fine droplets are formed [39].

In order to obtain nanofibers from a polymer solution, the electrospinning process as shown in Fig. 3.2 requires three major components: a high-voltage source, a pump providing a constant flow rate, e.g., a syringe pump on lab scale, and a collector which is normally grounded [5]. The voltage supply provides high electrical voltage to start the spinning process, a syringe pump holds a plastic or glass syringe with a needle attached to it and delivers the polymer solution at a constant flow rate throughout the electrospinning process. Deposition of formed fibers takes place at a collector. Fig. 3.3 shows formation of electrospun mat and its microscopic structure.

It is important to note that, the nozzle can be configured in either single or coaxial design and both are regarded as conventional approaches to process fibers in electrospinning. Single nozzle is the simplest used at laboratory level for ejecting single polymer solution out of the nozzle to form fibers. Coaxial design is an extension of single nozzle, where it has been modified to deliver two different liquids independently resulting in core-shell or hollow structured fibres [40] (Figs. 3.4 and 3.5). However, recent developments in electrospinning have led to needleless-electrospinning techniques e.g. use of rollers, discs, balls, bubbles, bearing the potential to produce nanofibers in large quantities including overcoming clogging issues faced with single nozzle electrospinning [41]. The major parameters affecting the outcome of fiber morphology are further explained below.

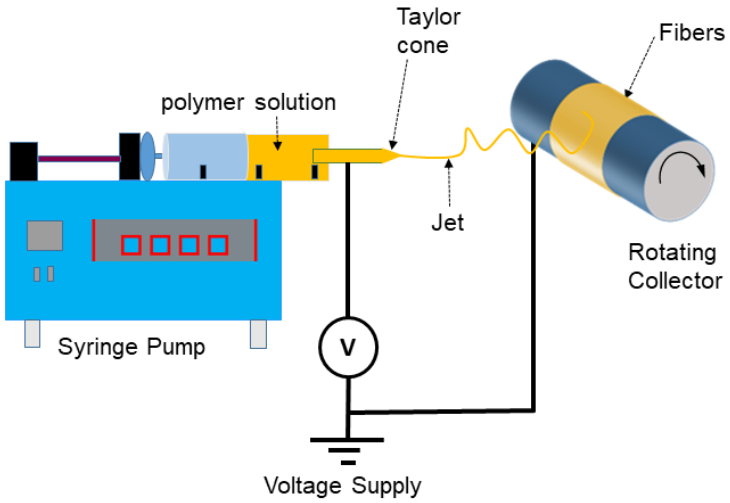

FIGURE 3.2. Single needle electrospinning set up.

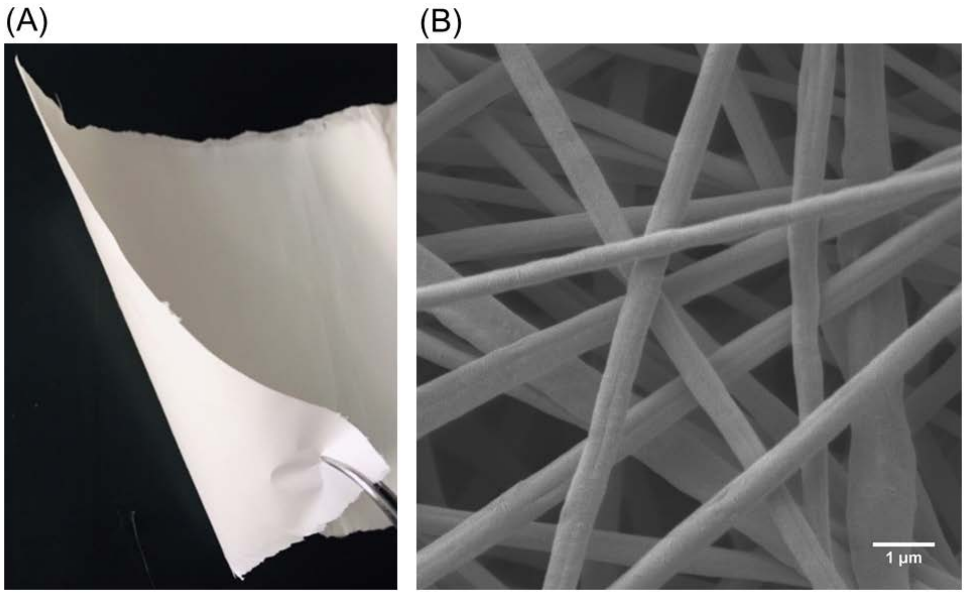

FIGURE 3.3. (A) Image of an electrospun fiber mat. (B) Scanning electron micrograph of electrospun Polyvinyl alcohol (PVA) fibers.

2.3.1 Process parameters

2.3.1.1 Voltage

A critical voltage value is the driving force needed for jet initiation and formation of nanofibers. An increase in the applied voltage leads to the formation of nanofibers with a smaller diameter due to the stretching of the electrospinning jet caused by increased charge repulsion. Further increase of voltage value causes high jet instability, resulting

in the formation of beaded nanofibers and poor fiber morphology [42, 43]. A typical voltage in electro-spinning ranges from 5 to 50 kV [44].

2.3.1.2 Flow rate

The feed rate of the polymer solution significantly effects fiber morphology and optimal flow rate is needed to obtain uniform nanofibers. High feed rates result in poor fiber morphology formation with beads. For instance, uniform nanofibers of polystyrene could be formed at 0.5 mL/hr, while increasing the flow rate to 1.5 mL/hr led to the formation of beaded nanofibers with flattened web-like structures. This is due to incomplete drying of the nanofibers in the space between the needle and the collector at high flow rates [45]. Also, increasing feed rate increases the mean fiber diameter [42].

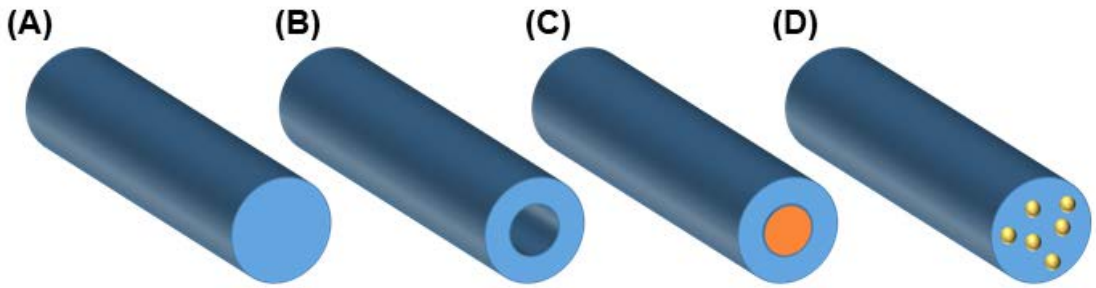

FIGURE 3.4. Morphology of electrospun fibers as drug-delivery systems from different approaches. (A) blend electrospinning; (B) hollow and (C) core-shell fibers through coaxial electrospinning; (D) emulsion electrospinning.

2.3.1.3 Collector

Electrospun fibers can be collected using a wide variety of collectors, mainly consisting of stationary or rotating platforms. These collectors will affect the final design of the electrospun fibers. Random or nonwoven fibers can be collected while using a plate collector whereas more aligned fibers are obtained with a rotating drum collector (mandrel). When using a rotating collector, the fiber diameter can be influenced by the circumferential speed of the collector. With increasing speed higher stretching forces are evolved which elongate the fibers and make them thinner. Motamedi et al. were able to collect polyvinylidine fluoride (PVDF) aligned fibers with decreasing mean fiber diameter by increasing the rotating collector speed from 1000 to 2500 rpm [42].

2.3.1.4 Nozzle tip-to-collector distance

The separating distance between nozzle tip and collector dictates the evaporation rate and deposition time of the electrospinning jet. When the spinning distance decreases to a critical length, poor fiber morphology with beads can be observed due to insufficient fiber stretching and solvent evaporation. Increasing the spinning distance provides a larger space for jet stretching and longer time for solvent evaporation from

the fibers and uniform fibers with thinner diameters can be formed [42, 43]. Shen et al. using melt-electrospinning of polypropylene fibers found out that if the distance between nozzle tip and collector is too long (> 8 cm) the strength of electric field weakens, resulting in the increase of fiber diameter [46]. Also, when the collector is kept too far away from the nozzle tip, a decrease or fail in fiber collection can occur [47].

2.3.1.5 Polymeric solution

It is reported that polymer solutions depending upon the molecular weights and concentration used, exhibit different electrospinnability, a good electrospinnability is directly related to optimum viscosity of polymeric solution. Usually at very low polymer concentration, the viscosity of the solution is low and not enough for polymer entanglements and fiber formation which results in electrospraying instead of electrospinning. Therefore, polymer viscosity plays a crucial role on the morphology of electrospun nanofibers where low viscosity results in the formation of beaded structures and increased viscosity leads to the formation of smooth bead free nanofibers. However, too high viscosity of polymer solution clogs the nozzle tip without fiber formation. Also, the conductivity of the polymer solution seems to affect the diameter of the electrospun nanofibers. Increased conductivity (> 0.55 mS/cm) induces higher stretching of the jet; which lead to a smaller diameter nanofiber [43].

The above-described parameters signify that the whole electrospinning process is a highly adjustable process. Thus, electrospinning process provides an opportunity for easy or free control over fiber diameter, morphology, surface characteristics, porosity and ease of getting fiber diameter in nanometer range. It is noteworthy that each polymer has an optimal working space taking into account both solution and process parameters in which it can be electrospun. Therefore, it is not possible to make a general recommendation for example for particular molecular weights / concentrations, flow rate, voltage, distance, and the resulting fiber morphology and diameter, because the optimal values of these parameters vary considerably with the polymer and solvent used. Hence, a critical optimization of both solution and process parameters is vital in order to achieve desirable fiber specifications beside a proper polymer selection [48] (Table 3.1).

TABLE 3.1 Some of the electrospun polymers and their parameters.

Polymer and Solvent type	Molecular weight	Electrospinning parameters	References
Collagen/PLGA, 1,1,1,3,3-hexafluoro-2-propanol (HFP)	90,000–126,000 Da	Collector distance: 17 cm, flow rate: 1 mL/h, voltage:29 kV	[49]
PVA, Water	89,000-98,000, ~125,000, 146,000-186,000 g/mol	Collector distance: 15 cm, flow rate: 0.5 mL/h, voltage:12, 15, 18 kV	[50]
PCL, HFP	~120,000–300,000 g/mol	Collector distance: 15 cm, flow rate: 0.8 mL/h, voltage:20 kV	[51]
PLA, chloroform:N, N-dimethylacetamide (DMAc): (80:20)	200,000 g/mol	Collector distance: 12 cm, flow rate: 1 mL/h, voltage:11 kV	[52]

2.4 Drug delivery applications

2.4.1 Electrospun fibers as drug-delivery systems

Electrospun fibers in drug delivery applications are administered mainly via oral, and topical routes or as implantable devices [53, 54]. Both natural and synthetic polymers have been widely used in the development of drug nanofibers as drug carriers to enable the release of drug in a controlled manner over a desired period (Table 3.2). Due to their characteristics like degradability, high porosity, high surface area-to-volume ratio of the fibers can be efficient in some processes, such as cell binding and proliferation, high drug loading, and mass transfer processes. Many drugs ranging from antimicrobials and anticancer drugs to bioactive molecules like DNA and RNA, proteins and other active agents have been incorporated into nanofibers producing drug delivery systems for various therapeutic applications [55].

TABLE 3.2 Electrospun drug-loaded nanofibers in drug-delivery applications.

Route	Drug incorporated	Polymer	References
Oral	Ofloxacin/gellan	PVA	[56]
	Ondansetron hydrochloride	PVA	[57]
	Ibuprofen/carvedilol	PCL	[58]
	Ibuprofen	Polyvinylpyrrolidone (PVP)	[59]
	Caffeine/riboflavin	PVA	[60]
	Donepezil HCl	PVA	[61]
	Clobetasol-17-propionate	Eudragit RS100 / PVP / PEO	[62]
	Salmon calcitonin (SCT)	Sodium alginate / PVA	[63]
Dermal	Ciprofloxacin.HCl	PVA / Chitosan / PCL	[64]
	Ketoprofen (KP)	PVA / Poly(acrylic acid) / Multi-walled carbon nanotubes (MWCNTs)	[65]
	Asiaticoside (AC)	Cellulose acetate	[66]
	Vitamin A acid/ Vitamin E	Cellulose acetate	[67]
	Meloxicam	PVA	[68]
	Curcumin/diclofenac/vitamin B12	Chitosan/phospholipids	[69]
	Tetracycline hydrochloride/phenytoin sodium	Cellulose acetate /PVA	[70]
Other implants	Collagen/salicylic acid (SA)	PVA	[71]
	Amoxicillin	Polyethylene glycol (PEG)/PLGA	[72]
	Cefradine/5-fluorouracil	PLGA/Gelatin	[73]
	Doxorubicin	PLA	[74]
	Paclitaxel	Polyurethane(PU) /Eudragit® L100-55	[75]

Several techniques are illustrated in the literature for drug incorporation using electrospinning devices, include blending, coaxial, emulsion, and surface modification. With these methods, drugs can either be attached to the fiber surface or encapsulated into the fiber core. And every technique has its own merits and demerits since not all drugs can be loaded with any method, the approach used heavily relies on the drug's physicochemical properties, intended application, polymeric characteristics, and the expected drug release rate [76, 77].

During blending technique, the active agent is mixed with polymer solution prior to electrospinning. Here, hydrophobic-hydrophilic properties of drug and polymer should always be thought-about. Mostly, issues of initial burst release of drugs from electrospun fibers is observed. This can be reduced through different combinations of hydrophilic and hydrophobic polymers or by use of emulsion and coaxial electrospinning method [76, 77]. Surface modification ensures that therapeutic agents are bound to the fiber surfaces. This can be for example used for gene or growth factor delivery. Electrospraying has been for example applied to load bioactive nanoparticles into electrospun scaffolds [77, 78].

Electrospinning using a coaxial nozzle design allows the production of core–shell structured nanofibers. The Coaxial process involves creating a drug loaded core which is sheathed by a drug-free (or drug-containing) polymer shell. In most cases, drugs sandwiched inside will be initially protected from environmental factors, such as the solvents used for electrospinning. Also, since the drug is encapsulated within the core portion of a nanofiber, a long-lasting biological stability can be achieved. Therefore, it gives a possibility to encapsulate and protect environmental or stress sensitive compounds like proteins [79, 80]. The release mode and kinetics of compounds from the inner core can be adjusted by controlling shell properties such as thickness and biodegradability [81].

Lastly, emulsion electrospinning is an efficient method to encapsulate drugs into the nanofibers (Table 3.3). With the help of two types of emulsions; oil-in-water (O/W) and water-in-oil (W/O), it is possible to manufacture nanofibers containing small drug enriched compartments and to modulate drug release rate by regulating the oil and water phase of the emulsions. Surfactants e.g., phospholipids play a key role for production of emulsions aiming to produce stable sub-micron sized droplet which are vital for encapsulation including proper stabilization in the polymeric system. Use of W/O emulsion electrospinning could improve the release of hydrophilic drugs, whereas, with O/W emulsions, encapsulation of lipophilic components to electrospun fiber can be useful [82].

TABLE 3.3 Applications of the emulsion electrospinning technique.

Application	Electrospun material	References
Wound dressing	PCL/hyaluronan/epidermal growth factor	[83]
	Ketoprofen/PCL/gelatin	[84]
	Human Epidermal Growth Factor (rhEGF) and Aloe vera/PLGA	[85]
	Gentamicin sulfate/metronidazole/PLA	[86]
Tissue engineering	PLGA/Chitosan/PVA	[87]
	Cefradine/5-fluorouracil/PLGA/Gelatin	[73]
	Hydroxyapatite/laminin/PLCL	[88]
	Alginate/PLA	[89]
	Silk Fibroin/PCL	[90]
Drug delivery	Metformin-hydrochloride/metoprolol tartrate/PCL/Poly(3-hydroxybutyric acid-co-3-hydroxyvaleric acid (PHBV)	[91]
	Phytoncide/PVA	[92]
	Doxorubicin hydrochloride /PEG-PLLA	[93]

Recent advances have seen smart nanofibers being developed as stimuli-responsive electrospun nanofibers for controlled release. Such stimuli can include pH, enzymes, oxidative stress, temperature, light and electric or magnetic fields. The idea here is to trigger the release of therapeutic agents at the targeted site by means of these stimuli [54, 94]. General mechanisms of drug release are found to be diffusion, desorption, matrix degradation / erosion, and swelling which is dependent on the nature of the polymer system used for delivery including the geometry of nanofibers. For example, fibers of smaller diameter exhibit faster drug release compared to fibers with larger diameters [95-97]. In most cases, based on the drug release profile, initial burst release process followed by a drug diffusion manner can be observed.

2.4.2 Needleless foam electrospinning

Several foam electrospinning techniques have been used to manufacture foam-based electrospun nanofibers apart from the commonly used nozzle-based electrospinning method. A new approach of needleless electrospinning involves utilizing foams to produce nanofibers was performed by Higham et al. [51]. They were using PVA and polyethylene oxide (PEO) solutions. They fed compressed carbon dioxide gas into polymer solutions through a fritted funnel. Upon immersion of a copper electrode coupled with a high voltage supply into the polymer solution, foam formation on the surface occurs and once the electric force is applied, jets are formed migrating towards the collector to form the nanofibers. This technique not only overcome the clogging problems encountered on the needle tip during electrospinning as the solvent evaporates, but also improves the production rate of fibers [98]. Furthermore, an addition of non-ionic surfactants e.g. Triton X-100 in small concentrations (0.01-0.1 wt.%) to electrospinnable solutions can improve foam formation, without negatively affecting the desired fiber morphology. In fact, syringe electrospinning and foam electrospinning have shown a relationship when it comes to electrospinnability of polymer solutions and the resulting fiber morphology. This suggests that optimal process and solution parameters found to electrospun fibers through syringe electrospinning can also be employed to deliver the same results via foam electrospinning [98].

Also, Sidaravicius et al. used this foam electrospinning principle to test electrospinnability of aqueous polymer solutions [99]. Ahirwal et al. developed PCL based 3D-cm thick foams with high porosity through the honeycomb self-organization of nanofibers and these foams could be ideal materials for tissue engineering applications [100].

Other nanofiber-based foams can be developed via freezing method by first producing a membrane through electrospinning. For instance, Si et al. 2014 constructed a foam by first cutting small pieces of polyacrylonitrile/benzoxazine (PAN/BA-a) and SiO2 electrospun membranes in water/tert-butanol mixture to form a dispersion and further freeze dried to a foam which can be used for various applications [101]. In general, nanofibers-based foams have been rarely used in drug delivery applications. However, Svagan et al. in 2016, successfully developed cellulose nanofiber (CNF)-based foam materials with a model drug riboflavin and a prolonged drug release was observed. Such materials could be useful in gastroretentive drug delivery [102].

2.4.3 Nanofibers impregnated with nanoparticles

Nanoparticles have particle sizes ranging from 100 to 500 nm [103]. Several methods like emulsification-solvent evaporation have been extensively applied to prepare such nanoparticles [104]. Nanoparticles in drug delivery come with advantages, such as they enhance the solubility of hydrophobic drugs, increase the physiochemical stability of therapeutic agents, can be used to modulate drug release rate, and improve the

bioavailability of therapeutic agents [105]. Recently, incorporation of nanoparticles (NPs) within electrospun fibres has emerged as one of most interesting research topics in the field of electrospinning. When these nanoparticles are combined with nanofibers, we can potentially maximise the effective functional output from nanoparticles as we widen the scope use of nanofibers in the field of pharmacy and medical devices. Silver nanoparticles have been widely incorporated into electrospun nanofibers by many researchers for antimicrobial applications and wound healing [106-108]. Nie and Wang in 2007 successfully prepared DNA/chitosan nanoparticles and PLGA/HAp composite scaffold for bone tissue engineering. This scaffold showed higher cell attachment, greater cell viability and improved DNA transfection efficiency in human marrow stem cells (hMSCs) [109]. Furthermore, it is also possible to load anticancer drugs e.g. Kim, Ebara and Aoyagi in 2013 electrospun the fibers from a solution of the polymer poly (NIPAAm-co-HMAAm, a copolymer of N-Isopropylacrylamide and N-hydroxymethylacrylamide) mixed with a solution of magnetic nanoparticles and doxorubicin. Using this scaffold, they effectively demonstrated of killing cancer cells, the human melanoma [110].

2.4.4 Wound dressings

Based on the nature of the healing process, wounds can be classified as acute or chronic wounds. Acute wounds include, mechanical injuries caused by knives, gun shots and surgical wounds including burns and chemical injuries. Acute wounds usually take short period (8-12 weeks) to heal completely, whereas chronic wounds such as those from diabetes ulcers, decubitis ulcers heal slowly and take beyond 12 weeks to recover [111]. Electrospun nanofibers have unique properties, such as high porosity, high encapsulation efficiency, and high surface-area-to-volume ratio, and thus high drug loading. These features make electrospun mats perfect materials for wound dressing. Besides mimicking the native extracellular matrix of human tissues, their high surface area and high porosity allow efficient gaseous exchange including removal of exudate, and they also act as a physical barrier against entry of microorganisms while preventing dehydration during wound healing [19, 112-114]. Many wound dressings based on electrospun fibrous mats have been developed and loaded with diverse active ingredients (Table 3.4) [85, 111, 115]. In particular, the incorporation of active ingredients with antibacterial properties in the electrospun wound dressing would prevent infection of the wound and accelerates the healing process. However, some of them have been reported to show adverse effects like allergic contact dermatitis [69] and use of dressings loaded with antibiotics has risk of developing antimicrobial resistance [70].

Table 3.4 Electrospun nanofibers used in wound dressing applications.

Application	Electrospun Scaffold	References
Wound dressing	Sodium alginate /PVA/moxifloxacin hydrochloride (MH)	[116]
	Gelatin/keratin/PVA	[117]
	PCL/PVA/curcumin (CU)	[118]
	Chitosan (CS)/PVA/ Ampicillin	[119]
	PVA/ zein nanoparticles (NPs)/diclofenac (DLF)	[120]
	Chitosan/silver-NPs/PVA	[121]
	PVA/Chitosan/Tetracycline hydrochloride	[122]
	PVA/Soursop Leaves Extract (SLE)	[123]
	Silk fibroin/gelatin	[124]
	Hyaluronic Acid/PLGA	[125]
	PLA/Ag NPs/ Momordica charantia fruit extract	[126]
	PLA-Hyperbranched polyglycerol/ curcumin	[126]
	Spirulina extract-alginate PCL	[127]
	Collagen/ Silver nanoparticles (AgNPs)	[128]
	PLGA/metformin	[129]

Moreover, frequent dressing changes have to be avoided as this causes a lot of pain and trauma to patients, damage to new sensitive epithelial cells and even affecting the wound healing pattern. These problems can be solved by careful selection of the ingredients especially with respect to the irritation and sensitization potential. Moreover, polymers with good biocompatibility and which are biodegradable should be preferred as they do not require an invasive and / or traumatic intervention for dressing removal. In wound treatment, an initial burst release frequently observed from release profiles of drug loaded nanofibers could be of great importance; if for example the drug has antimicrobial and/or anti-inflammatory properties, it can provide immediate relief, while a subsequent slow release of drug prevents reinfection [111, 130]. Furthermore, sustained drug release also supports less frequent dressing changes and could thus improve patient compliance. Therefore, the main goal should be to develop an electrospun wound dressing with less or free of adverse effects suitable for human use with effective wound therapy even after long term usage. To this end, in our

laboratories we have developed a bioactive PVA based electrospun wound dressing through emulsion electrospinning containing birch bark extract, an active ingredient clinically proven to improve wound healing [131, 132].

2.5 Tissue engineering

2.5.1 Biomimetic scaffolds

The goal of tissue engineering (TE) in regenerative medicine is to use cells, biomaterials, and bioactive molecules such as growth factors to restore or replace damaged human tissues or organs. Hence, suitable scaffolds for tissue engineering applications should be biodegradable, biocompatible, nontoxic, non-mutagenic, and nonimmunogenic [20]. Biodegradability is very important and ideally the scaffold should degrade within the same period of time as it is replaced with newly regenerated tissues. Natural tissue consists of a structural component, the ECM, and other tissue-specific cells that occupy it. Electrospun scaffolds aims to resemble the natural tissue as closely as possible so that they can serve as a perfect material for cell regeneration. For this purpose, electrospun based polymeric scaffolds play a vital role in tissue engineering through cell seeding, proliferation followed by new tissue formation. Another advantage of electrospun nanofiber scaffolds is that their morphology can be modified by controlling the electrospinning parameters to obtain the architecture that best fits the intended application. Studies have shown that electrospun fibrous scaffolds with aligned fibers both in vitro and in vivo to enhance better cell migration and differentiation as they tend to mimic ECM well compared to other forms of scaffolds [14, 133]. In addition, nanofiber sheets can be formed into almost any shape e.g. tubes based on the site of desired implantation [134]. Through electrospinning, many researchers have utilized a variety of biocompatible synthetic and natural polymers to produce electrospun products, such as vascular grafts including bone grafts for tissue engineering.

2.5.2 Bone scaffolds

Bone matrix mainly consists of aligned collagen and hydroxyapatite materials which gives bone its balance of stiffness, strength and toughness [135]. The versatility of electrospinning has enabled many researchers to investigate various ways of manufacturing scaffolds for bone healing and repair. An ideal material must be biocompatible and bioactive to be able to initiate osteogenesis, and eventually lead to bone repair [136]. Several research groups have utilized electrospun scaffolds to develop bone grafts by incorporating bioactive substances to assist proliferation and mineralization of osteoblasts, enhancing bone regeneration. For example, Abdal-hay et al. used scaffolds of polyamide 6 nanofibers and coated them with hydroxyapatite (HA). An in vitro culture test revealed that HA-Polyamide nanofibers showed good biocompatibility and faster cell growth and proliferation compared to pristine scaffolds [137].

In addition, both natural and synthetic polymers have been used to design scaffolds in bone tissue engineering (Table 3.5). Studies have also shown that natural polymers like chitosan that exhibit weak mechanical properties but with excellent bioactivity can be combined with other synthetic polymers, e.g., PCL, to produce bone grafts with both improved physical and biological characteristics. Numerous studies combined biodegradable synthetic polymers like PGA, PLA, PLGA and PCL, PVA with stem cells, e.g., bone marrow-derived mesenchymal stem cells (BM-MSCs) and osteoblasts and obtained excellent bone scaffolds [136, 138-141]. Lim et al. demonstrated that alignment of fibers influences bone cell growth behaviour as they favoured more mesenchymal stem cells (MSCs) proliferation than random-oriented fibers [142]. Moreover, physicochemical properties including porosity, pore geometry, surface chemistry as well as biological and mechanical properties have been found to be important parameters when designing a bone scaffold [138].

TABLE 3.5 Electrospun nanofibers used in various biomedical applications.

Application	Electrospun Scaffold	References
Tissue engineering:	PCL/collagen (type I)	[143]
	Gelatin/PCL and collagen/PLCL	[144]
	Chitosan/PCL	[145]
vascular grafts	Tecophilic/gelatin	[146]
	PLA/PCL	[147]
	PLGA/smooth muscle cells (SMCs) and endothelial cells (ECs)	[148]
Bone grafts	Cellulose/nano-hydroxyapatite	[149]
	PCL/octacalcium phosphate	[141]
	Silk fibroin/bone morphogenetic protein 2 (BMP-2)/ hydroxyapatite	[150]
	PLGA/nHA/insulin	[151]
	PCL/carboxymethyl chitosan (PCL/CMC)	[152]
	Nanohydroxyapatite/ cellulose nanofibers/PVA (nHAp/CNF/ PVA)	[140]

2.6 Scaling-up and electrospun-based commercial products

The use of biocompatible polymers in the biomedical sector has promoted the production of electrospinning-based artificial tissue and the development of drug-delivery systems. However, the single nozzle electrospinning approach is a simple way to produce nanofibers on lab scale but with low production rates. Usually, it is only possible to process up to several liters of polymer solution under constant runs. Therefore it is only useful in academic research and product development where majority of the experiments are performed under few millilitres [153]. In order to economically and efficiently manufacture fibers in large scale needed in commercial applications, strategies for scaling up the process of electrospinning are required. This has led to development of new equipment and technological solutions with many electrospun materials paving their way to commercialization.

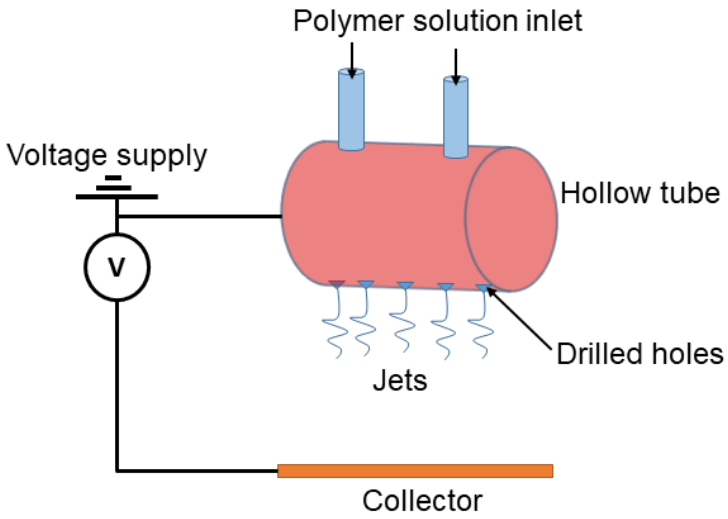

FIGURE 3.5. Multiple-hole electrospinning technique using a hollow tube [154].

New emerging companies are dedicated to supply electrospinning equipment from laboratory level to industrial scale or even offering services such as supplying nanofibrous products. Even contract manufacturing companies are already in the market offering electrospinning services. To increase the production rate of fibers, multi-spinneret components have been employed where the polymer injection system has been modified. Other techniques for manufacturing of nanofibers in large scale include, use of needleless electrospinning systems, e.g., rotating disks, rollers, balls and bubbles and centrifugal spinning [155, 156].

For example, the Nanospider developed by the Czech company Elmarco and Nanospinner416 from Inovenso Ltd., INFL8100 by FNM company and Yflow from Spain have been developed as industrial-scale instruments.

Nanospider technology, for example, is a needle-free high voltage electrospinning process. The principle behind this technology is, that Taylor cones, and the subsequent jet formation, occur from a thin film of a polymer solution (Fig. 3.6).

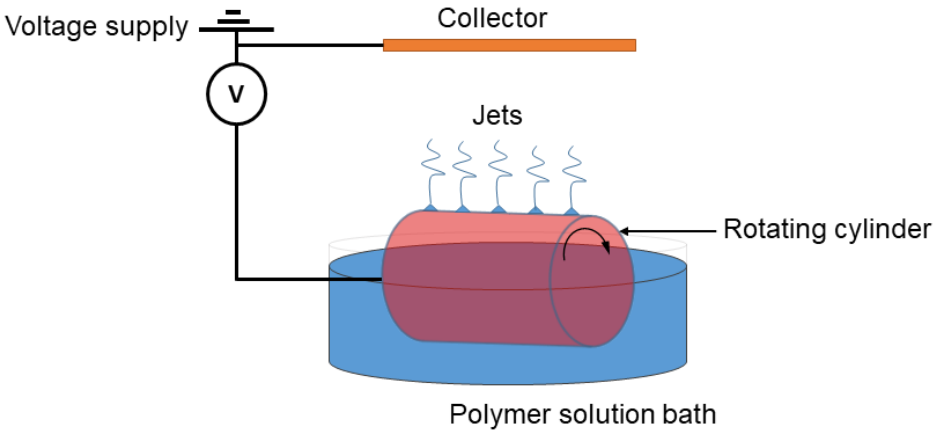

FIGURE 3.6. Schematic diagram of rotating cylinder electrospinning method (Nanospider) [157].

By utilizing such production lines, nanofibers can be produced at large scale level while cutting off high production costs. Table 3.6 summarizes a few electrospinning-based companies and their developed biomedical products.

TABLE 3.6 List of electrospun-applied commercial products in biomedical applications.

Product	**Company**	**Country**	**Application**
RIVELIN patch	Bioinicia	Spain	Drug delivery
PK Papyrus	Biotronik	Germany	Covered stent
ReDura dura patch	Medprin	Germany	Duraplasty
Nanofiber scaffolds	Stellenbosch (SNC)	South Africa	biomedical
Scaffolds for tissue regeneration	The electrospinning company	United Kingdom	biomedical
Antimicrobial Dressings	PolyRemedy	United States	Wound care
AVflo™ vascular graft	Nicast	Israel	biomedical
ReBOSSIS	Ortho Rebirth	Japan	Biomedical, synthetic bone

2.7 Regulatory aspects

The primarily goal of the International Organization for Standardization (ISO) is to ensure that products and services for the consumer are safe, reliable and of good quality. Electrospun-based products meant for biomedical applications, and depending on their intended use, are highly regulated or controlled using different international standards. Therefore, electrospinning companies across the globe should acquire and harmonize with these regulatory requirements to help them design, develop, manufacture and supply scaffolds meant for biomedical applications. ISO 9001 and ISO 13485 are two important guidelines for medical device manufacturers. Both are revised every five years and have been recently updated to ISO 9001:2015 and ISO 13485:2016 [158].

ISO 13485 is the most commonly adhered to standard for the efficient production of the intended medical device. ISO 13485 certification adapts ISO 9001 model except that this is specifically for medical device. ISO 13485:2016 as the latest standard contains requirements for a quality management system whereby a company can produce medical devices and services that are consistent with consumer safety and ensuring that applicable regulations are adhered to. It deals with all aspects of the device such as product development, risk management, complains, labelling and manufacturing [159, 160].

In addition, there are specific standards and guidelines dealing with compatibility and safety requirements for the medical device that comes into direct contact with the body. For this matter, ISO 10993 is used which covers biological evaluation of medical devices. Several testing such as cytotoxicity, implantation, genotoxicity, irritation and skin sensitization, carcinogenicity, biodegradation, etc. are carried out under the regulations of Good Laboratory Practice upon registration through regulatory authorities like FDA and the European union (EU) [161]. If the medical device is an electrical system, it should satisfy International Electrotechnical Commission (IEC) 60601 requirements [162].

2.8 Possible challenges and future directions

Electrospinning has been fully recognized as a simple way to produce (drug eluting) wound dressings and scaffolds for biomedical applications because of their special characteristics and that it has an enormous potential for innovative drug delivery systems. Despite the tremendous advances seen in this field in the last decade, there are still some challenges encountered while developing electrospun products. It remains a challenge to overcome clogging of spinneret during fiber preparation with needle-based systems. Low production rates are limiting when scaffolds for biomedical applications have to be produced in larger amounts. Nevertheless, single-needle electrospinning will remain beneficial to many researchers especially in the academic area, for example, to preinvestigate the behaviour and electrospinnability of a polymer. Thanks to the current advances in the industry, for example by use of needleless electrospinning devices, it renders possible to produce scaffolds at large scale level. However, more work is necessary to evaluate the morphology and performance of the nanofibers produced using the large-scale equipment and for ensuring consistent fiber quality is guaranteed throughout.

Another challenge is the frequent use of organic solvents, of which most of them are toxic and harmful to humans limiting the use of electrospun products. Current advances in electrospinning technology has also brought the emergence of green electrospinning. Use of degradable materials, green solution electrospinning, and solvent-free electrospinning are concepts revolving around green electrospinning. The idea here is to use raw materials which are not only biodegradable but also friendly to our environment, e.g., a solvent which is nontoxic and pollution-free [163]. Furthermore, the residual solvent in the fibers may not only restrict many promising potential applications, especially in biomedical field, but also removal of solvent residues from nanofibers and the corresponding analytic are very costly. Within this context, green electrospinning for example by use of water as the solvent, enables electrospun products to be further used in the biomedical field, such as tissue engineering, wound healing, and drug delivery, without any obstacles, since there is no organic solvent residue in the nanofibers. This could enhance a low-cost production and easier commercialization of electrospun-based biomedical products that are not only eco-friendly but also widely acceptable.

One of the challenges that needs to be further investigated is the ability of electrospun scaffolds to recreate the complexity of the human tissues. The development of scaffolds going forward for wound-healing therapies will need to address these issues of creating an environment that closely resembles that of native skin, where materials in the future should mimic the dermis in terms of their structure as well as it’s biological function. Moreover, drug-eluting wound dressings should be able to deliver several drugs in a time dependant manner to set the stage for an enhancement of the subsequent phases of wound healing. Nevertheless, use of scaffolds, for example, in tissue engineering will remain helpful when it comes to biomedical research, especially when testing new drug formulations. Although most of the biodegradable polymers

have been already approved by the FDA for clinical use, in vivo stability, degradation rate and more extensive toxicity studies should be undertaken, especially on humans, in the future for the electrospun products to be clinically approved.

When it comes to large-scale production, it seems to be still challenging to repeatedly produce complex electrospun scaffolds with precise dimensions and morphology as each polymer will likely respond differently to the control system. Hence, careful selection of correct polymer / solvent combination including proper manipulation of process parameters, such as flow rate and the electrical field between Taylor cone and collector, is needed.

Studies involving smart electrospun nanofibers, their advantages, and shortcomings, should be further investigated, especially in drug delivery, to come up with more interesting electrospun products.

Overall, with the ongoing significant developments and with what have already occurred so far, the future of electrospinning technology in both biomedical and pharmaceutical field is bright, and more innovations will continue to evolve.

2.9 References

1. Formhals, A., *Process and apparatus for preparing artificial threads.* US Patent No. 1,975,504, 1934.
2. Jaeger, R., et al., *Electrospinning of ultra-thin polymer fibers.* Macromolecular Symposia, 1998. **127**(1): p. 141-150.
3. Panda, P. and B. Sahoo, *Synthesis and applications of electrospun nanofibers—A review.* Nanotechnology, 1990. **1**: p. 399-416.
4. Dzenis, Y.A. and D. Reneker, *Polymer hybrid nano/micro composites*. 1994, Technomic Publishing Co., Inc., Lancaster, PA (United States).
5. Doshi, J. and D.H. Reneker, *Electrospinning process and applications of electrospun fibers.* Journal of Electrostatics, 1995. **35**(2): p. 151-160.
6. Fang, X. and D. Reneker, *DNA fibers by electrospinning.* Journal of Macromolecular Science, Part B: Physics, 1997. **36**(2): p. 169-173.
7. Kim, J.s. and D.H. Reneker, *Mechanical properties of composites using ultrafine electrospun fibers.* Polymer composites, 1999. **20**(1): p. 124-131.
8. Huang, Z.-M., et al., *A review on polymer nanofibers by electrospinning and their applications in nanocomposites.* Composites Science and Technology, 2003. **63**(15): p. 2223-2253.
9. Thenmozhi, S., et al., *Electrospun nanofibers: New generation materials for advanced applications.* Materials Science and Engineering: B, 2017. **217**: p. 36-48.
10. El-hadi, A.M. and F.Y. Al-Jabri, *Influence of Electrospinning Parameters on Fiber Diameter and Mechanical Properties of Poly(3-Hydroxybutyrate) (PHB) and Polyanilines (PANI) Blends.* Polymers, 2016. **8**(3): p. 97.
11. Reneker, D.H. and I. Chun, *Nanometre diameter fibres of polymer, produced by electrospinning.* Nanotechnology, 1996. **7**(3): p. 216-223.
12. Jian, S., et al., *Nanofibers with diameter below one nanometer from electrospinning.* RSC Advances, 2018. **8**(9): p. 4794-4802.
13. Lee, J.B., et al., *Highly porous electrospun nanofibers enhanced by ultrasonication for improved cellular infiltration.* Tissue Engineering Part A, 2011. **17**(21-22): p. 2695-2702.
14. Wang, X., B. Ding, and B. Li, *Biomimetic electrospun nanofibrous structures for tissue engineering.* Materials Today, 2013. **16**(6): p. 229-241.
15. Al-Enizi, A.M., M.M. Zagho, and A.A. Elzatahry, *Polymer-Based Electrospun Nanofibers for Biomedical Applications.* Nanomaterials (Basel, Switzerland), 2018. **8**(4): p. 259.
16. Thakkar, S. and M. Misra, *Electrospun polymeric nanofibers: New horizons in drug delivery.* European Journal of Pharmaceutical Sciences, 2017. **107**: p. 148-167.
17. Frantz, C., K.M. Stewart, and V.M. Weaver, *The extracellular matrix at a glance.* Journal of cell science, 2010. **123**(Pt 24): p. 4195-4200.
18. Tian, H., et al., *Biodegradable synthetic polymers: Preparation, functionalization and biomedical application.* Progress in Polymer Science, 2012. **37**(2): p. 237-280.
19. Kai, D., S.S. Liow, and X.J. Loh, *Biodegradable polymers for electrospinning: Towards biomedical applications.* Materials Science and Engineering: C, 2014. **45**: p. 659-670.
20. Asghari, F., et al., *Biodegradable and biocompatible polymers for tissue engineering application: a review.* Artificial Cells, Nanomedicine, and Biotechnology, 2017. **45**(2): p. 185-192.
21. Nair, L.S. and C.T. Laurencin, *Biodegradable polymers as biomaterials.* Progress in Polymer Science, 2007. **32**(8): p. 762-798.
22. Jammalamadaka, U. and K. Tappa, *Recent Advances in Biomaterials for 3D Printing and Tissue Engineering.* Journal of functional biomaterials, 2018. **9**(1): p. 22.
23. Rampichová, M., et al., *Composite 3D printed scaffold with structured electrospun nanofibers promotes chondrocyte adhesion and infiltration.* Cell adhesion & migration, 2017. **12**(3): p. 271-285.

24. Mohammadian, F. and A. Eatemadi, *Drug loading and delivery using nanofibers scaffolds.* Artificial Cells, Nanomedicine, and Biotechnology, 2017. **45**(5): p. 881-888.
25. Hansen, C.M., *50 Years with solubility parameters—past and future.* Progress in Organic Coatings, 2004. **51**(1): p. 77-84.
26. Doktorovova, S., E.B. Souto, and A.M. Silva, *Hansen solubility parameters (HSP) for prescreening formulation of solid lipid nanoparticles (SLN): in vitro testing of curcumin-loaded SLN in MCF-7 and BT-474 cell lines.* Pharmaceutical Development and Technology, 2018. **23**(1): p. 96-105.
27. Casasola, R., N.L. Thomas, and S. Georgiadou, *Electrospinning of poly(lactic acid): Theoretical approach for the solvent selection to produce defect-free nanofibers.* Journal of Polymer Science Part B: Polymer Physics, 2016. **54**(15): p. 1483-1498.
28. Yazgan, G., et al., *Steering surface topographies of electrospun fibers: understanding the mechanisms.* Scientific reports, 2017. **7**(1): p. 158-158.
29. Koski, A., K. Yim, and S. Shivkumar, *Effect of molecular weight on fibrous PVA produced by electrospinning.* Materials Letters, 2004. **58**(3): p. 493-497.
30. Zhang, J., et al., *Molecular weight-modulated electrospun poly(ε-caprolactone) membranes for postoperative adhesion prevention.* RSC Advances, 2014. **4**(79): p. 41696-41704.
31. Ngadiman, N.H.A., et al., *Influence of polyvinyl alcohol molecular weight on the electrospun nanofiber mechanical properties.* Procedia Manufacturing, 2015. **2**: p. 568-572.
32. Shenoy, S.L., et al., *Role of chain entanglements on fiber formation during electrospinning of polymer solutions: good solvent, non-specific polymer–polymer interaction limit.* Polymer, 2005. **46**(10): p. 3372-3384.
33. Machotová, J., et al., *Electrospinning of Styrene–Ethyl Acrylate Emulsion Copolymers: Exploring the Impact of Polymer Polarity and Glass Transition Temperature on Fiber Formation and Hydrophobicity.* Polymer-Plastics Technology and Engineering, 2016. **55**(4): p. 423-431.
34. Burgess, K., et al., *The Effect of Molecular Properties on Active Ingredient Release from Electrospun Eudragit Fibers.* Pharmaceutics, 2018. **10**(3): p. 103.
35. Taylor, G., *Disintegration of Water Drops in an Electric Field.* Proceedings of the Royal Society of London A: Mathematical, Physical and Engineering Sciences, 1964. **280**(1382): p. 383-397.
36. Yarin, A.L., S. Koombhongse, and D.H. Reneker, *Taylor cone and jetting from liquid droplets in electrospinning of nanofibers.* Journal of Applied Physics, 2001. **90**(9): p. 4836-4846.
37. Shin, Y.M., et al., *Electrospinning: A whipping fluid jet generates submicron polymer fibers.* Applied Physics Letters, 2001. **78**(8): p. 1149-1151.
38. Reneker, D.H., et al., *Bending instability of electrically charged liquid jets of polymer solutions in electrospinning.* Journal of Applied Physics, 2000. **87**(9): p. 4531-4547.
39. Garg, K. and G.L. Bowlin, *Electrospinning jets and nanofibrous structures.* Biomicrofluidics, 2011. **5**(1): p. 013403.
40. Loscertales, I.G., et al., *Micro/Nano Encapsulation via Electrified Coaxial Liquid Jets.* Science, 2002. **295**(5560): p. 1695.
41. Yu, M., et al., *Recent advances in needleless electrospinning of ultrathin fibers: From academia to industrial production.* Macromolecular Materials and Engineering, 2017. **302**(7): p. 1700002.
42. Motamedi, A.S., et al., *Effect of electrospinning parameters on morphological properties of PVDF nanofibrous scaffolds.* Progress in Biomaterials, 2017. **6**(3): p. 113-123.
43. Haider, A., S. Haider, and I.-K. Kang, *A comprehensive review summarizing the effect of electrospinning parameters and potential applications of nanofibers in biomedical and biotechnology.* Arabian Journal of Chemistry, 2018. **11**(8): p. 1165-1188.
44. Zhang, C.-L. and S.-H. Yu, *Spraying functional fibres by electrospinning.* Materials Horizons, 2016. **3**(4): p. 266-269.

45. Zargham, S., et al., *The effect of flow rate on morphology and deposition area of electrospun nylon 6 nanofiber.* Journal of Engineered Fibers and Fabrics, 2012. **7**(4): p. 155892501200700414.
46. Shen, Y., et al., *Experimental study and prediction of the diameter of melt-electrospinning polypropylene fiber.* Fibers and Polymers, 2016. **17**(8): p. 1227-1237.
47. Jabur, A.R., L.K. Abbas, and S.M.M. Aldain, *The effects of operating parameters on the morphology of electrospun polyvinyl alcohol nanofibres.* journal of kerbala university, 2015(المؤتمر العلمي الثالث لكلية العلوم): p. 35-46.
48. Pillay, V., et al., *A Review of the Effect of Processing Variables on the Fabrication of Electrospun Nanofibers for Drug Delivery Applications.* Journal of Nanomaterials, 2013. **2013**: p. 22.
49. Sadeghi-Avalshahr, A., et al., *Synthesis and characterization of collagen/PLGA biodegradable skin scaffold fibers.* Regenerative biomaterials, 2017. **4**(5): p. 309-314.
50. Akduman, C., E.P.A. Kumabasar, and A. Çay. *Effect of Molecular weight on the Morphology of Electrospun Poly (vinyl alcohol) Nanofibers*. in *Proc. XIIIth International Izmir Textile and Apparel Symposium*. 2014.
51. Baker, S.R., et al., *Determining the mechanical properties of electrospun poly-ε-caprolactone (PCL) nanofibers using AFM and a novel fiber anchoring technique.* Materials Science and Engineering: C, 2016. **59**: p. 203-212.
52. Nguyen, T.T.T., et al., *Characteristics of curcumin-loaded poly (lactic acid) nanofibers for wound healing.* Journal of Materials Science, 2013. **48**(20): p. 7125-7133.
53. Ignatious, F., et al., *Electrospun Nanofibers in Oral Drug Delivery.* Pharmaceutical Research, 2010. **27**(4): p. 576-588.
54. Weng, L. and J. Xie, *Smart electrospun nanofibers for controlled drug release: recent advances and new perspectives.* Current pharmaceutical design, 2015. **21**(15): p. 1944-1959.
55. Torres-Martinez, E.J., et al., *A Summary of Electrospun Nanofibers as Drug Delivery System: Drugs Loaded and Biopolymers Used as Matrices.* Current drug delivery, 2018. **15**(10): p. 1360-1374.
56. Vashisth, P., et al., *Ofloxacin loaded gellan/PVA nanofibers - Synthesis, characterization and evaluation of their gastroretentive/mucoadhesive drug delivery potential.* Materials Science and Engineering: C, 2017. **71**: p. 611-619.
57. Vuddanda, P.R., A.P. Mathew, and S. Velaga, *Electrospun nanofiber mats for ultrafast release of ondansetron.* Reactive and Functional Polymers, 2016. **99**: p. 65-72.
58. Potrč, T., et al., *Electrospun polycaprolactone nanofibers as a potential oromucosal delivery system for poorly water-soluble drugs.* European Journal of Pharmaceutical Sciences, 2015. **75**: p. 101-113.
59. Yu, D.-G., et al., *Oral fast-dissolving drug delivery membranes prepared from electrospun polyvinylpyrrolidone ultrafine fibers.* Nanotechnology, 2009. **20**(5): p. 055104.
60. Li, X., et al., *Electrospun polyvinyl-alcohol nanofibers as oral fast-dissolving delivery system of caffeine and riboflavin.* Colloids and Surfaces B: Biointerfaces, 2013. **103**: p. 182-188.
61. Nagy, Z.K., et al., *Electrospun water soluble polymer mat for ultrafast release of Donepezil HCl.* Express polymer letters, 2010. **4**(12): p. 763-772.
62. Colley, H.E., et al., *Pre-clinical evaluation of novel mucoadhesive bilayer patches for local delivery of clobetasol-17-propionate to the oral mucosa.* Biomaterials, 2018. **178**: p. 134-146.
63. Li, C., et al., *Preparation and characterization of an electrospun colon-specific delivery system for salmon calcitonin.* RSC Advances, 2018. **8**(18): p. 9762-9769.
64. Nageh, H., et al., *Evaluation of antibacterial activity and drug release behavior of chitosan-based nanofibers (In Vitro Study).* UK J. Pharm. Biosci, 2014. **2**: p. 1-5.
65. Yun, J., et al., *Electro-responsive transdermal drug delivery behavior of PVA/PAA/MWCNT nanofibers.* European Polymer Journal, 2011. **47**(10): p. 1893-1902.

66. Suwantong, O., U. Ruktanonchai, and P. Supaphol, *Electrospun cellulose acetate fiber mats containing asiaticoside or Centella asiatica crude extract and the release characteristics of asiaticoside.* Polymer, 2008. **49**(19): p. 4239-4247.
67. Taepaiboon, P., U. Rungsardthong, and P. Supaphol, *Vitamin-loaded electrospun cellulose acetate nanofiber mats as transdermal and dermal therapeutic agents of vitamin A acid and vitamin E.* European Journal of Pharmaceutics and Biopharmaceutics, 2007. **67**(2): p. 387-397.
68. Ngawhirunpat, T., et al., *Development of Meloxicam-Loaded Electrospun Polyvinyl Alcohol Mats as a Transdermal Therapeutic Agent.* Pharmaceutical Development and Technology, 2009. **14**(1): p. 73-82.
69. Mendes, A.C., et al., *Hybrid electrospun chitosan-phospholipids nanofibers for transdermal drug delivery.* International Journal of Pharmaceutics, 2016. **510**(1): p. 48-56.
70. Souriyan-Reyhani pour, H., et al., *Cellulose acetate/poly (vinyl alcohol) hybrid fibrous mat containing tetracycline hydrochloride and phenytoin sodium: Morphology, drug release, antibacterial, and cell culture studies.* Journal of Bioactive and Compatible Polymers, 2018. **33**(6): p. 597-611.
71. Zhang, X., K. Tang, and X. Zheng, *Electrospinning and Crosslinking of COL/PVA Nanofiber-microsphere Containing Salicylic Acid for Drug Delivery.* Journal of Bionic Engineering, 2016. **13**(1): p. 143-149.
72. Zhang, L., et al., *Electrospun PEGylated PLGA nanofibers for drug encapsulation and release.* Materials Science and Engineering: C, 2018. **91**: p. 255-262.
73. Hu, J., et al., *Preparation and characterization of electrospun PLGA/gelatin nanofibers as a drug delivery system by emulsion electrospinning.* Journal of Biomaterials Science, Polymer Edition, 2013. **24**(8): p. 972-985.
74. Doustgani, A., *Doxorubicin release from optimized electrospun polylactic acid nanofibers.* Journal of Industrial Textiles, 2017. **47**(1): p. 71-88.
75. Aguilar, L.E., et al., *Electrospun polyurethane/Eudragit® L100-55 composite mats for the pH dependent release of paclitaxel on duodenal stent cover application.* International Journal of Pharmaceutics, 2015. **478**(1): p. 1-8.
76. Manuel, C.B.J., V.G.L. Jesús, and S.M. Aracely, *Electrospinning for drug delivery systems: drug incorporation techniques*, in *Electrospinning-Material, Techniques, and Biomedical Applications*. 2016, InTech.
77. Zamani, M., M.P. Prabhakaran, and S. Ramakrishna, *Advances in drug delivery via electrospun and electrosprayed nanomaterials.* International journal of nanomedicine, 2013. **8**: p. 2997-3017.
78. Gupta, D., et al., *Nanostructured biocomposite substrates by electrospinning and electrospraying for the mineralization of osteoblasts.* Biomaterials, 2009. **30**(11): p. 2085-2094.
79. Wen, P., et al., *Preparation and Characterization of Protein-Loaded Electrospun Fiber Mat and Its Release Kinetics.* Journal of Agricultural and Food Chemistry, 2017. **65**(23): p. 4786-4796.
80. Li, C., et al., *Coaxial Electrospinning and Characterization of Core-Shell Structured Cellulose Nanocrystal Reinforced PMMA/PAN Composite Fibers.* Materials (Basel, Switzerland), 2017. **10**(6): p. 572.
81. Lu, Y., et al., *Coaxial electrospun fibers: applications in drug delivery and tissue engineering.* Wiley Interdisciplinary Reviews: Nanomedicine and Nanobiotechnology, 2016. **8**(5): p. 654-677.
82. Nikmaram, N., et al., *Emulsion-based systems for fabrication of electrospun nanofibers: Food, pharmaceutical and biomedical applications.* RSC Advances, 2017. **7**(46): p. 28951-28964.
83. Wang, Z., et al., *Evaluation of emulsion electrospun polycaprolactone/hyaluronan/epidermal growth factor nanofibrous scaffolds for wound healing.* Journal of Biomaterials Applications, 2015. **30**(6): p. 686-698.

84. Basar, A.O., et al., *Novel poly(ε-caprolactone)/gelatin wound dressings prepared by emulsion electrospinning with controlled release capacity of Ketoprofen anti-inflammatory drug.* Materials Science and Engineering: C, 2017. **81**: p. 459-468.
85. Garcia-Orue, I., et al., *Novel nanofibrous dressings containing rhEGF and Aloe vera for wound healing applications.* International Journal of Pharmaceutics, 2017. **523**(2): p. 556-566.
86. Chitrattha, S. and T. Phaechamud, *Porous poly(dl-lactic acid) matrix film with antimicrobial activities for wound dressing application.* Materials Science and Engineering: C, 2016. **58**: p. 1122-1130.
87. Ajalloueian, F., et al., *Emulsion electrospinning as an approach to fabricate PLGA/chitosan nanofibers for biomedical applications.* BioMed research international, 2014. **2014**: p. 475280-475280.
88. Tian, L., et al., *Biocompatibility evaluation of emulsion electrospun nanofibers using osteoblasts for bone tissue engineering.* Journal of Biomaterials Science, Polymer Edition, 2013. **24**(17): p. 1952-1968.
89. Xu, W., et al., *Preparation and characterization of electrospun alginate/PLA nanofibers as tissue engineering material by emulsion eletrospinning.* Journal of the Mechanical Behavior of Biomedical Materials, 2017. **65**: p. 428-438.
90. Roy, T., et al., *Core-Shell Nanofibrous Scaffold Based on Polycaprolactone-Silk Fibroin Emulsion Electrospinning for Tissue Engineering Applications.* Bioengineering, 2018. **5**(3): p. 68.
91. Hu, J., et al., *Drug-loaded emulsion electrospun nanofibers: characterization, drug release and in vitro biocompatibility.* RSC Advances, 2015. **5**(121): p. 100256-100267.
92. Shin, J. and S. Lee, *Encapsulation of phytoncide in nanofibers by emulsion electrospinning and their antimicrobial assessment.* Fibers and Polymers, 2018. **19**(3): p. 627-634.
93. Xu, X., et al., *Ultrafine medicated fibers electrospun from W/O emulsions.* Journal of Controlled Release, 2005. **108**(1): p. 33-42.
94. Agrahari, V., et al., *Chapter 9 - Electrospun Nanofibers in Drug Delivery: Fabrication, Advances, and Biomedical Application*s, in *Emerging Nanotechnologies for Diagnostics, Drug Delivery and Medical Devices*, A.K. Mitra, K. Cholkar, and A. Mandal, Editors. 2017, Elsevier: Boston. p. 189-215.
95. Chou, S.-F., D. Carson, and K.A. Woodrow, *Current strategies for sustaining drug release from electrospun nanofibers.* Journal of Controlled Release, 2015. **220**: p. 584-591.
96. Wen, P., et al., *Electrospinning: A novel nano-encapsulation approach for bioactive compounds.* Trends in Food Science & Technology, 2017. **70**: p. 56-68.
97. Hrib, J., et al., *Nanofibers for drug delivery - incorporation and release of model molecules, influence of molecular weight and polymer structure.* Beilstein journal of nanotechnology, 2015. **6**: p. 1939-1945.
98. Higham, A.K., et al., *Foam electrospinning: A multiple jet, needle-less process for nanofiber production.* AIChE Journal, 2014. **60**(4): p. 1355-1364.
99. Sidaravicius, J., et al., *Predicting the electrospinnability of polymer solutions with electromechanical simulation.* Journal of Applied Polymer Science, 2014. **131**(22).
100. Ahirwal, D., et al., *From self-assembly of electrospun nanofibers to 3D cm thick hierarchical foams.* Soft Matter, 2013. **9**(11): p. 3164-3172.
101. Si, Y., et al., *Ultralight nanofibre-assembled cellular aerogels with superelasticity and multifunctionality.* Nature Communications, 2014. **5**: p. 5802.
102. Svagan, A.J., et al., *Solid cellulose nanofiber based foams – Towards facile design of sustained drug delivery systems.* Journal of Controlled Release, 2016. **244**: p. 74-82.
103. Rizvi, S.A.A. and A.M. Saleh, *Applications of nanoparticle systems in drug delivery technology.* Saudi pharmaceutical journal : SPJ : the official publication of the Saudi Pharmaceutical Society, 2018. **26**(1): p. 64-70.

104. Crucho, C.I.C. and M.T. Barros, *Polymeric nanoparticles: A study on the preparation variables and characterization methods.* Materials Science and Engineering: C, 2017. **80**: p. 771-784.
105. Kumar, B., et al., *Recent advances in nanoparticle-mediated drug delivery.* Journal of Drug Delivery Science and Technology, 2017. **41**: p. 260-268.
106. Aadil, K.R., S.I. Mussatto, and H. Jha, *Synthesis and characterization of silver nanoparticles loaded poly(vinyl alcohol)-lignin electrospun nanofibers and their antimicrobial activity.* International Journal of Biological Macromolecules, 2018. **120**: p. 763-767.
107. Celebioglu, A., et al., *One-step green synthesis of antibacterial silver nanoparticles embedded in electrospun cyclodextrin nanofibers.* Carbohydrate Polymers, 2019. **207**: p. 471-479.
108. Kurtz, I.S. and J.D. Schiffman, *Current and Emerging Approaches to Engineer Antibacterial and Antifouling Electrospun Nanofibers.* Materials, 2018. **11**(7): p. 1059.
109. Nie, H. and C.-H. Wang, *Fabrication and characterization of PLGA/HAp composite scaffolds for delivery of BMP-2 plasmid DNA.* Journal of Controlled Release, 2007. **120**(1): p. 111-121.
110. Kim, Y.-J., M. Ebara, and T. Aoyagi, *A Smart Hyperthermia Nanofiber with Switchable Drug Release for Inducing Cancer Apoptosis.* Advanced Functional Materials, 2013. **23**(46): p. 5753-5761.
111. Boateng, J.S., et al., *Wound Healing Dressings and Drug Delivery Systems: A Review.* Journal of Pharmaceutical Sciences, 2008. **97**(8): p. 2892-2923.
112. Zhong, S.P., Y.Z. Zhang, and C.T. Lim, *Tissue scaffolds for skin wound healing and dermal reconstruction.* Wiley Interdisciplinary Reviews: Nanomedicine and Nanobiotechnology, 2010. **2**(5): p. 510-525.
113. Zahedi, P., et al., *A review on wound dressings with an emphasis on electrospun nanofibrous polymeric bandages.* Polymers for Advanced Technologies, 2010. **21**(2): p. 77-95.
114. *Drug-loaded electrospun materials in wound-dressing applications and in local cancer treatment.* Expert Opinion on Drug Delivery, 2013. **10**(4): p. 469-483.
115. Wang, J. and M. Windbergs, *Functional electrospun fibers for the treatment of human skin wounds.* European Journal of Pharmaceutics and Biopharmaceutics, 2017. **119**: p. 283-299.
116. Fu, R., et al., *A novel electrospun membrane based on moxifloxacin hydrochloride/poly(vinyl alcohol)/sodium alginate for antibacterial wound dressings in practical application.* Drug Delivery, 2016. **23**(3): p. 818-829.
117. Yao, C.-H., et al., *Novel bilayer wound dressing based on electrospun gelatin/keratin nanofibrous mats for skin wound repair.* Materials Science and Engineering: C, 2017. **79**: p. 533-540.
118. Saeed, S.M., et al., *Designing and fabrication of curcumin loaded PCL/PVA multi-layer nanofibrous electrospun structures as active wound dressing.* Progress in Biomaterials, 2017. **6**(1): p. 39-48.
119. Wang, M., A.K. Roy, and T.J. Webster, *Development of Chitosan/Poly(Vinyl Alcohol) Electrospun Nanofibers for Infection Related Wound Healing.* Frontiers in physiology, 2017. **7**: p. 683-683.
120. Ghalei, S., H. Asadi, and B. Ghalei, *Zein nanoparticle-embedded electrospun PVA nanofibers as wound dressing for topical delivery of anti-inflammatory diclofenac.* Journal of Applied Polymer Science, 2018. **135**(33): p. 46643.
121. Abdelgawad, A.M., S.M. Hudson, and O.J. Rojas, *Antimicrobial wound dressing nanofiber mats from multicomponent (chitosan/silver-NPs/polyvinyl alcohol) systems.* Carbohydrate Polymers, 2014. **100**: p. 166-178.
122. Alavarse, A.C., et al., *Tetracycline hydrochloride-loaded electrospun nanofibers mats based on PVA and chitosan for wound dressing.* Materials Science and Engineering: C, 2017. **77**: p. 271-281.

123. Aruan, N.M., et al., *Polyvinyl Alcohol/Soursop Leaves Extract Composite Nanofibers Synthesized Using Electrospinning Technique and their Potential as Antibacterial Wound Dressing.* Procedia Engineering, 2017. **170**: p. 31-35.
124. Shan, Y.-H., et al., *Silk fibroin/gelatin electrospun nanofibrous dressing functionalized with astragaloside IV induces healing and anti-scar effects on burn wound.* International Journal of Pharmaceutics, 2015. **479**(2): p. 291-301.
125. Shin, Y.C., et al., *Hyaluronic Acid/PLGA Core/Shell Fiber Matrices Loaded with EGCG Beneficial to Diabetic Wound Healing.* Advanced Healthcare Materials, 2016. **5**(23): p. 3035-3045.
126. Alippilakkotte, S., S. Kumar, and L. Sreejith, *Fabrication of PLA/Ag nanofibers by green synthesis method using Momordica charantia fruit extract for wound dressing applications.* Colloids and Surfaces A: Physicochemical and Engineering Aspects, 2017. **529**: p. 771-782.
127. Choi, J.I., et al., *Spirulina extract-impregnated alginate-PCL nanofiber wound dressing for skin regeneration.* Biotechnology and Bioprocess Engineering, 2017. **22**(6): p. 679-685.
128. Rath, G., et al., *Collagen nanofiber containing silver nanoparticles for improved wound-healing applications.* Journal of Drug Targeting, 2016. **24**(6): p. 520-529.
129. Lee, C.-H., et al., *Enhancement of Diabetic Wound Repair Using Biodegradable Nanofibrous Metformin-Eluting Membranes: in Vitro and in Vivo.* ACS Applied Materials & Interfaces, 2014. **6**(6): p. 3979-3986.
130. Huang, X. and C.S. Brazel, *On the importance and mechanisms of burst release in matrix-controlled drug delivery systems.* Journal of Controlled Release, 2001. **73**(2): p. 121-136.
131. Ebeling, S., et al., *From a Traditional Medicinal Plant to a Rational Drug: Understanding the Clinically Proven Wound Healing Efficacy of Birch Bark Extract.* PLoS ONE, 2014. **9**(1): p. e86147.
132. Färber, A. and R. Daniels, *Ex vivo Skin Permeation of Betulin from Water-in-Oil Foams.* Skin Pharmacology and Physiology, 2016. **29**(5): p. 250-256.
133. Wu, S., et al., *Fabrication of Aligned Nanofiber Polymer Yarn Networks for Anisotropic Soft Tissue Scaffolds.* ACS Applied Materials & Interfaces, 2016. **8**(26): p. 16950-16960.
134. Xie, J., X. Li, and Y. Xia, *Putting Electrospun Nanofibers to Work for Biomedical Research.* Macromolecular rapid communications, 2008. **29**(22): p. 1775-1792.
135. Buehler, M.J., *Molecular nanomechanics of nascent bone: fibrillar toughening by mineralization.* Nanotechnology, 2007. **18**(29): p. 295102.
136. Prabhakaran, M.P., J. Venugopal, and S. Ramakrishna, *Electrospun nanostructured scaffolds for bone tissue engineering.* Acta Biomaterialia, 2009. **5**(8): p. 2884-2893.
137. Abdal-hay, A., et al., *Preparation and characterization of vertically arrayed hydroxyapatite nanoplates on electrospun nanofibers for bone tissue engineering.* Chemical Engineering Journal, 2014. **254**: p. 612-622.
138. Pramanik, S., B. Pingguan-Murphy, and N.A. Abu Osman, *Progress of key strategies in development of electrospun scaffolds: bone tissue.* Science and technology of advanced materials, 2012. **13**(4): p. 043002-043002.
139. Kim, M.S. and G. Kim, *Three-dimensional electrospun polycaprolactone (PCL)/alginate hybrid composite scaffolds.* Carbohydrate Polymers, 2014. **114**: p. 213-221.
140. Enayati, M.S., et al., *Development of electrospun poly (vinyl alcohol)-based bionanocomposite scaffolds for bone tissue engineering.* Journal of Biomedical Materials Research Part A, 2018. **106**(4): p. 1111-1120.
141. Heydari, Z., D. Mohebbi-Kalhori, and M.S. Afarani, *Engineered electrospun polycaprolactone (PCL)/octacalcium phosphate (OCP) scaffold for bone tissue engineering.* Materials Science and Engineering: C, 2017. **81**: p. 127-132.
142. Lim, J., et al., *Emerging bone tissue engineering via Polyhydroxyalkanoate (PHA)-based scaffolds.* Materials Science and Engineering: C, 2017. **79**: p. 917-929.

143. Tan, G.Z. and Y. Zhou, *Tunable 3D Nanofiber Architecture of Polycaprolactone by Divergence Electrospinning for Potential Tissue Engineering Applications.* Nano-Micro Letters, 2018. **10**(4): p. 73.
144. Fu, W., et al., *Electrospun gelatin/PCL and collagen/PLCL scaffolds for vascular tissue engineering.* International journal of nanomedicine, 2014. **9**: p. 2335-2344.
145. Du, F., et al., *Gradient nanofibrous chitosan/poly ε-caprolactone scaffolds as extracellular microenvironments for vascular tissue engineering.* Biomaterials, 2012. **33**(3): p. 762-770.
146. Vatankhah, E., et al., *Electrospun tecophilic/gelatin nanofibers with potential for small diameter blood vessel tissue engineering.* Biopolymers, 2014. **101**(12): p. 1165-1180.
147. Sankaran, K.K., et al., *Development and evaluation of axially aligned nanofibres for blood vessel tissue engineering.* Journal of Tissue engineering and regenerative medicine, 2014. **8**(8): p. 640-651.
148. Kim, M.J., et al., *In vitro andin vivo application of PLGA nanofiber for artificial blood vessel.* Macromolecular Research, 2008. **16**(4): p. 345-352.
149. Ao, C., et al., *Fabrication and characterization of electrospun cellulose/nano-hydroxyapatite nanofibers for bone tissue engineering.* International Journal of Biological Macromolecules, 2017. **97**: p. 568-573.
150. Li, C., et al., *Electrospun silk-BMP-2 scaffolds for bone tissue engineering.* Biomaterials, 2006. **27**(16): p. 3115-3124.
151. Haider, A., K.C. Gupta, and I.-K. Kang, *PLGA/nHA hybrid nanofiber scaffold as a nanocargo carrier of insulin for accelerating bone tissue regeneration.* Nanoscale research letters, 2014. **9**(1): p. 314-314.
152. Sharifi, F., et al., *Polycaprolactone/carboxymethyl chitosan nanofibrous scaffolds for bone tissue engineering application.* International Journal of Biological Macromolecules, 2018. **115**: p. 243-248.
153. Persano, L., et al., *Industrial Upscaling of Electrospinning and Applications of Polymer Nanofibers: A Review.* Macromolecular Materials and Engineering, 2013. **298**(5): p. 504-520.
154. Varabhas, J.S., G.G. Chase, and D.H. Reneker, *Electrospun nanofibers from a porous hollow tube.* Polymer, 2008. **49**(19): p. 4226-4229.
155. Moon, S., M. Gil, and K.J. Lee, *Syringeless Electrospinning toward Versatile Fabrication of Nanofiber Web.* Scientific Reports, 2017. **7**: p. 41424.
156. Valipouri, A., *Production scale up of nanofibers: a review.* J Text Polym, 2017. **5**(1): p. 8-16.
157. Cengiz-Çallıoğlu, F., O. Jirsak, and M. Dayik, *Investigation into the relationships between independent and dependent parameters in roller electrospinning of polyurethane.* Textile Research Journal, 2013. **83**(7): p. 718-729.
158. Geremia, F., *Quality aspects for medical devices, quality system and certification process.* Microchemical Journal, 2018. **136**: p. 300-306.
159. Zyga, S. and J. Stathoulis, *Application of ISO 13485: 2003 in Biomedical Engineering: a Systematic.* International Journal of Caring Sciences, 2011. **4**(2): p. 58.
160. ISO, *https://www.iso.org/obp/ui/#iso:std:iso:13485:ed-3:v1:en.* 2016.
161. ISO, *https://www.iso.org/obp/ui/#iso:std:iso:10993:-1:ed-5:v2:en.* 2018.
162. ISO, *https://www.iso.org/obp/ui/#iso:std:iso:80601:-2-13:ed-1:v1:en.* 2011.
163. Lv, D., et al., *Green Electrospun Nanofibers and Their Application in Air Filtration.* Macromolecular Materials and Engineering, 2018. **303**(12): p. 1800336.

3 Chapter 3: Optimized Birch Bark Extract loaded Colloidal Dispersion using Hydrogenated Phospholipids as stabilizer.

Francis Kamau Mwiiri, Rolf Daniels

Department of Pharmaceutical Technology, Eberhard Karls University,

Tuebingen, Germany

Reprinted from Pharmaceutics 2020, 12(9), 832; Special Issue: Advanced Colloidal Systems for Multimodal Drug Delivery

DOI: 10.3390/pharmaceutics12090832

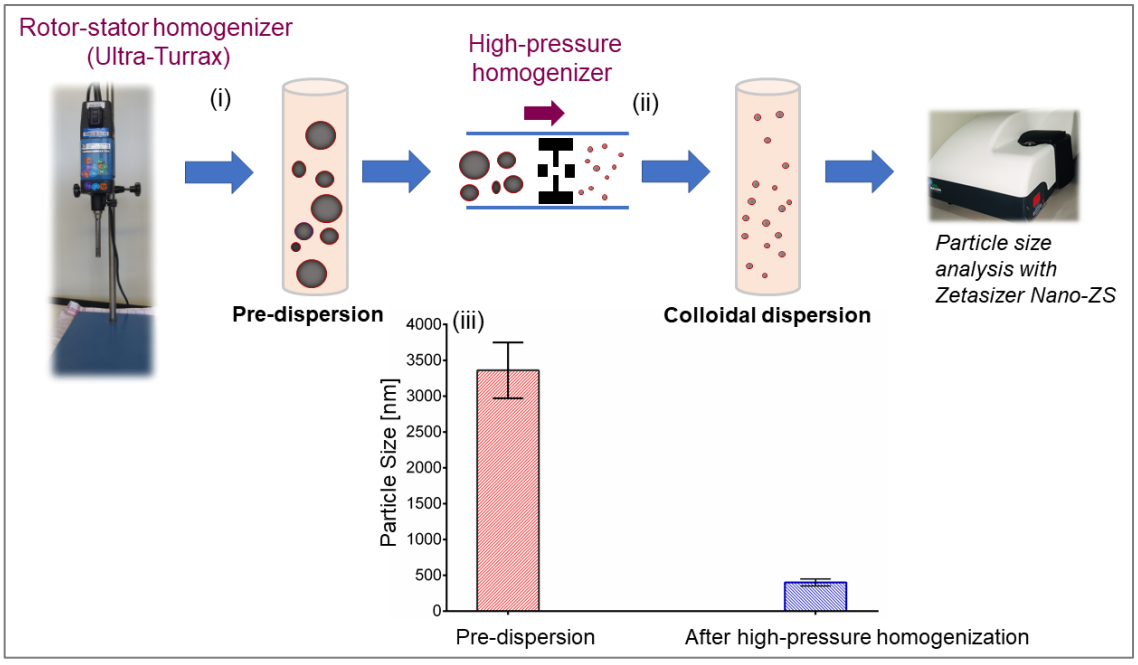

Graphical Abstract

3.1 Abstract

This study investigated the formulation and processing of aqueous colloidal dispersions containing a birch bark dry extract (TE) as the active substance and hydrogenated phospholipids (Phospholipon 90H) as stabilizer, which can be used in the preparation of electrospun wound dressings. Colloidal dispersions manufactured using a two-stage homogenization process had a bimodal particle size distribution, which was most significantly ($p < 0.0001$) affected by the phospholipid content. The size of the single particles decreased from an average particle size of about 4 µm to a particle size of approximately 400 nm. Dynamic interfacial tension studies performed using a profile analysis tensiometer (PAT) showed that the phospholipids strongly declined the interfacial tension, whereas a further decrease was observed when phospholipids were combined with birch bark extract. Interfacial viscoelasticity properties analyzed using the oscillating drop technique resulted in an increase of both interfacial elasticity and viscosity values. These results indicated that the phospholipids are preferentially located at the lipophilic/water interface and a stable film is formed. Furthermore, the results point to a synergistic interaction between phospholipids and TE. Confocal Raman microscopy (CRM) suggested that the TE is predominantly located in the oil phase and the phospholipids at the interface.

Keywords: colloidal dispersions; birch bark extract; phospholipids; sunflower oil; high-pressure homogenization; interfacial rheology

3.2 Introduction

Dry extracts from the outer bark of birch consist mainly of pentacyclic triterpenes, which are known for various pharmacological properties such as anti-inflammatory, anti-viral, anti-cancer activity, and wound-healing effects [1–8]. A well-characterized commercially used triterpene dry extract from the outer bark of birch contains about 80% (*w/w*) betulin and is obtained by accelerated solvent extraction with n-heptane [9]. Other disclosed triterpenes of the dry extract include lupeol (LU), erythrodiol (ER), betulinic acid (BA), and oleanolic acid (OA), as shown in Table 1 [10]. However, the low solubility of these triterpenes in polar and non-polar solvents makes formulation a challenging task, which might limit their therapeutic application [7,11,12]. For topical application, only a few formulation concepts are known. These include cosmetic water-in-oil creams, water-in-oil foams [8], and an oleogel consisting of TE and sunflower oil, which received the European marketing authorization in January 2016 [12]. To the best of our knowledge, an aqueous colloidal dispersion of TE has not been described so far.

However, such a colloidal dispersion would be a prerequisite as we intend to develop a bioactive wound dressing containing colloidal dispersions of birch bark extract through a blend electrospinning technique [13]. In this case, the colloidal TE dispersions will be blended with a suitable water-soluble polymer, e.g., polyvinyl alcohol (PVA) or polyvinyl pyrrolidone (PVP), to create sub-micron-sized electrospun fibers even without further modification of the spinneret.

Table 1. Physical–chemical characteristics of the birch bark dry extract (TE) used [8].

TE Composition	Specific Surface Area	Particle Size D50%
Betulin 81.60%, lupeol 2.08%, betulinic acid 3.84%, erythrodiol 1.05%, oleanolic acid 0.97%, betulinic acid methyl ester 0.52%, unidentified substances 9.94%	42 ± 0.4 m^2/g	5.8 µm

Phospholipids (PL) are commonly found in all cell membranes and therefore exist in all living organisms where they serve both structural and functional purposes. Lecithin is the most common form of phospholipids, where phosphatidylcholine (PC) is the major component [14,15]. Phospholipids are amphiphilic in nature, having a polar head group and two lipophilic tails. The polar head unit containing a phosphate group can be esterified with an alcohol to an organic molecule such as PC with choline, in phosphatidylethanolamine (PE) with ethanolamine, phosphatidylglycerol (PG) with glycerol, etc. Examples of these phospholipid derivatives can be found here [14]. Due to their amphiphilic characteristics, they have been shown to form

bilayers and liposomes or micelles under certain conditions [15]. As a result, PLs are frequently used as emulsifiers in the pharmaceutical, cosmetic, and food industry [14,16–18]. Being amphiphilic in nature, they can form a viscoelastic interfacial film that provides excellent colloidal stability [19–22]. Studies have shown that the dispersion particle size depends on the surfactant concentration whereby the particles significantly decrease in size as the surfactant concentration was increased [23–26]. Beyond that, many studies suggest that there is a direct interaction between PL and pentacyclic triterpenes [27,28]. This is also supported by preliminary studies in our group indicating that colloidal aqueous dispersions of TE are feasible in the presence of hydrogenated PL. These unique features make phospholipids most suitable to be used in this study in the preparation of colloidal dispersions containing birch bark extract.

Colloidal dispersions, e.g., nanoemulsions or solid-lipid nanoparticles, are widely known as drug carriers for various potential therapeutic applications i.e., oral, ocular, dermal, and parenteral [29–33]. More exclusively, they have been used to incorporate poorly water-soluble drugs, increase their bioavailability, or minimize the side effects of potent drugs [34–37]. Several methods have been utilized to manufacture such colloidal dispersions. Mostly, they can be formed by first forming a primary coarse dispersion with larger particle sizes in the micron range (1–5 µm) and then after subjecting them to high-energy dispersion methods, e.g., high-pressure homogenization, they can be reduced to the colloidal range (<500 nm). Usually, pre-dispersions formed in the first step by high shear mixing have high variable particle sizes, whereas the subsequent high-pressure homogenization produces dispersions with smaller and also more uniform particle sizes [30,38,39]. However, a simple preparation of TE-based aqueous or oily colloidal suspensions have been reported to be challenging due to the unique structure of the extract particle, which has been described as a “cauliflower-like” structure. These highly porous triterpene particles cannot be crushed by common techniques to reach particles in the colloidal size range, even when high-energy dispersion techniques, e.g., sonication or high-pressure homogenization, were utilized [40].

The aim of this study was (1) to study the role played by PL with respect to the distribution of TE in particular at the oil–water interface, (2) to develop a suitable workflow for the production of aqueous colloidal dispersions containing TE with particle sizes in colloidal range through a homogenization process, and (3) to investigate the influence of PL and sunflower content on particle size reduction.

3.3 Materials and Methods

3.3.1 Materials

Hydrogenated phospholipids from soybean lecithin (Phospholipon 90H) were supplied by Lipoid GmbH (Ludwigshafen, Germany). Sunflower oil was purchased from Caesar & Loretz GmbH (Hilden, Germany). Birch bark extract was obtained from Amryt AG, (Niefern-Öschelbronn, Germany). Reverse osmosis water (ELGA Labwater, Celle, Germany) was used for the preparation of all aqueous solutions.

3.3.2 Experimental Design and Statistical Analysis

All statistical calculations, experimental design generation, and optimization procedures were performed with JMP version 14.2 software (SAS Institute, Cary, NC, USA). A full factorial design of experiment (DoE) was used to generate combinations of formulations with a 3 × 4 design as shown in Table 2. Phospholipon 90H (PL90H) and sunflower oil (SO) content were taken as independent variables, whereas the amount of TE was kept constant at 0.5%. Thereafter, the respective formulations were prepared and assessed for particle size and polydispersity index (PDI). The observed response (particle size (nm)) was analyzed and compared with the predicted values. Beyond that, 3-D surface representations and leverage plots were constructed. The significance of each factor was evaluated by analysis of variance (ANOVA), and *P* values less than 0.05 were considered significant.

Table 2. Design of experiment (DoE) employed for the preparation of aqueous colloidal dispersions.

Batch Code	Pattern	TE (wt %)	PL90H (wt %)	SO (wt %)
F1	111	0.5	0.5	0
F2	112	0.5	0.5	0.3
F3	113	0.5	0.5	0.5
F4	114	0.5	0.5	1
F5	121	0.5	1	0
F6	122	0.5	1	0.3
F7	123	0.5	1	0.5
F8	124	0.5	1	1
F9	131	0.5	2.5	0
F10	132	0.5	2.5	0.3
F11	133	0.5	2.5	0.5
F12	134	0.5	2.5	1

3.3.3 Preparation of Aqueous Colloidal Dispersions

The colloidal dispersions prepared in this work consisted of PL90H, sunflower oil, and TE as the dispersed phase (1–4%) and water as the continuous phase (96–99%). A set of formulations as suggested by the corresponding DoE (Table 2) were prepared with varying concentrations of PL90H (0.5%, 1% and 2.5%) and sunflower oil (0%, 0.3%, 0.5%, and 1%), whereas birch bark extract (TE) concentration was kept constant at 0.5% in all runs. Briefly, during the preparation of each formulation, a pre-dispersion (PD) was prepared by first dispersing PL90H and TE in water at 70 °C for 30 min under magnetic stirring at 400 rpm using a MR 3001 K magnetic hotplate stirrer (Heidolph, Schwabach, Germany). Then, this mixture was homogenized for 5 min using a rotor-stator system (Ultra Turrax T25, IKA, Staufen, Germany) at 9500 rpm. Thereafter, the formed dispersion was added into the SO and homogenized for 3 min. Finally, the pre-dispersion was homogenized using a high-pressure homogenizer (Emulsiflex C-3, Avestin, Mannheim, Germany) for 8 cycles at a pressure of 100 MPa.

3.3.4 Particle Size Analysis

Dispersion particle size distribution and polydispersity were determined using dynamic light scattering (DLS) (Zetasizer Nano-ZS, Malvern Instruments, Herrenberg, Germany). In general, samples were diluted (1:10,000) with reversed osmosis water in 1.5 mL polystyrene disposable cuvettes prior to analysis to avoid multiple scattering effects. The results are reported as mean particle diameter (Z-average), size distribution by volume, and uniformity of the distribution (polydispersity index (PDI)). All formulations were analyzed on the day of manufacture, and DLS measurements were carried out at 25 °C in triplicate.

3.3.5 Density Measurements

Density was measured at 25 °C by means of a DMA 4500 density meter with an oscillating U-tube (Anton Paar, Filderstadt, Germany).

3.3.6 Interfacial Tension and Elasticity

Dynamic interfacial tension and elasticity was measured using a profile analysis tensiometer PAT-1D (Sinterface Technologies, Berlin, Germany) by applying the buoyant drop method. This method involves imaging the drop and fitting the shape to the Young–Laplace equation. To prepare the test solutions, TE and/or PL90H were dissolved completely in SO by sonication at 65 °C and cooled down to room

temperature before performing further experiments. A buoyant drop was formed in a cuvette made of optical glass 35 × 35 × 32 (mm) containing the aqueous phase, and its shape was imaged via a charge coupled device (CCD) camera and fitted to the Young–Laplace equation using the profile drop analysis software provided (Sinterface Technologies, Berlin, Germany). The interfacial tension, given as a function of time, was calculated from the drop shape using the Young–Laplace Equation:

$$\gamma\left(\frac{1}{R_1}+\frac{1}{R_2}\right)=\Delta P_0+(\Delta\rho)gz \quad (1)$$

where R_1 and R_2 are main radii of interface curvature, γ is the interfacial tension, ΔP_0 is the pressure difference at a reference plane, $\Delta\rho$ is the density difference, g is the gravitational constant, and z is the vertical height measured from the reference plane [41]. Hence, the interfacial tension values in equilibrium were manually extracted from the extrapolation of the measured data by a γ (1/√t) plot to infinite time [19]. The diffusion rates of all the samples were also determined from the slope of the plot.

Interfacial rheology was measured by applying the oscillating drop method using the buoyant drop technique with the profile analysis tensiometer PAT-1D (Sinterface Technologies, Berlin, Germany). The principle of the oscillating drop method involves changes of the size of the interface, where PL molecules are located, by continuously altering the drop volume. In a sinusoidal change of drop volume, and thus also the interface, the following can be observed: as the interface narrows, stabilizer molecules desorb from the interface (interfacial tension increases) and during the subsequent enlargement adsorb the molecules again (interfacial tension decreases) [41,42]. Hence, the rheological properties of adsorption layers are expressed by the relationship between the variation of the interfacial tension, from its initial value, and the expansion of the surface area. The interfacial elastic (E) and viscosity modulus can be expressed as [43].

$$E=\frac{\mathrm{d}\gamma}{\mathrm{d}\ \ln(A)} \quad (2)$$

$$\eta_d=\frac{\mathrm{d}\gamma}{(\mathrm{d}A/dt)/A} \quad (3)$$

where E is the interfacial elasticity, γ is the interfacial tension, A is the area of the interface, and η_d is the interfacial dilational viscosity.

The experiments were started after 10 min to allow equilibration of the interface. A single frequency of 0.1 Hz was used to study interfacial elasticity and viscosity. A drop volume of 10 µL ± 2 µL was formed at the capillary tip. Subsequently, the data were fitted, and the interfacial elasticity and viscosity values were calculated through a Fourier Transformation (FT) with the associated software. All measurements were performed at 25 °C.

To calculate the interfacial characteristics, the densities of the involved phases are required. The following values have been used: SO (0.91761 g/cm^3), SO + 0.1% TE (0.91782 g/cm^3): SO + 0.1% PL90H (0.91782 g/cm^3), and SO + 0.1% TE + 0.1% PL90H (0.91798 g/cm^3)).

3.3.7 Confocal Raman Spectral Imaging

A pre-dispersion containing sunflower oil, water, TE, and phospholipids was imaged using an alpha 500R Raman microscope (WiTec GmbH, Ulm, Germany) equipped with a DV401-BV CCD detector, connected via an optical fiber to a UHTS 300 spectrometer and a 532 nm laser excitation source. A 100× air objective (EC Epiplan-Neofluor, Carl Zeiss, Oberkochen, Germany) with a numerical aperture of 0.9 was used to view the sample, while the laser intensity was adjusted to 35 mW. The spectral range covered the fingerprint region between 710 and 1820 cm^{-1} and the region between 2700 and 3580 cm^{-1}. The spectra of all single components (PL90H, SO, and TE) were first collected and used as a reference to monitor the presence of each component in the dispersion. Subsequently, the test samples were presented to the microscope on glass slides (VWR-International, Darmstadt, Germany) and covered with a coverslip. Image scans of dispersion using 25 µm × 25 µm area of the surface were taken at an integration time of 0.01 s. Henceforth, color-coded images were obtained by initial cosmic ray removal and spectral background subtraction using the WiTec Project data analysis software 4.1 (WiTec GmbH, Ulm, Germany). By assigning the spectrum of each component to a color, the distribution of all components within the sample can be indicated, resulting in the color-coded image of the scanned area [44].

3.4 Results and Discussion

3.4.1 Confocal Raman Spectral Imaging

This study focused on colloidal systems consisting of PL, SO, and water, which to the best of our knowledge enabled for the first time the preparation of a colloidal TE dispersion. To get a first insight into the spatial distribution of the components, Raman microspectral imaging was applied to a coarse pre-dispersion consisting of 2.5% PL90H, 1% SO, and 0.5% TE. As can be seen in Figure 1, TE (red) enriches predominantly in the oil phase (yellow), meaning that the extract has high affinity to sunflower oil. On the other hand, no isolated TE particles dispersed in the aqueous phase have ever been detected on Raman images. As expected, the images clearly reveal that the PL90H (green) forms an interfacial layer between the lipophilic droplet (TE and SO) and water (blue). Consequently, this will lead to a reduction of the interfacial tension and stabilizes the dispersion of the two lipophilic components in the aqueous phase. Due to the limited spatial resolution, the Raman microscopic images could neither give hints on a direct interaction of TE and PL90H in these coarse dispersions nor could it seriously be applied to colloidal dispersions.

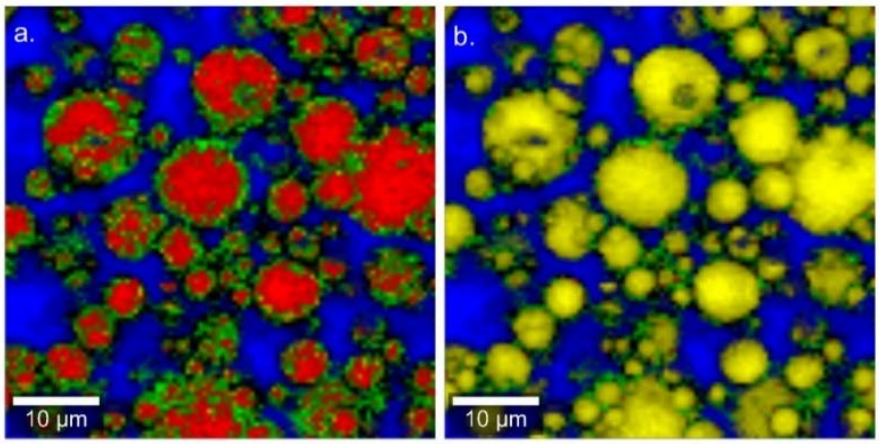

Figure 1. Confocal Raman microscopic color-coded images of aqueous pre-dispersion (**a**) Red: TE, Green: PL90H, Blue: Water, (**b**) shows TE removed in the image to facilitate the better identification of the yellow sunflower oil (SO).

3.4.2 Interfacial Tension and Viscoelasticity

To gain further insights into the potential role of PL90H in the dispersions process and its interaction with TE, we have conducted dynamic interfacial tension experiments at the oil–water interface in the absence and presence of PL90H. Figure 2 illustrates the results of the interfacial tension measurements of SO, reference

(21.58 ± 0.27 mN/m), SO + 0.1% TE (19.96 ± 0.39 mN/m): SO + 0.1% PL90H (8.4 ± 0.58 mN/m), and SO + 0.1% TE + 0.1% PL90H (4.75 ± 0.54 mN/m).

It is evident that where PL90H is present, a significant reduction of interfacial tension occurs, whereas TE displays only marginal interfacial activity. From the slope of the plot (interfacial tension versus $1/\sqrt{t}$), diffusion rates toward the interface can be calculated. This seems to be of particular interest when comparing the ternary system water, SO, and PL90H with the quaternary system consisting of water, SO, PL90H, and TE. 17.22 mN/m $s^{-1/2}$ or SO + 0.1% PL and SO + 0.1% TE + 0.1% PL90H exhibited the highest diffusion rate of 55.91 mN/m $s^{-1/2}$. This reveals that PL90H and TE strongly interact with each other, probably synergistically forming a film/membrane at the interface, which leads to a faster and more effective reduction of the interfacial tension.

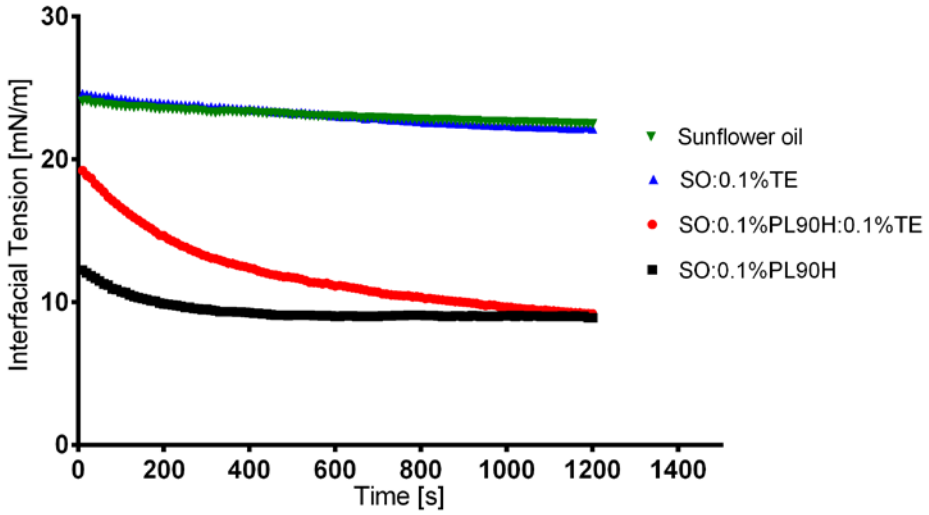

Figure 2. Dynamic interfacial tension curves of PL90H, TE, and PL90H + TE mixture dispersed in SO with water (*n* = 10).

The interfacial elasticity and viscosity of the test samples obtained from the oscillatory perturbation at a frequency of 0.1 Hz. Pure SO presented low interfacial elastic and viscosity values whereas for samples containing TE and PL90H, both values strongly increased. With an addition of PL90H to triterpene extract, both interfacial elastic and viscosity values significantly shifted toward higher values as compared to reference oil. It seems with the observed higher interfacial elastic values (Figure 3), that PL90H adsorbs at the interface and over the time, a plateau is formed; consequently, the interface becomes more elastic and more structured. Studies have shown that phospholipid molecules can adsorb at the interface, forming

a strong elastic film [15,45,46]. Therefore, the obtained high interfacial elasticity values indicate a stable rigid film formation at the interface. Moreover, low elasticity in the interface would require less energy to break the dispersion particles during the emulsification process. High interfacial elasticity is necessary in the stability of dispersions, as a stable film can hinder various instabilities such as the coalescence of dispersion particles from taking place [22,25,47]. Hence, the interfacial elasticity and viscosity can play a key role in the assessment of the deformability of dispersion particles and thus their stability [48]. In this study, the results indicate that a mixture of phospholipid + triterpene extract forms together a combined film with the highest elasticity at the interface, and such a complex again reveals that these two substances interact and do have a synergetic action. Further studies have shown that triterpenes interact with phospholipids (PL) and fluidize lipid membranes controlled by their free polar groups where tetracyclic triterpenes (e.g., cortisol) tend to be located at the head group, whereas pentacyclic ones (e.g., erythrodiol) being more hydrophobic are incorporated deeply in the lipid bilayers [28,49]. Cyclic triterpenes share similar structural properties with cholesterol, and it has been reported that such a monolayer containing cholesterol and PL is highly ordered. On the other hand, binary films of triterpenes and PLs are amorphous [27].

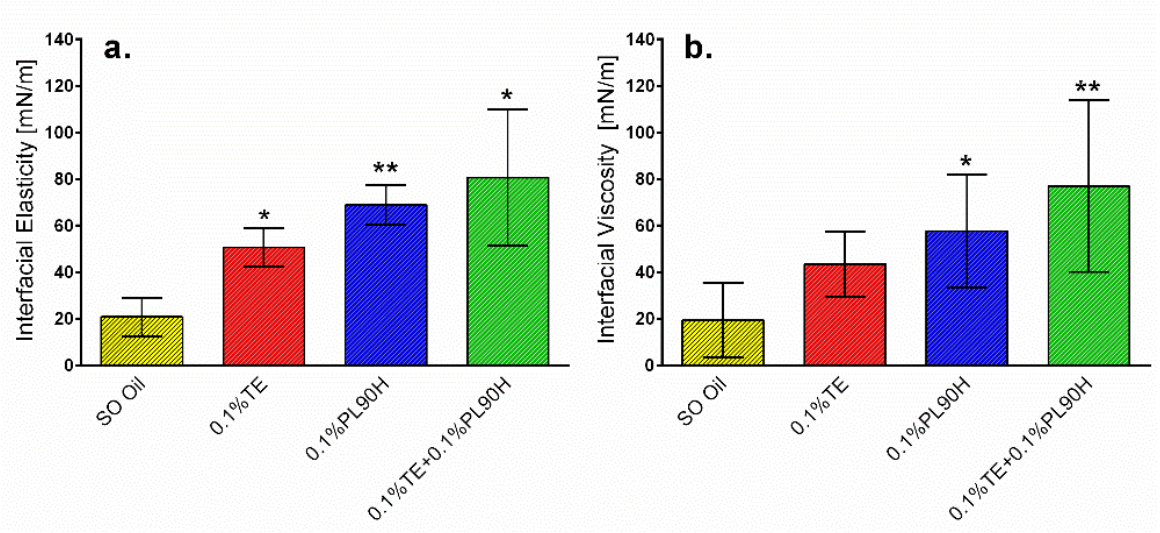

Figure 3. Interfacial elasticity (**a**) and viscosity (**b**) of 0.1% PL90H, 0.1% TE and PL90H + TE dispersed in sunflower oil (Mean ± SD, n = 6). statistically significant, * $p < 0.05$; ** $p < 0.01$ vs. sunflower oil (reference).

3.4.3 Particle Size Reduction

The suitability of high-pressure homogenization to produce colloidal dispersions of TE, PL90H, and SO in water was first tested with a formulation consisting of 2.5% PL90H, 0.5% TE, and 1% SO. After mixing and homogenizing with an Ultra Turrax, a mean particle size of 3400 ± 390 nm (pre-dispersion (PD), PDI: 0.9) was achieved. This could be reduced to 400 ± 49 nm (PDI: 0.5) by high-pressure homogenization, yielding a bimodal distribution function. The intensity weighed particle size distribution revealed a major peak at 364 nm comprising 81% and a smaller one at 76 nm representing 19% (Figure 4).

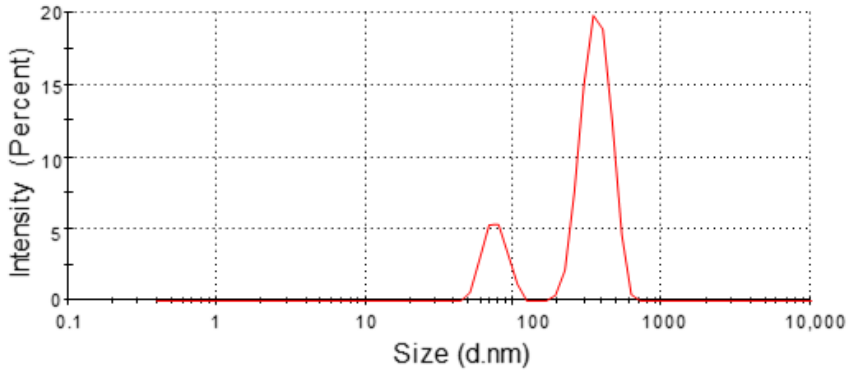

Figure 4. Bimodal particle size distribution by intensity of colloidal dispersion (2.5% PL90H:1% SO:0.5% TE).

To gain further insight, a DoE has been applied in order to identify the composition variables that influence the particle size distribution of the colloidal dispersions consisting of PL90H, SO, water, and a constant amount of 0.5% TE. The design space has to be restricted with respect to maximal PL90H (<2.5%) and SO concentration (<1%) in order to obtain sufficiently fluid systems necessary for high-pressure homogenization. Table 3 summarizes the respective results.

As expected, and shown in Table 3, pre-dispersions (PD) in all prepared formulations exhibited large particle sizes that were significantly reduced after high-pressure homogenization. Increasing either or both the content of SO and PL90H affected the size and distribution width (expressed as PDI) positively, whereby PL90H had a more pronounced effect. By increasing the concentration of PL90H from 0.5% (1033 nm) to 1% (730 nm) in the system while concentrations of SO and TE are kept constant (0.5%), the particle size could be reduced by a percentage of approximately 30%. A further increase of PL90H to 2.5% revealed a mean particle size of 400 nm which equals to a reduction by ca. 90%.

Table 3. Observed and predicted particle size and polydispersity index values of aqueous TE dispersions measured using Zetasizer, (Mean ± SD, *n* = 3). PD: pre-dispersion, PDI: polydispersity index.

Batch Code	Pattern	TE (wt %)	PL90H (wt %)	SO (wt %)	PD (nm)	Particle Size [nm]	Dv (d.nm)	Span	PDI	Predicted Particle Size (nm)	Predicted PDI
F1	111	0.5	0.5	0	2486 ± 379	1049 ± 176	D10: 93 D50: 510 D90: 769	1.3	0.7	1063	0.8
F2	112	0.5	0.5	0.3	1838 ± 405	1174 ± 365	D10: 33 D50: 407 D90: 642	1.5	0.8	1013	0.8
F3	113	0.5	0.5	0.5	1738 ± 220	1033 ± 160	D10: 54 D50: 392 D90: 547	1.3	0.8	981	0.8
F4	114	0.5	0.5	1	1988 ± 343	878 ± 292	D10: 82 D50: 690 D90: 930	1.2	0.7	898	0.7
F5	121	0.5	1	0	1147 ± 167	866 ± 215	D10: 61 D50: 451 D90: 748	1.5	0.7	930	0.7
F6	122	0.5	1	0.3	1968 ± 59	935 ± 39	D10: 85 D50: 554 D90: 788	1.3	0.7	881	0.7
F7	123	0.5	1	0.5	2982 ± 25	730 ± 114	D10: 36 D50: 72 D90: 403	5.1	0.7	848	0.7
F8	124	0.5	1	1	1127 ± 108	655 ± 48	D10: 76 D50: 429 D90: 596	1.2	0.7	766	0.7
F9	131	0.5	2.5	0	1799 ± 165	382 ± 35	D10: 58 D50: 299 D90: 554	1.7	0.5	533	0.5
F10	132	0.5	2.5	0.3	2420 ± 556	589 ± 36	D10: 415 D50: 678 D90: 1070	0.9	0.4	484	0.5
F11	133	0.5	2.5	0.5	1892 ± 253	525 ± 48	D10: 59 D50: 524 D90: 866	1.5	0.5	451	0.5
F12	134	0.5	2.5	1	3400 ± 390	400 ± 49	D10: 57 D50: 152 D90: 400	2.3	0.5	370	0.5

Dv: Size distribution by Volume; Span = $\frac{(D90 - D10)}{D50}$.

The whole model actual versus predicted plot with the details of ANOVA (p-value < 0.0001, R^2 of 0.86) in Figure 6 shows that all data points are close to the straight line, indicating that the plot is suitable, and the model fits well. The regression line and the 95% confidence curves crossed the horizontal line at the mean of the response (particle size (nm)). This implies that the whole factorial model with all combined effects (Figure 5) explains a significant proportion of the variation in particle size [50].

Furthermore, the constructed leverage plots in Figures 6–8 revealed that the factor that caused the most significant effect on reducing particle size was the PL90H concentration (p-value < 0.0001), followed by the SO (p-value < 0.085). In addition, the leverage plot for PL90H showed that both the regression line and the 95% confidence curves crossed the horizontal line; thus, the independent variable significantly influenced and contributed to variations of particle size.

Full model prediction equations for particle size and PDI including independent variables were found to be:

Particle size (nm) = 715.66 − 264.81 × (PL90H − 1.5) − 82.01 × ((SO − 0.5) / 0.5)

PDI = 0.63 − 0.13 × (PL90H − 1.5) − 0.025 × ((SO − 0.5) / 0.5).

Using the optimization and desirability function of the JMP software, it was predicted that a formulation consisting of 2.5% PL90H, 1% SO, and 0.5%TE allowed to achieve particle sizes as low as 370 nm and with a PDI of 0.5. This is in perfect accordance to our experimental results, where we measured for such an optimal formulation a particle size of 400 nm and a PDI of 0.5.

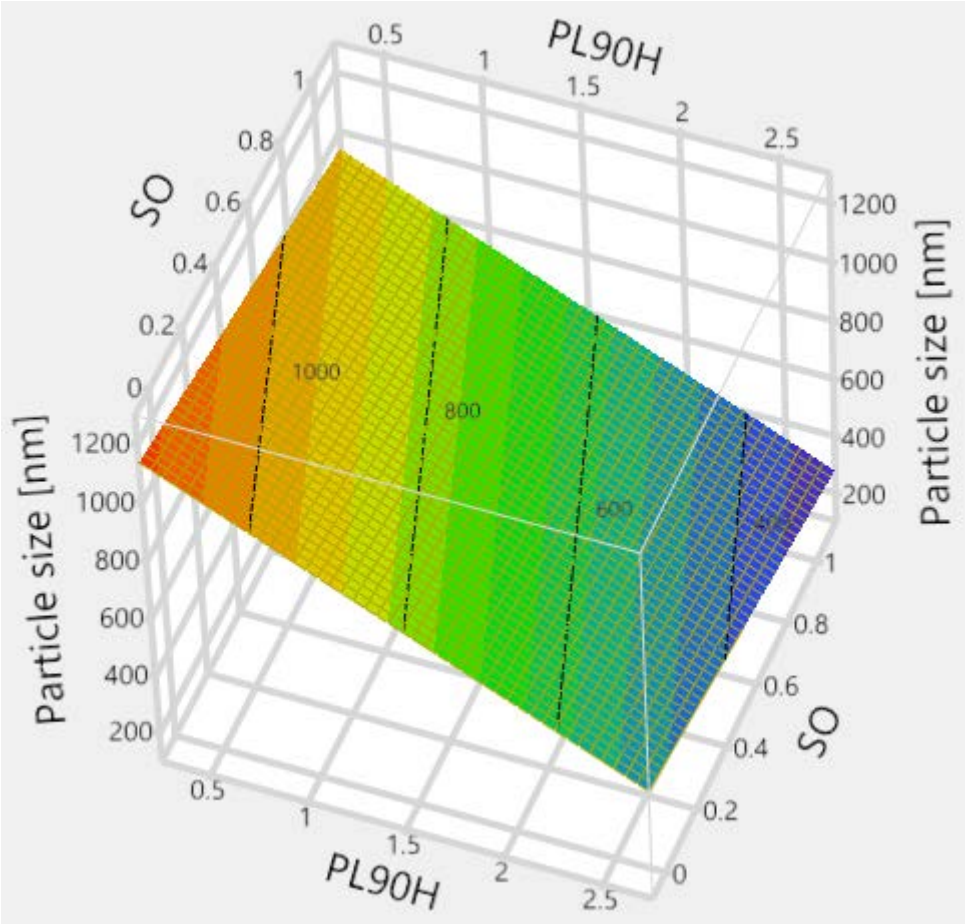

Figure 5. Effect of independent variables on particle size presented in 3D response surface.

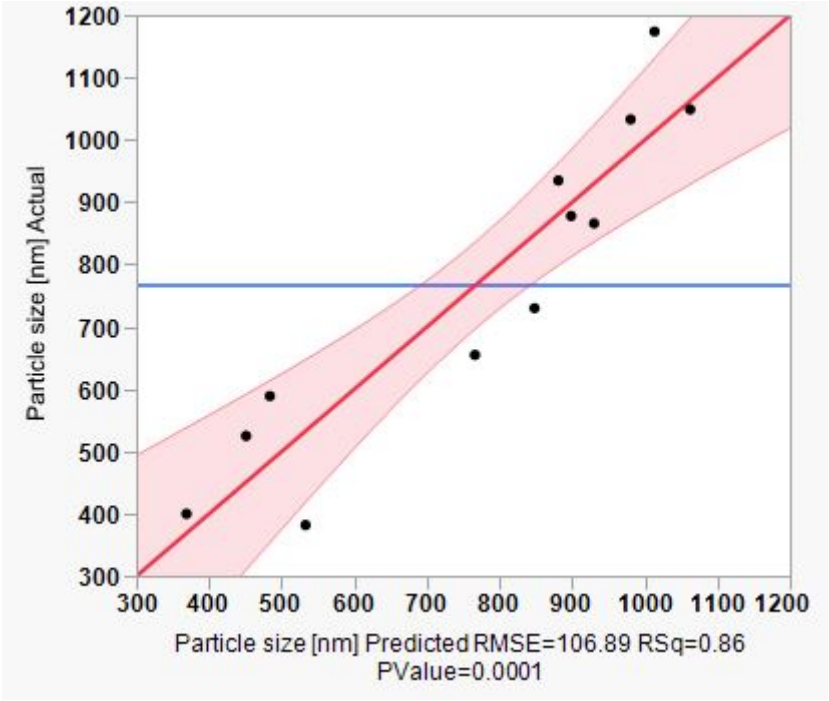

Figure 6. Leverage plot for the whole model of actual vs. predicted particle size.

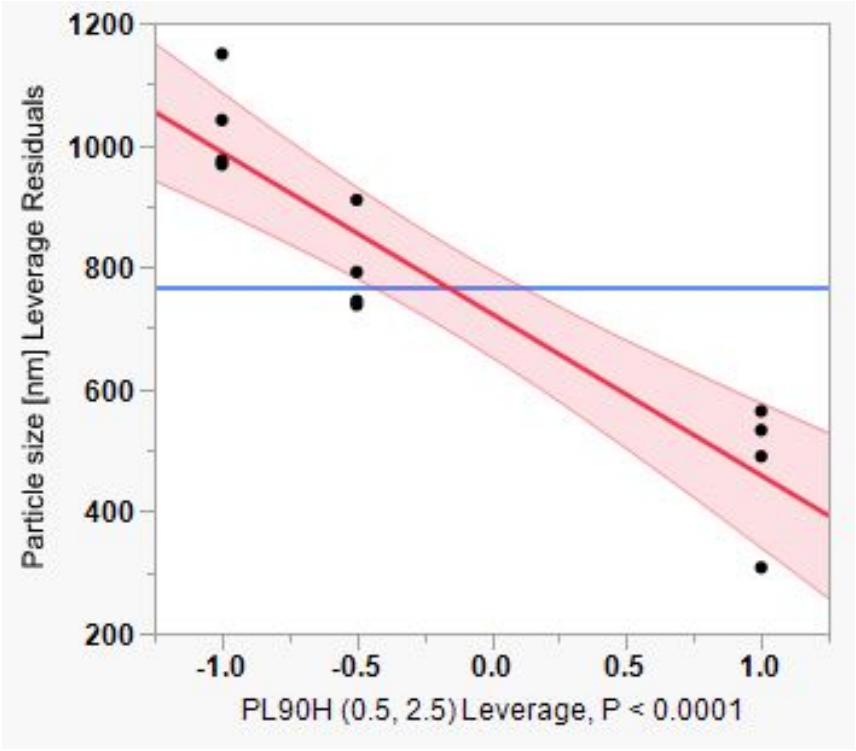

Figure 7. Leverage plot for Phospholipon 90H (PL90H).

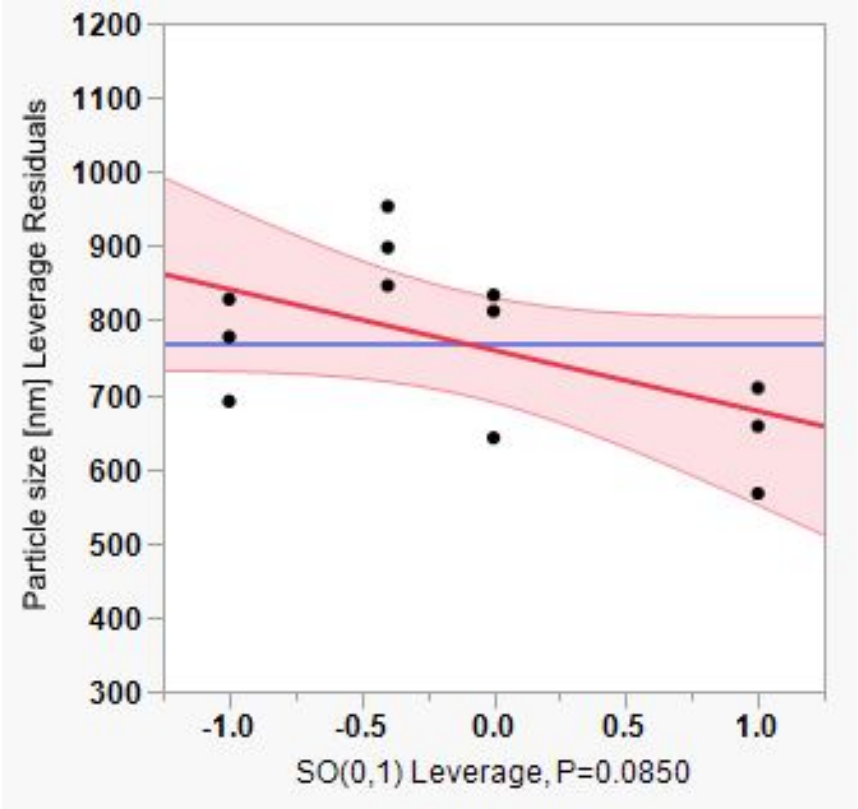

Figure 8. Leverage plot for sunflower oil (SO).

3.5 Conclusions

A suitable two-stage homogenization process was successfully developed to produce aqueous colloidal dispersions containing TE. The interfacial properties of the PL90H with its SO–TE dispersions were evaluated, and the results showed differences in terms of equilibrium interfacial tension and viscoelastic characteristics, clearly indicating an interaction of PL90H and TE. Confocal Raman spectral imaging allowed visualizing that the two lipophilic components namely, triterpene extract and sunflower oil, were predominantly co-located whereas hydrogenated PL was preferably detected at the oil/water interface. The characteristics of aqueous colloidal dispersions with varied phospholipid-to-sunflower oil ratio were evaluated through particle size measurement. The particle size produced was highly depending on the PL-to-oil ratio. Increasing the PL-to-oil ratio decreased significantly the mean particle sizes. The production of colloidal dispersions with particle sizes of below 1 µm was feasible, as it was our main goal. The optimal composition in the tested design space could be predicted by means of a statistic software.

Author Contributions: Conceptualization, F.K.M. and R.D.; Data curation, F.K.M.; Funding acquisition, F.K.M. and R.D..; Investigation, F.K.M.; Methodology, F.K.M. and R.D.; Project administration, R.D.; Supervision R.D.; Writing—original draft, F.K.M.; Writing—review and editing, R.D. Both authors have read and agreed to the published version of the manuscript.

Funding: This research was funded (PRC20170703) by the Phospholipid Research Center in Heidelberg, Germany.

Acknowledgments: The authors would like to thank Lipoid GmbH for the kind donation of the phospholipids.

Conflicts of Interest: The authors declare no conflict of interest.

3.6 References

1. Aiken, C.; Chen, C.H. Betulinic acid derivatives as HIV-1 antivirals*. Trends Mol. Med.* **2005**, *11*, 31–36.
2. Haque, S.; Nawrot, D.A.; Alakurtti, S.; Ghemtio, L.; Yli-Kauhaluoma, J.; Tammela, P. Screening and Characterisation of Antimicrobial Properties of Semisynthetic Betulin Derivatives*. PLoS ONE* **2014**, *9*, e102696.
3. Dehelean, C.A.; Soica, C.M.; Toma, C.-C.; Feflea, S.; Gruia, A.T.; Kasa, P., Jr. Antitumoral activity of betulin, a compound present in birch tree, in formulations with cyclodextrin*. Studia Univ. VgSer. St. Vietii* **2010**, *20*, 55–58.
4. Dehelean, C.A.; Şoica, C.; Ledeţi, I.; Aluaş, M.; Zupko, I.; Găluşcan, A.; Cinta-Pinzaru, S.; Munteanu, M. Study of the betulin enriched birch bark extracts effects on human carcinoma cells and ear inflammation*. Chem. Cent. J.* **2012**, *6*, 137–137.
5. Ebeling, S.; Naumann, K.; Pollok, S.; Wardecki, T.; Vidal-y-Sy, S.; Nascimento, J.M.; Boerries, M.; Schmidt, G.; Brandner, J.M.; Merfort, I. From a Traditional Medicinal Plant to a Rational Drug: Understanding the Clinically Proven Wound Healing Efficacy of Birch Bark Extract*. PLoS ONE* **2014**, *9*, e86147.
6. Metelmann, H.-R.; Podmelle, F.; Waite, P.D. Long-term cosmetic benefit of wound healing by betuline*. Am. J. Cosmet. Surg.* **2012**, *29*, 19–24.
7. Steinbrenner, I.; Houdek, P.; Pollok, S.; Brandner, J.M.; Daniels, R. Influence of the Oil Phase and Topical Formulation on the Wound Healing Ability of a Birch Bark Dry Extract*. PLoS ONE* **2016**, *11*, e0155582.
8. Färber, A.; Daniels, R. Ex vivo Skin Permeation of Betulin from Water-in-Oil Foams*. Ski. Pharmacol. Physiol.* **2016**, *29*, 250–256.
9. Laszczyk, M.; Jäger, S.; Simon-Haarhaus, B.; Scheffler, A.; Schempp, C.M. Physical, Chemical and Pharmacological Characterization of a New Oleogel-Forming Triterpene Extract from the Outer Bark of Birch (Betulae Cortex)*. Planta Med.* **2006**, *72*, 1389–1395.
10. Krasutsky, P.A. Birch bark research and development*. Nat. Prod. Rep.* **2006**, *23*, 919–942.
11. Jäger, S.; Laszczyk, M.N.; Scheffler, A. A preliminary pharmacokinetic study of betulin, the main pentacyclic triterpene from extract of outer bark of birch (Betulae alba cortex)*. Molecules* **2008**, *13*, 3224–3235.
12. Scheffler, A. The Wound Healing Properties of Betulin from Birch Bark from Bench to Bedside*. Planta Med.* **2019**, *85*, 524–527.
13. Mwiiri, F.K.; Brandner, J.M.; Daniels, R. Electrospun Bioactive Wound Dressing Containing Colloidal Dispersions of Birch Bark Dry Extract. *Pharmaceutics* **2020**, *12*, 770.
14. van Hoogevest, P.; Wendel, A. The use of natural and synthetic phospholipids as pharmaceutical excipients*. Eur. J. Lipid Sci. Technol.* **2014**, *116*, 1088–1107.
15. Pichot, R.; Watson, R.L.; Norton, I.T. Phospholipids at the Interface: Current Trends and Challenges*. Int. J. Mol. Sci.* **2013**, *14*, 11767–11794.

16. Van Nieuwenhuyzen, W. The industrial uses of special lecithins: A review. *J. Am. Oil Chem. Soc.* **1981**, *58*, 886–888.
17. Hasenhuettl, G.L.; Hartel, R.W. (Eds.) *Food Emulsifiers and Their Applications*; Springer: New York, NY, USA, 2008; pp. 1–9.
18. Cabezas, D.M.; Madoery, R.; Diehl, B.W.K.; Tomás, M.C. Emulsifying Properties of Different Modified Sunflower Lecithins. *J. Am. Oil Chem. Soc.* **2012**, *89*, 355–361.
19. Hildebrandt, E.; Nirschl, H.; Kok, R.J.; Leneweit, G. Adsorption of phospholipids at oil/water interfaces during emulsification is controlled by stress relaxation and diffusion. *Soft Matter* **2018**, *14*, 3730–3737.
20. Grandell, D.; Murtomäki, L. *Sur*face Pressure Control of Phospholipid Monolayers at the Water/1,2-Dichloroethane Interface. *Langmuir* **1998**, *14*, 556–559.
21. Shchipunov, Y.A.; Schmiedel, P. Phase Behavior of Lecithin at the Oil/Water Interface. *Langmuir* **1996**, *12*, 6443–6445.
22. Langevin, D. Influence of interfacial rheology on foam and emulsion properties. *Adv. Colloid Interface Sci.* **2000**, *88*, 209–222.
23. Güell, C.; Ferrando, M.; Trentin, A.; Schroën, K. Apparent Interfacial Tension Effects in Protein Stabilized Emulsions Prepared with Microstructured Systems. *Membranes* **2017**, *7*, 19.
24. Pan, L.G.; Tomás, M.C.; Añón, M.C. Oil-in-water emulsions formulated with sunflower lecithins: Vesicle formation and stability. *J. Am. Oil Chem. Soc.* **2004**, *81*, 241–244.
25. Amine, C.; Dreher, J.; Helgason, T.; Tadros, T. Investigation of emulsifying properties and emulsion stability of plant and milk proteins using interfacial tension and interfacial elasticity. *Food Hydrocoll.* **2014**, *39*, 180–186.
26. Henry, J.V.L.; Fryer, P.J.; Frith, W.J.; Norton, I.T. The influence of phospholipids and food proteins on the size and stability of model sub-micron emulsions. *Food Hydrocoll.* **2010**, *24*, 66–71.
27. Broniatowski, M.; Flasiński, M.; Wydro, P. Investigation of the interactions of lupane type pentacyclic triterpenes with outer leaflet membrane phospholipids—Langmuir monolayer and synchrotron X-ray scattering study. *J. Colloid Interface Sci.* **2012**, *381*, 116–124.
28. Abboud, R.; Charcosset, C.; Greige-Gerges, H. Tetra- and Penta-Cyclic Triterpenes Interaction with Lipid Bilayer Membrane: A Structural Comparative Study. *J. Membr. Biol.* **2016**, *249*, 327–338.
29. Sznitowska, M.; Janicki, S.; Dabrowska, E.; Zurowska-Pryczkowska, K. Submicron emulsions as drug carriers: Studies on destabilization potential of various drugs. *Eur. J. Pharm. Sci.* **2001**, *12*, 175–179.
30. Benita, S.; Levy, M.Y. Submicron emulsions as colloidal drug carriers for intravenous administration: Comprehensive physicochemical characterization. *J. Pharm. Sci.* **1993**, *82*, 1069–1079.

31. Fang, J.-Y.; Leu, Y.-L.; Chang, C.-C.; Lin, C.-H.; Tsai, Y.-H. Lipid Nano/Submicron Emulsions as Vehicles for Topical Flurbiprofen Delivery. *Drug Deliv.* **2004**, *11*, 97–105.
32. Klang, S.H.; Baszkin, A.; Benita, S. The stability of piroxicam incorporated in a positively-charged submicron emulsion for ocular administration. *Int. J. Pharm.* **1996**, *132*, 33–44.
33. Aviv, H.; Friedman, D.; Bar-Ilan, A.; Vered, M. Submicron Emulsions as Ocular Drug Delivery Vehicles. Google Patents US5496811A, 1996,03-05.
34. Youenang Piemi, M.P.; Korner, D.; Benita, S.; Jean-Paul, M. Positively and negatively charged submicron emulsions for enhanced topical delivery of antifungal drugs. *J. Control. Release* **1999**, *58*, 177–187.
35. Rubinstein, A.; Pathak, Y.V.; Kleinstern, J.; Reches, A.; Benita, S. In Vitro Release and Intestinal Absorption of Physostigmine Salicylate from Submicron Emulsions. *J. Pharm. Sci.* **1991**, *80*, 643–647.
36. Schwarz, J.S.; Weisspapir, M.R.; Friedman, D.I. Enhanced Transdermal Delivery of Diazepam by Submicron Emulsion (SME) Creams. *Pharm. Res.* **1995**, *12*, 687–692.
37. Sznitowska, M.; Dabrowska, E.A.; Janicki, S. Solubilizing potential of submicron emulsions and aqueous dispersions of lecithin. *Int. J. Pharm.* **2002**, *246*, 203–206.
38. Cortés-Muñoz, M.; Chevalier-Lucia, D.; Dumay, E. Characteristics of submicron emulsions prepared by ultra-high pressure homogenisation: Effect of chilled or frozen storage. *Food Hydrocoll.* **2009**, *23*, 640–654.
39. Sjöström, B.; Bergenståhl, B.; Kronberg, B. A method for the preparation of submicron particles of sparingly water-soluble drugs by precipitation in oil-in-water emulsions. II: Influence of the emulsifier, the solvent, and the drug substance. *J. Pharm. Sci.* **1993**, *82*, 584–589.
40. Rott, C. Herstellung und Charakterisierung Betulinhaltiger Zubereitungen für Berührungsempfindliche Haut. Ph.D. Thesis, University of Tuebingen, Tuebingen, Germany, 2016.
41. Miller, R.; Ferri, J.K.; Javadi, A.; Krägel, J.; Mucic, N.; Wüstneck, R. Rheology of interfacial layers. *Colloid Polym. Sci.* **2010**, *288*, 937–950.
42. Javadi, A.; Mucic, N.; Karbaschi, M.; Won, J.; Lotfi, M.; Dan, A.; Ulaganathan, V.; Gochev, G.; Makievski, A.; Kovalchuk, V. Characterization methods for liquid interfacial layers. *Eur. Phys. J. Spec. Top.* **2013**, *222*, 7–29.
43. Miller, R.; Wüstneck, R.; Krägel, J.; Kretzschmar, G. Dilational and shear rheology of adsorption layers at liquid interfaces. *Colloids Surf. A Physicochem. Eng. Asp.* **1996**, *111*, 75–118.
44. Heck, R.; Hermann, S.; Lunter, D.J.; Daniels, R. Film-forming formulations containing porous silica for the sustained delivery of actives to the skin. *Eur. J. Pharm. Biopharm.* **2016**, *108*, 1–8.
45. Li, J.B.; Kretzschmar, G.; Miller, R.; Möhwald, H. Viscoelasticity of phospholipid layers at different fluid interfaces. *Colloids Surf. A Physicochem. Eng. Asp.* **1999**, *149*, 491–497.

46. Flasiński, M.; Hąc-Wydro, K.; Broniatowski, M. Incorporation of Pentacyclic Triterpenes into Mitochondrial Membrane—Studies on the Interactions in Model 2D Lipid Systems. *J. Phys. Chem. B* **2014**, *118*, 12927–12937.
47. Sommerling, J.-H.; de Matos, M.B.C.; Hildebrandt, E.; Dessy, A.; Kok, R.J.; Nirschl, H.; Leneweit, G. Instability Mechanisms of Water-in-Oil Nanoemulsions with Phospholipids: Temporal and Morphological Structures. *Langmuir* **2018**, *34*, 572–584.
48. Opawale, F.O.; Burgess, D.J. Influence of Interfacial Rheological Properties of Mixed Emulsifier Films on the Stability of Water-in-Oil-in-Water Emulsions*. J. Pharm. Pharmacol.* **1998**, *50*, 965–973.
49. Tsuchiya, H. Membrane interactions of phytochemicals as their molecular mechanism applicable to the discovery of drug leads from plants. *Molecules* **2015**, *20*, 18923–18966.
50. Proust, M. *JMP, Introductory Guide*. SAS Statistical Software: Cary, NC, USA, 2007.

4 Chapter 4: Electrospun Bioactive Wound Dressing Containing Colloidal dispersions of Birch Bark Dry Extract.

Francis Kamau Mwiiri [1], Johanna M. Brandner [2] and Rolf Daniels [1] *

[1] Department of Pharmaceutical Technology, Eberhard Karls University, Auf der Morgenstelle 8, 72076 Tuebingen, Germany

[2] Department of Dermatology and Venerology, University Hospital Hamburg-Eppendorf, Martinistraße 52, 20246 Hamburg, Germany

Reprinted from Pharmaceutics 2020, 12(8), 770; Special Issue: Recent Development of Electrospinning for Drug Delivery Volume II

DOI: 10.3390/pharmaceutics12080770

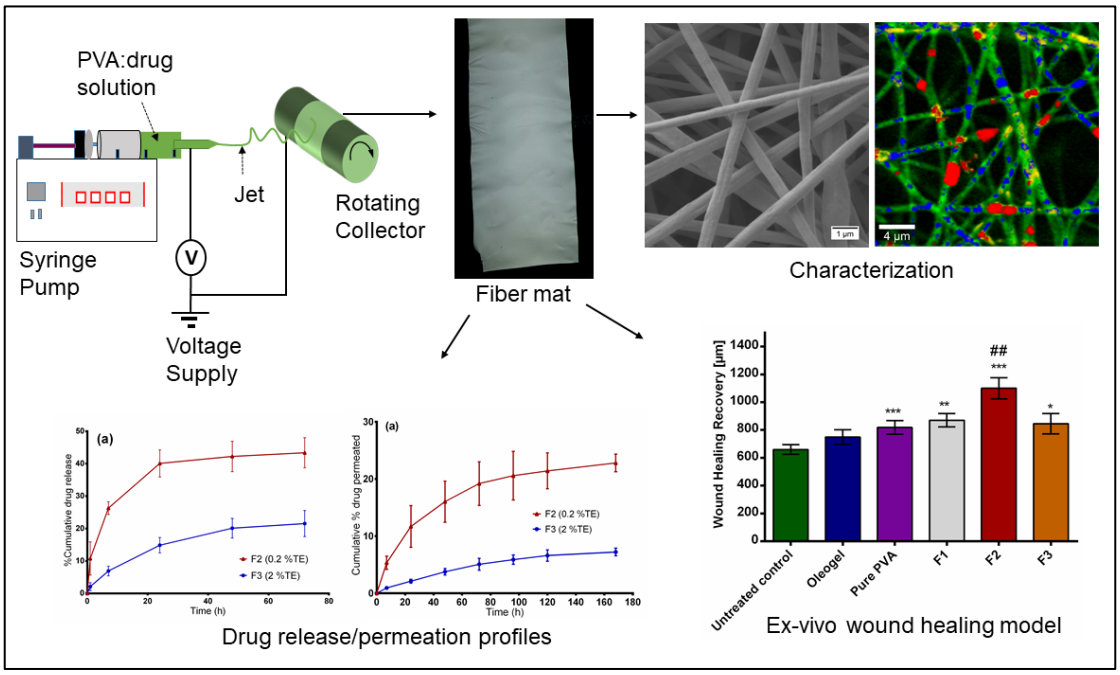

Graphical Abstract

4.1 Abstract

Novel birch bark dry extract (TE)-loaded polyvinyl alcohol (PVA) fiber mats intended for wound therapy were developed through an electrospinning process. Colloidal dispersions containing TE as the active substance were prepared by the high-pressure homogenization (HPH) technique using hydrogenated phospholipids as stabilizer. Subsequently, the colloidal dispersions were blended with aqueous PVA solutions in the ratio of 60:40 (wt.%) and electrospun to form the nanofiber mats. Fiber morphology examined using scanning electron microscopy (SEM) indicated that fibers were uniform and achieved diameters in the size range of 300–1586 nm. Confocal Raman spectral imaging gave good evidence that triterpenes were encapsulated within the electrospun mats. In vitro drug release and ex vivo permeation studies indicated that the electrospun nanofibers showed a sustained release of betulin, the main component of birch bark dry extract, making the examined dressings highly applicable for several wound care applications. Ex vivo wound healing studies proved that electrospun fiber mats containing TE accelerated wound healing significantly more than TE oleogel, which was comparable to an authorized product that consists of TE and sunflower oil and has proved to enhance wound healing. Therefore, our results conclude that the developed TE-PVA-based dressings show promising potential for wound therapy, an area where effective remedy is needed.

Keywords: electrospinning; PVA; birch bark extract, wound dressing; phospholipids

4.2 Introduction

The human skin serves as a barrier between the body and the environment. Therefore, it is prone to microbial, thermal, mechanical, and chemical threats, which can cause acute or chronic wounds. Triterpenes have been shown to improve wound healing recovery by inducing cell migration, cell proliferation, and collagen deposition [1]. Outer birch bark extracts have a high content of triterpenes, which are known for various pharmacological properties such as anti-inflammatory, antimicrobial, antiviral, anticancer activity, and wound healing effects [2–10]. A well characterized commercially used triterpene dry extract from the outer bark of birch (TE) contains about 80% (*w/w*) betulin as the main component and is obtained by accelerated solvent extraction with n-heptane [11]. Other disclosed triterpenes of the dry extract include lupeol (LU), erythrodiol (ER), betulinic acid (BA), and oleanolic acid (OA) as shown in Table 1 [12]. However, the low solubility of these triterpenes in polar and nonpolar solvents may lead to a poor bioavailability, which might limit their therapeutic application [8,13].

A study conducted by Ebeling et al. showed the molecular mechanism of the effects of birch bark extract on wound healing properties in human primary keratinocytes and porcine ex vivo wound healing models. They showed that TE and betulin mainly accelerated reepithelialization in a porcine ex vivo wound healing model after wound

treatment with TE-oleogel (10% TE, 90% sunflower oil). Beyond that, they found out that TE led to upregulation of proinflammatory mediators such as COX-2 and IL-6, which play a key role in wound healing und epidermal barrier repair [6,14]. Additionally, the effects of TE-based formulations have been already investigated in vivo on different types of wounds including dystrophic epidermolysis bullosa where treatments promote wound healing and was found out to be safe and well tolerated [15–17]. It is good to note that TE together with sunflower oil (SFO) supports wound healing better than in combination with other oils as examined by Steinbrenner et al. [8]. At the moment, there are a few available topical formulations containing these triterpenes, including water-in-oil foams [9], cosmetic water-in-oil creams, and an oleogel consisting of TE and sunflower oil that received European marketing authorization in January 2016 [18].

Table 1. Physicochemical characteristics of the dry birch bark extract used [**9**].

TE Composition	Specific surface area	Particle size D50%
Betulin 81.60%, lupeol 2.08%, betulinic acid 3.84%, erythrodiol 1.05%, oleanolic acid 0.97%, Betulinic acid methyl ester 0.52%, unidentified substances 9.94%	42 ± 0.4 m^2/g	5.8 µm

The electrospinning technique is a simple and versatile process for preparing fibers having a diameter from few micrometers down to several nanometers [19,20]. The resulting nanofibers have special features, such as high surface area to volume ratio, and can form mats/fleeces with high porosity which makes them attractive materials for wound dressing [21,22]. Beyond that, electrospun fibrous scaffolds mimic the structure of the native extracellular matrix (ECM) and hence facilitate cell proliferation, improve gaseous exchange, removal of exudate, and act as a physical barrier against entry of microorganisms during wound healing and regeneration of damaged tissues [21, 23–26].

Polymeric nanofibers made from biodegradable and biocompatible synthetic or natural polymers have been utilized to develop drug delivery systems to treat various ailments. One of the potential areas to use them is medicated wound dressing [21,23]. PVA is a biocompatible and biodegradable hydrophilic polymer with good chemical and mechanical properties, and has been approved by the U. S. Food and Drug Administration (FDA) for different biomedical and pharmaceutical applications [27,28]. For instance, PVA has been used to create hydrogels for wound dressing [29] or electrospun together with active substances, such as silver nanoparticles [30], and curcumin [31], to produce wound dressings. Several wound dressings in the market containing active agents such as hydrocolloids or silver dressings often used on wound healing have shown negative effects such as allergic contact dermatitis [32], and use of dressings loaded with antibiotics has risk of developing antimicrobial resistance [33]. Our interest in this study is to develop a dressing loaded with birch bark extract with a sustained drug release that is suitable for human use on wound healing with effective therapy even after long-term usage. To satisfy this requirement, we ensured that all the components used in this study are biocompatible and biodegradable when applied to the human body, such that an invasive and/or traumatic intervention for dressing

removal, like in the case of deep wounds, is unnecessary. Furthermore, sustained drug release could lead to less frequent dressing changes, which are painful, especially in treatment of chronic wounds, and thereby resulting in better patient compliance. In addition to that, our concept allows one to avoid organic solvents and uses water as the only solvent throughout the whole processing of the wound dressing. This guarantees not only that the solvent is nontoxic and affordable, but also that it is eco-friendly and can thus be regarded as green electrospinning. However, encapsulation of birch bark dry extract into nanofibers may present a challenge. For instance, earlier studies showed that due to their unique structure, the particle sizes of the dry extract cannot be grinded by common techniques to reach sufficiently small particles even when high energy dispersion techniques, e.g., sonication or high-pressure homogenization, were used with aqueous and organic suspensions of the material [34]. This was solved through processing of oil in water (O/W) colloidal dispersions with birch bark dry extract as the active substance, phospholipids as stabilizer, sunflower oil, and the water phase through a step-wise homogenization process. Hydrogenated soybean phosphatidylcholine (HSPC) types of phospholipids containing mainly esterified stearic and palmitic acid enhanced the producibility of colloidal dispersions with particle sizes < 1 µm and enabled miscibility and stabilization of the lipophilic components in the hydrophilic PVA matrix prior to electrospinning.

The purpose of this study was to (1) develop wound dressing materials with incorporated colloidal dispersions of TE and to (2) study their efficiency related to wound healing performance and (3) drug release. The surface properties of electrospun fiber mats were characterized by using SEM, thermal analysis with differential scanning calorimetry (DSC) and confocal Raman spectral imaging for visualization of all components within the fiber mats. We also conducted ex vivo permeation and in vitro release studies using Franz diffusion cell. The efficacy of the developed wound dressings was evaluated through an ex vivo wound healing assay. Here, low and highly TE-loaded dressings were tested and compared to an oleogel similar to the authorized product. To the best of our knowledge, there are no reports focusing on the development of this kind of wound dressing; therefore, this will be the first polymer-based wound dressing containing birch bark dry extract aimed for future potential use in wound therapy.

4.3 Materials and methods

4.3.1 Materials

PVA with a molecular weight of 146–186 kDa was purchased from Sigma Aldrich (Steinheim, Germany), hydrogenated phospholipids from soybean lecithin (Phospholipon 90 H) were supplied by Lipoid GmbH (Ludwigshafen, Germany). SO was purchased from Caesar & Loretz GmbH (Hilden, Germany). Birch bark extract was obtained from Amryt AG (Niefern-Öschelbronn, Germany). Reverse osmosis water (ELGA Labwater, Celle, Germany) was used for the preparation of all solutions. Parafilm® was from Bemis Company Inc., (Oshkosh, WI, USA). Whatman Nuclepore polycarbonate membrane filters were purchased from Sigma-Aldrich (Steinheim, Germany). Pig ears for permeation studies were obtained from the Department of Experimental Medicine at the University of Tuebingen [35] and for wound healing studies from a slaughterhouse in Schleswig-Holstein after slaughtering the pigs for human consumption.

4.3.2 Preparing the Colloidal Dispersions

Three different dispersions were prepared with varying concentrations of TE as shown in Table 2. Dispersions 1 and 2 (D1 and D2) were necessary to investigate the impact of high or low TE concentration on wound healing, whereas dispersion 3 (D3) was used as a placebo. It is important to mention that it was only practically possible to produce dispersions consisting of high TE (5%) loading by use of high concentrations of PL90H (8%). That is why 8% PL90H was used in preparation of dispersion consisting 5% TE. Dispersion containing 2.5% PL90H was the optimized colloidal dispersion from our previous study. Briefly, during preparation of each formulation, a predispersion was prepared by first dispersing Phospholipon 90H (PL90H) and TE in water at 70 °C for 30 min under magnetic stirring at 400 rpm using Heidolph MR 3001 K magnetic hotplate stirrer (Schwabach, Germany). Then, this mixture was homogenized for 5 min using a rotor-stator system (Ultra Turrax T25, IKA, Staufen, Germany), at 9500 rpm. Thereafter, the formed dispersion was added into the SO and homogenized for 3 min. Finally, the predispersion was homogenized using a high-pressure homogenizer (Emulsiflex C-3, Avestin, Mannheim, Germany) for eight cycles at a pressure of 100 MPa and their particle sizes measured with a Zetasizer Nano-ZS (Malvern Instruments, Herrenberg, Germany).

Table 2. Composition (wt.%) of the prepared aqueous dispersions with their particle sizes.

Dispersion	Composition	Particle Size (nm)
D1	2.5% PL90H, 1% SO and 0.5% TE	400 ± 49
D2	8% PL90H, 10% SO and 5% TE	840 ± 17
D3	8% PL90H, 10% SO and 0% TE	477 ± 58

4.3.3 Preparation of Electrospinning Solutions

The 12 wt.% PVA solution was prepared by dissolving PVA in water at 90 °C under magnetic stirring for 5 h. The solution was allowed to cool to room temperature and used the following day. Subsequently, for colloidal dispersion-PVA electrospinning experiments, the above aqueous dispersions (D1–D3) were blended with a PVA polymer solution in the ratio of 60:40 using a magnetic stirrer for 2 h at 40 °C to form a homogeneous solution. Samples were then cooled down to room temperature prior to electrospinning.

4.3.4 Electrospinning of nanofibers

The electrospinning setup purchased from Nanolab Instruments Sdn. Bhd., Subang Jaya, Malaysia consisted of a syringe pump holding a 5 mL plastic syringe with a blunt-end needle (18-gauge), a grounded rotating collector, and a high-voltage power supply. Electrospun fibers were prepared from solutions and dispersions as listed in Table 3. Pure polymer solution serves as a reference mainly for the physicochemical characterization. F1 represents the placebo formulation. F2 and F3 were chosen to investigate the effect of high and low TE concentration. The syringe was filled with the solution and electrospun at a target collector distance of 10 cm and an applied voltage of 15 kV. Solutions were pumped through the syringe at a flow rate of 0.5 mL/h and the rotating speed of the collector was fixed at 1000 rpm. All electrospinning studies were carried out at ambient temperature (24 °C) and a relative humidity of 45%.

Table 3. Final composition (wt.%) of formulation blends for electrospinning.

Component	Formula 1 (F1) [%]	Formula 2 (F2) [%]	Formula 3 (F3) [%]
PVA	7.2	7.2	7.2
PL90H	3.2	1	3.2
Sunflower oil	4	0.4	4
TE	-	0.2	2
Purified water	ad 100	ad 100	ad 100

4.3.5 Characterization of Nanofiber Morphology

Fiber morphology was analyzed through SEM, Zeiss DSM 940 A, (Carl Zeiss GmbH, Oberkochen, Germany). Fiber mats of 0.5 cm × 0.5 cm sizes were placed of a conductive double-sided tape and sputter coated with gold using Biorad E 5100 Sputter Coater (Bio-Rad GmbH, Munich, Germany) at 2.1 kV and 20 mA for 240 s and imaged using the microscope. Thereafter, the average fiber diameters were determined from the SEM images by randomly selecting a minimum of 30 segments and their diameters calculated using ImageJ software (National Institute of Health, Bethesda, MD USA). For fiber diameter distribution, numbers of fiber diameters were converted into their percentage total values and plotted against grouped fiber diameter. The thicknesses of the fiber mats were measured with a digital micrometer using both magnetic induction and eddy current methods (Dualscope FMP20, Helmut Fischer GmbH,

Sindelfingen Germany) taking the average of 15 measurements at randomly selected places.

4.3.6 Confocal Raman Spectral Imaging

Raman images of wound dressings were acquired using an alpha 500R Raman microscope (WiTec GmbH, Ulm, Germany) equipped with a DV401-BV charge coupled device (CCD) detector, connected via an optical fiber to a UHTS 300 spectrometer and a 532 nm laser excitation source. A 100× air objective (EC Epiplan-Neofluor, Carl Zeiss, Oberkochen, Germany) with a numerical aperture of 0.9 was used to view the sample while the laser intensity was adjusted to 35 mW. The spectral range covered the fingerprint region between 710 and 1820 cm^{-1} and region between 2700 and 3580 cm^{-1}. Spectra of all single components (PL90H, SO, PVA and TE) were first collected and used to monitor the presence of each component in the wound dressing. Subsequently, nanofiber mats were presented to the microscope on glass slides (VWR-International, Darmstadt, Germany) without the use of a coverslip. Image scans of wound dressings using 25 µm × 25 µm area of the surface were taken at an integration time of 0.01 s. Henceforth, color-coded images were obtained by initial cosmic ray removal and spectral background subtraction using the WiTec Project data analysis software 4.1 (WITec GmbH, Ulm, Germany, 2016). By assigning the spectrum of each component to a color, the distribution of all components within the formulation can be indicated, resulting in a color-coded image of the scanned area [36].

4.3.7 Differential Scanning Calorimetry (DSC)

Differential scanning calorimetry (DSC) studies of the produced nanofiber mats were carried out using a DSC 820 differential scanning calorimeter (Mettler-Toledo GmbH, Gießen, Germany). The DSC was calibrated for temperature and enthalpy using indium as a standard. Samples of 4–7 mg were sealed in an aluminium pan with one pinhole in the lid. The furnace was purged with nitrogen at a flow rate of 80 mL/min. The DSC scans were obtained by heating in the range of 25-250 °C at a rate of 10 °C/min.

4.3.8 Skin Permeation and In Vitro Drug Release Studies

Both permeation and release studies were performed using modified vertical Franz diffusion cells (Gauer Glas, Püttlingen, Germany) with a receptor volume of 12 mL. For in vitro release studies, synthetic polycarbonate membranes with a pore size diameter of 0.4 µm were used to separate donor and receptor compartments. For permeation studies, pig ears were obtained from the Department of Experimental Medicine of the University Hospital Tuebingen. The live animals were kept at the Department of Experimental Medicine and sacrificed during their experiments, with the approval of the ethics committee of the University Hospital Tuebingen. The ears were delivered directly after the death of the animals. The Department of Pharmaceutical Technology is registered for the use of animal products at the District Office of Tuebingen (registration number: DE 08 416 1052 21). Fresh pig ears were first cleaned with

isotonic saline using cotton balls and after postauricular skin excision, they were wrapped in aluminium foil and stored at −30 °C until use. During the day of experiment, the skin samples were thawed at room temperature, skin strips of 3 cm width were made and pinned to a block of Styrofoam precovered with aluminium foil. Thereafter, wounded skin samples were prepared according to [9] by a skin grafting method using a Dermatom (Dermatom GA 630, Aesculap AG & Co. KG, Tüttlingen, Germany). The skin was first "wounded" through removal of the outermost layers of the skin with a thickness of 0.2 mm using Dermatom. Subsequently, the remaining skin was then dermatomed to a thickness of 0.4 mm. From the prepared porcine skin, a specimen was punched to obtain discs of 25 mm in diameter using a circular hole punch (Eduard Gottfried Ferne, Remscheid, Germany) [37].

The synthetic membrane/dermal porcine skin was mounted between the compartments of diffusion cells, and the effective diffusion area was 1.77 cm^2. For both in vitro release and ex vivo permeation experiments studies, samples of 20 mg fiber mats (F2 and F3), exactly weighed, were used. Consequently, all samples were loaded in the donor compartments and covered with parafilm to prevent solvent evaporation. A mixture of ethanol and water, 50:50 (*v/v*), was used as the receptor medium and the diffusion cells were maintained at 32 °C under constant magnetic stirring at 500 rpm. At predetermined time intervals, samples of 1 mL were taken from the receptor compartment and replaced with the same volume of fresh prewarmed receptor medium to maintain sink condition. The samples removed were analyzed directly using the HPLC-UV method as described below. The experiments were conducted in triplicate.

4.3.9 Entrapment Efficiency

The amount of betulin entrapped within fiber mats was estimated by dissolving approximately 20 mg of electrospun fiber mat, exactly weighed, in 30 mL ethanol:water (50:50 *v/v*) solution by means of sonication at 65 °C (Sonorex RK 31H, Bandelin, Berlin). Samples were then filtered using hydrophilic polyethersulfone (PES) syringe filters (Macherey-Nagel, Düren, Germany), and the total amount of drug extracted was quantified by High Performance Liquid Chromatography with Ultraviolet detection (HPLC-UV). The percentage entrapment efficiency (%EE) was calculated by the following equation:

$$\% \text{ EE} = \frac{\text{Total mass of drug extracted from nanofiber}}{\text{Mass of total drug added}} \times 100\% \quad (4)$$

4.3.10 Betulin Permeation/Release Kinetics Studies

The release/permeation kinetics were estimated by linear regression analysis of the in vitro release and ex vivo permeation data using various mathematical models [38]. The four models included zero order (Equation 2), first order (Equation 3), Korsmeyer–Peppas (Equation 4), and Higuchi (Equation 5) and the mathematical model that best fitted the kinetic release profile was selected based on the highest coefficient of

determination, R^2. In all equations, M_t represents the amount of betulin released at time t.

Zero-order model, where k_0 is the zero-order release constant:

$$M_t = k_0 t \quad (5)$$

First order model where K_1 is the first order release rate constant:

$$\ln (1 - M_t) = -K_1 t \quad (6)$$

Korsmeyer–Peppas model: $Mt = kt^n$; where K is the Korsmeyer–Peppas constant, which is connected to the characteristics of the delivery system and the encapsulated drug. The n is the diffusional exponent that shows the drug release mechanism; where *n* equal to 0.45 represents a Fickian diffusion mechanism and $0.45 < n < 1$ is referred to as a non-Fickian diffusion mechanism (anomalous transport) in which both Fickian diffusion and Case-II transport occurs [39]. (4)

Higuchi model, where k is Higuchi constant:

$$Mt = kt^{0.5} \quad (5)$$

4.3.11 HPLC Analysis

Betulin quantification was performed using an LC-20A prominence HPLC system (Shimadzu, Kyoto, Germany). The mobile phase, a mixture of acetonitrile and water with the addition of 0.1% (*v/v*) phosphoric acid, was used as a gradient system for chromatographic separation. For efficient separation, gradient conditions were used according to the isocratic/gradient modes developed by Armbruster et al. [40]. A Nucleosil 100-5 C18 EC 125/4 column with a precolumn Universal RP EC 4/3 (Macherey-Nagel, Düren, Germany) was kept at 40 °C and a flow rate of 1.2 mL/min was used. A sample volume of 100 µL was injected and the peaks were detected at 210 nm. The retention time of betulin was approximately 7.5 min.

4.3.12 Ex Vivo Wound Healing Assay

In order to characterize the wound healing efficiency, a porcine ex-vivo wound healing assay was performed as described elsewhere [8]. Briefly, pig ears were immediately delivered after slaughtering for human consumption to the laboratory, cleaned, and disinfected. Thereafter, 6 mm punch biopsies were taken from the plicae of the ears and fat and subcutis were removed. Consequently, wounds were generated by the removal of the epidermis and upper dermis in a central area of 7.1 mm^2. Then, the so formed ex vivo wound healing model was placed dermis-down on gauze in culture dishes and incubated at the air–liquid interface with Dulbecco's modified Eagle´s medium supplemented with hydrocortisone, 2% fetal calf serum, penicillin, and streptomycin. The tested sample groups were divided into six groups (n = 10): (i) untreated control, (ii) TE-oleogel, (iii) pure PVA mat (iv) F1, (v) F2, and (vi) F3 fiber

mats. Subsequently, sections of the electrospun fiber mats (4 mm in diameter)/5 µL of the oleogel were immediately applied after wounding, and the models were incubated for 48 h at 37 °C and 5% CO_2. Further steps involved shock freezing, preparations of cryostat sections of the central parts of the wound healing models, and staining with hematoxylin and eosin. Wound healing progress (reepithelialization) was assessed by measuring the distance between the wound margin and the tip of the regenerated epidermis using a Leica DMLS microscope (10 ×), a Leica MC 170 HD CCD camera, and the Leica LAS V4.9 software (Leica, Wetzlar, Germany, 2017). Means of left and right wound margins were calculated.

4.3.13 Statistical Analysis

All the experiments unless mentioned otherwise were carried out in triplicate and the results were expressed as mean ± standard deviation (mean ± SD). Statistical analysis of the acquired data was performed by Student's *t*-test and analysis of variance (ANOVA). *p*-value less than 0.05 was considered statistically significant, and where significance has been proven, it is indicated by *$p < 0.05$, **$p < 0.01$, and ***$p < 0.001$.

4.4 Results and Discussion

4.4.1 Fiber Preparation and Morphological Characterization Using SEM

Preparation of the electrospun fibers building the wound dressing mats followed the optimized protocol as given in section 2.4. In our previous preliminary studies, we varied all typical parameters that might have an impact on the fiber's properties. Parameters investigated included (1) flow rate, which was varied between 0.1, 0.5, and 2 mL/h, (2) needle tip-to-collector distances were in range of 5, 10, and 20 cm, (3) speed of the collector was fixed at 1000 rpm, and (4) voltage was varied at 7, 15, and 20 kV. The electrospinning parameters used to manufacture fiber mats as highlighted in Section 2.4 were optimized to a flow rate of 0.5 mL/h, needle tip-to-collector distance of 10 cm, and an applied voltage of 15 kV.

Figure 1 shows SEM images of the electrospun wound dressings and the correspondingly measured fiber diameters. Pure PVA fiber mats had a thickness of about 51.67 ± 4.9 µm, F1 of 100 ± 9.09 µm, F2 of 39.59 ± 3.4 µm, and F3 exhibited the highest thickness of 110 ± 5.4 µm. Pure PVA electrospun fibers were randomly oriented with smooth surface and a few interconnected web-like structures in several points, while their fiber diameter ranged from approximately 750 to 1600 nm. The fiber diameter of F1 was between 390 and 600 nm without formation of beads. F2 fibers were observed as smooth and uniform with fiber diameters of 340 to 500 nm without beads. On the other hand, F3 fibers were observed as uniform but rough surfaces with presence of interconnected beads and their fiber diameter ranged from 350 to 900 nm.

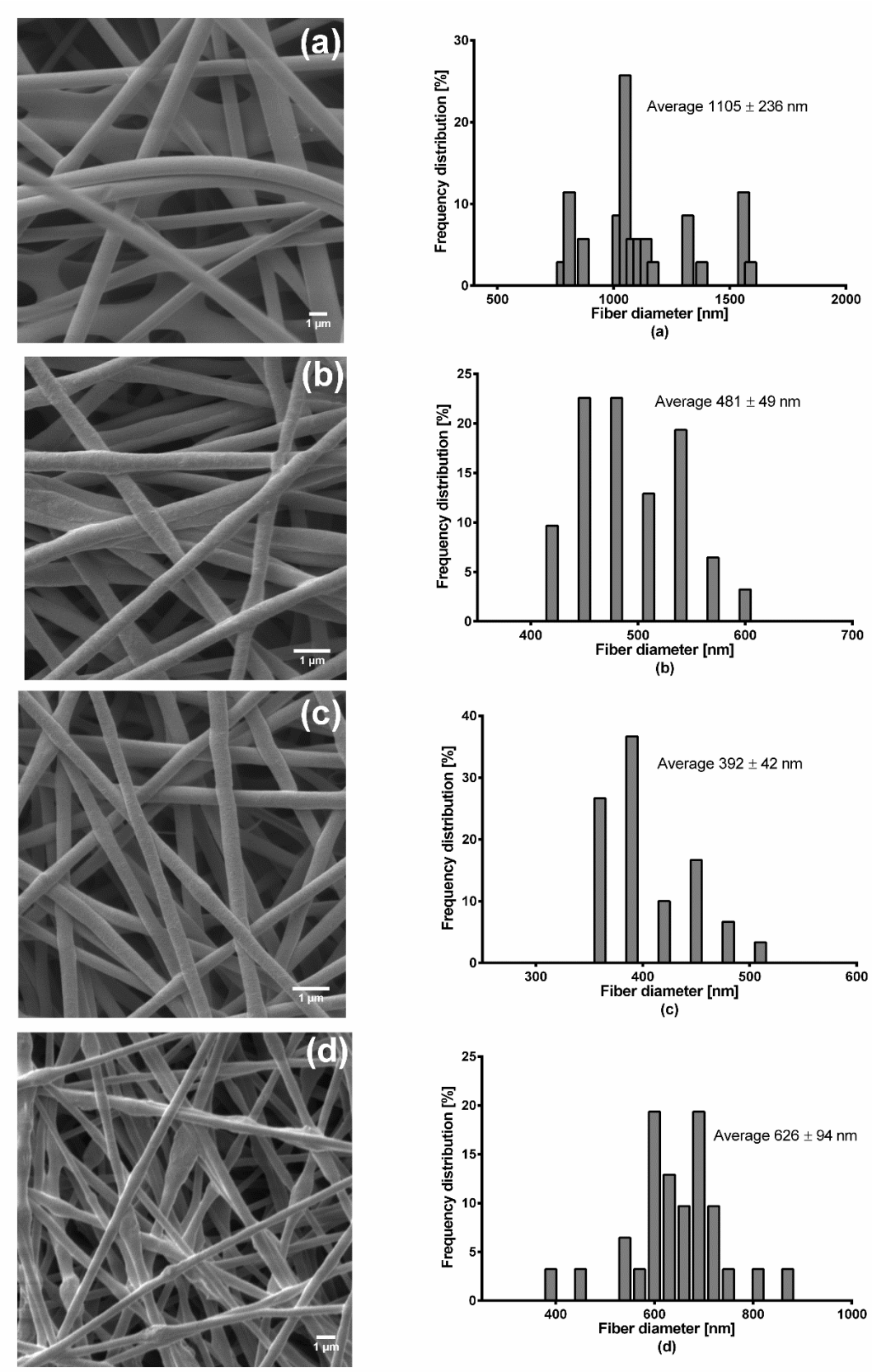

Figure 1. SEM micrographs and fiber diameter distribution of (**a**) pure PVA, (**b**) F1 (**c**) F2, and (**d**) F3 electrospun fiber mats.

The results clearly show that not only the morphology of electrospun fibers, but also the resulting fiber diameter was changed after PVA was blended with the aqueous dispersions. In general, the addition of colloidal dispersions resulted in a decrease of the average fiber diameter due to the reduced viscosity of polymeric solutions shown in Figure 2. However, the increase of TE concentration in the mixture influenced the structure of the fibers, and the average diameter of the nanofibers also increased (Table 4). The observed web-like interconnected structures/beads were due to high viscosity, which caused resistance to jet stretching during the electrospinning process. In addition, it was very difficult to process F3 with a high amount of TE (2%) because unstable Taylor cone and discontinuous jet during electrospinning with intermediate clogging of the needle occurred. The discontinuous jet formation led to loss of the electrospinning solution, meaning that much drug was also lost in the process. Therefore, lower amounts of constituents in the colloidal dispersions led to reduction of viscosity, which resulted in better and stable stretching of the jet with an overall good performance during the electrospinning process even over a long production run (4 h). As a result, improved fiber morphology with smooth, thinner fibers was observed [41,42]. The two formulations showed good drug entrapment efficiencies of about 76% for F2 and 69% for F3.

Table 4. Fiber diameters of the obtained electrospun fibers.

Formulation	Average Diameter (nm)	Minimum Diameter (nm)	Maximum Diameter (nm)
Pure PVA	1105 ± 236	768	1586
F1	481 ± 49	399	577
F2	392 ± 42	341	499
F3	626 ± 94	390	853

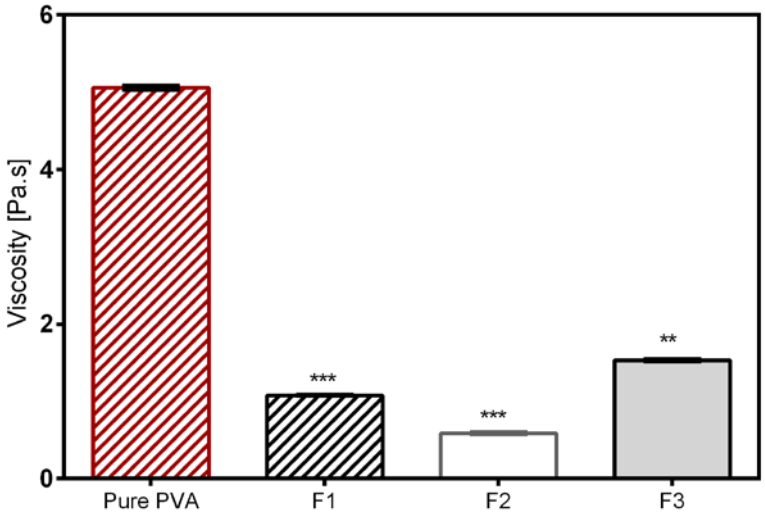

Figure 2. Viscosity of non-loaded and TE-loaded PVA solutions. * statistically significant, ** $p < 0.01$; *** $p < 0.001$ vs. pure PVA.

4.4.2 Differential Scanning Calorimetry Analysis

DSC measurements of the pure constituents of the electrospun fiber mats as well as of the final fiber mats were performed to observe the effect of the addition of colloidal dispersions in PVA matrix; their thermograms are presented in Figure 3. The DSC thermogram of the TE extract showed the melting process of a metastable modification at the beginning, accompanied by subsequent exothermic recrystallization in a more stable form, which melts at about 248 °C [43]. PL90H showed a major endothermic peak at around 119 °C where a partial melting of side chains as well as phosphatidylcholine transition to a thermotropic liquid crystalline state occurs. The peaks at around 141 °C, 153 °C, and 178 °C were thought to show further phase transitions, and lastly, the peak at 231 °C is where melting of phosphatidylcholine takes place [44]. The DSC thermograms of the electrospun products are characterized by two major endothermic peaks, one broader band between 70–100°C associated with evaporation of water, and a melting peak at 177 °C. This melting peak is in good accordance with the melting of pure PVA fibers (Table 5). Interestingly, the electrospun fibers show neither the melting peaks and phase transitions of the phospholipid, nor the melting peak of the TE. This indicates that the colloidal dispersions embedded in nanofibers were present mostly in the amorphous state. However, a final decision on the crystallinity requires further analytical methods, e.g., X-ray diffraction [45,46].

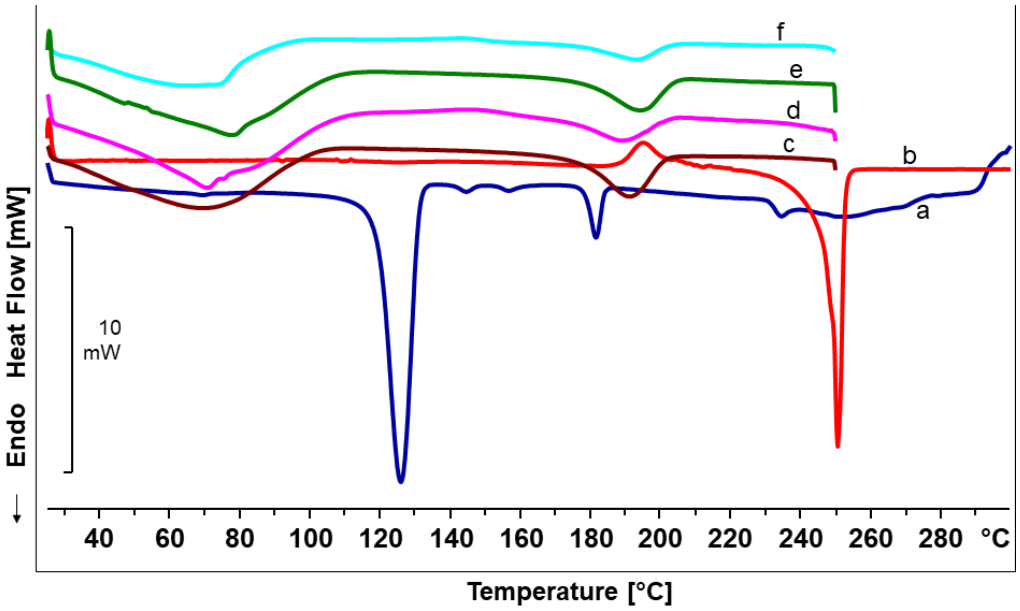

Figure 3. DSC thermograms for (**a**) Phospholipon 90H, (**b**) birch bark extract (TE), (**c**) Pure PVA mat, (**d**) F1, (**e**) F2, and (**f**) F3 fiber mats.

Table 5. Thermal properties of nonloaded and TE-loaded electrospun PVA-based fiber mats.

Sample	T_m (°C)
Birch bark extract	248 ± 2.92
Phospholipon 90H	231 ± 1.11
Pure PVA mat	177 ± 0.42
F1	177 ± 0.27
F2	178 ± 1.53
F3	177 ± 0.14

4.4.3 Confocal Raman Spectral Imaging

The obtained Raman images of the nanofiber mats of F2 and F3 are shown in Figure 4. By observing the red spots, these color-coded images clearly show that F3 contained higher amount of the incorporated TE. TE (red spots) is found predominantly colocated with the oil phase (yellow spots), demonstrating that the extract has high affinity to sunflower oil. Although spatial resolution of Raman microscopy is in the submicron range and not on the molecular level, the images give, as expected, clear hints that the phospholipon 90H (blue spots) forms an interfacial layer between the lipophilic components (TE and sunflower oil) and PVA (green). Consequently, this will ensure better encapsulation as well as stabilization of the two lipophilic substances within the hydrophilic PVA matrix. Indeed, the color-coded images not only show homogeneous TE distribution throughout the fiber mats, but also strengthens a good encapsulation of TE within the nanofiber mats. Accordingly, confocal Raman microscopy allowed the investigation of the spatial distribution of all components within the fiber mats.

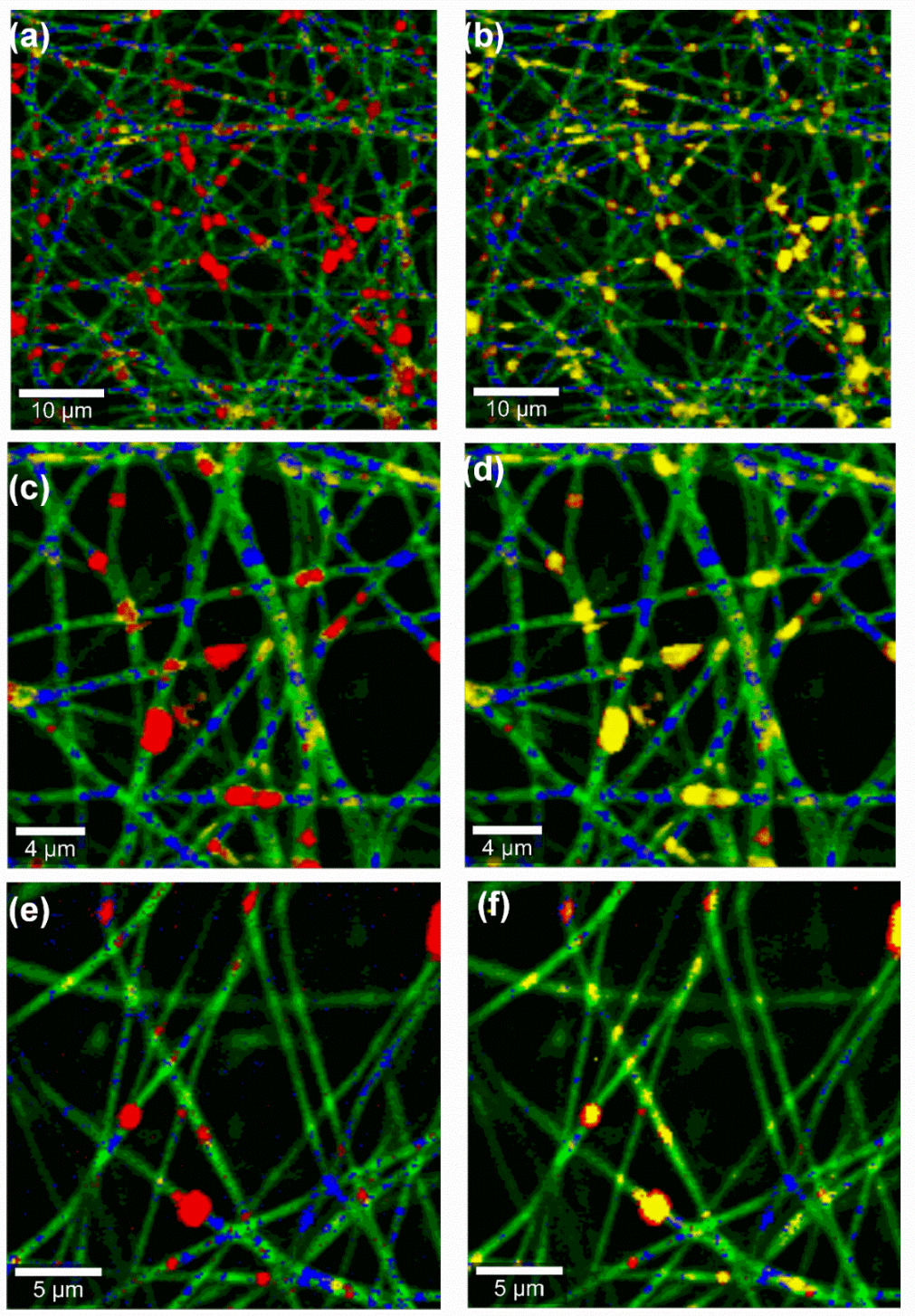

Figure 4. Confocal Raman microscopic color-coded images of TE-loaded fiber mats from (**a**) to (**d**) F3 (**e**), and (**f**) F2, Color code: Red: TE, Blue: PL90H, Green: PVA, Yellow: Sunflower oil; stack order of color code left column: green, yellow, blue, red; stack order of color code right column: green, red, blue, yellow.

4.4.4 In Vitro Release Studies

Figure 5 shows the cumulative betulin release from PVA-based wound dressings for a period of 72 h at 32 °C represented in percent and μg/cm^2 for the two TE-containing wound dressings. The release in μg/cm^2 units could be vital for a possible clinical therapy, which makes it easier to calculate the dose needed based on the size of the wound dressing. Besides, the release in percentage would thereby be helpful to estimate the encapsulation efficiency. By observing the percentage amount released after 3 days, 44% of betulin was released from the F2 nanofibers whereas only 22% was released from F3 fiber mats. Although the amount of TE incorporated in F3 blend was high, this formulation shows a slower percentage drug release than F2 ($p < 0.05$) where a faster release is observed. The reason behind this was F3 blend contained components at very high concentrations (3.2% PL90H, 4% SO), which slowed the release of the drug, whereas the F2 blend had only 1% PL90H and 0.4% SO, hence quicker release of the drug from the hydrophilic matrix. Obviously, the amount released in μg/cm^2 from F3 formulation was higher than F2 blend due to large differences in the amount initially incorporated. From these results, we can conclude that, initially, the drug is being released faster from the wound dressings, followed by a sustained release manner.

Table 6 shows the modelling results obtained from the four kinetic models. On comparing the R^2 values of the two formulations, it was found that betulin release from the electrospun PVA wound dressings closely fitted Korsmeyer–Peppas model as this model showed higher R^2 values followed by Higuchi square root model than other models. From the Korsmeyer–Peppas model, n values were found to be between 0.42 and 0.62 for both dressings, indicating that betulin release from PVA/TE fiber mats can be largely described as matrix diffusion [47,48].

In addition, the obtained results show that, by regulating the sunflower oil and PL90H concentrations in both formulations, betulin release can be controlled. Several mechanisms could be responsible for betulin's controlled release. In our previous study, we observed through interfacial tension measurements that PL90H and TE strongly interact with each to form a stable film. Moreover, studies have shown that triterpenes interact with PL and fluidize lipid membranes controlled by their free polar groups where tetracyclic triterpenes (e.g., cortisol) tend to be located at the head group, whereas pentacyclic ones (e.g., erythrodiol), being more hydrophobic, are incorporated deeply in the lipid bilayers [49]. The ratios between PL90H:TE were 2:0.4 for F2 and 6.4:4 for F3 which demonstrates that increasing the concentration of PL90H reduces rate of drug release. On the other hand, the F2 contained lower concentrations of sunflower oil and PL90H which allows release medium to easily penetrate through the hydrophilic matrix, hence allowing faster betulin release. Another possible reason is that the F2 dressing had thinner fibers, with an average fiber diameter of 392 nm, than the thicker fibers of F3 (626 nm) where betulin has to travel a longer distance through the polymeric matrix, leading to a slower release [50]. It is also known that through emulsion electrospinning, core–shell nanofibers can be produced while

designing controlled release drug delivery systems such that the drug release rate can be modulated, for example, by just adjusting the oil phase and the water phase of the emulsions [51].

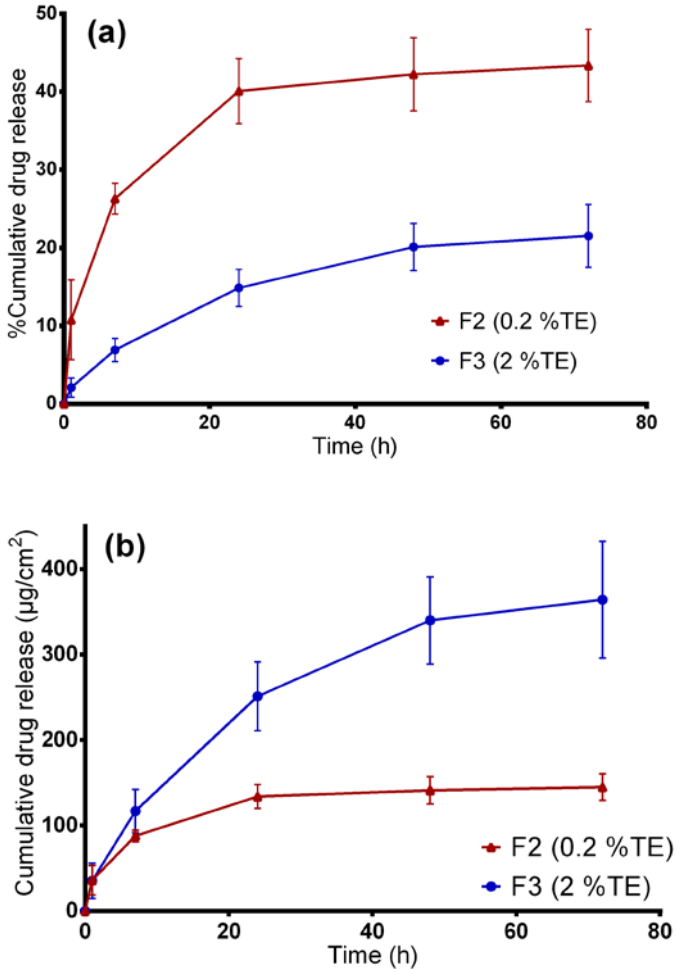

Figure 5. In vitro drug release studies. (**a**) Percentage of released betulin and (**b**) amount of betulin released (µg/cm^2) from TE-loaded wound dressings.

Table 6. In vitro release kinetics data of the two TE-loaded electrospun fiber mats fitted to mathematical models.

Sample	Zero-Order	First-Order	Higuchi	Korsmeyer–Peppas Model	
	R^2	R^2	R^2	R^2	n
F2	0.9105	0.9405	0.9847	0.9943	0.42
F3	0.9834	0.9877	0.9975	1	0.62

4.4.5 Ex vivo Permeation Through Wounded Skin

The developed wound dressings are intended to be applied on wounded skin. Figure 6 shows the cumulative amount of betulin permeated from the two wound dressings through stimulated “injured skin”. Again, the data is represented in both percent and µg/cm^2. The cumulative amount of drug permeated from the F3 formulation was 124.24 ± 11.5 µg/cm^2, and 74.58 ± 4.7 µg/cm^2 for the F2 dressing at 168 h. The large

differences in permeation profiles are due to the high amount of TE incorporated in the F3 formulation. However, the drug permeated much faster from the F2 dressing (permeation coefficient: 6.2×10^{-3} mg/cm^2.h), reaching about 22.81%, than the F3 formulation (permeation coefficient: 3.6×10^{-3} mg/cm^2.h) where only 7.21% was achieved at 168 h. Beyond that, as shown in Figure 6, the ex vivo drug permeation profiles were similar to in vitro drug-release profiles. On comparing the R^2 values of the two formulations, again, betulin permeation profiles closely fitted to Korsmeyer–Peppas model (R^2: 0.9914 for F2, 0.9934 for F3) and Higuchi square root model (R^2: 0.9844 for F2, 0.9968 for F3) than other models. From the Korsmeyer–Peppas model, *n* values were found to be between 0.42 and 0.75 for both dressings, showing that betulin permeation from PVA/TE fiber mats can be mainly attributed to diffusion of the drug from the polymer matrix. Mostly, the release of the drug from drug-loaded electrospun nanofibers is mainly governed by diffusion through the polymer matrix, including release by polymer matrix degradation and drug desorption from the surface of the nanofibers [52,53].

As expected, in vitro drug release and skin permeation studies are markedly different ($p < 0.05$) in that the drug release with the use of synthetic membrane is much faster in comparison to the dermatomed skin. For instance, only 19% (62.78 ± 12.5 µg/cm^2) of betulin from F2 permeated through the skin, whereas about 44% (145 ± 15.5 µg/cm^2) was released through the synthetic membrane after 3 days. These data suggest that the diffusion of betulin across the synthetic membrane demonstrates how the skin due to its complexity, presents as a barrier leading to a slower permeation even when injured skin was tested.

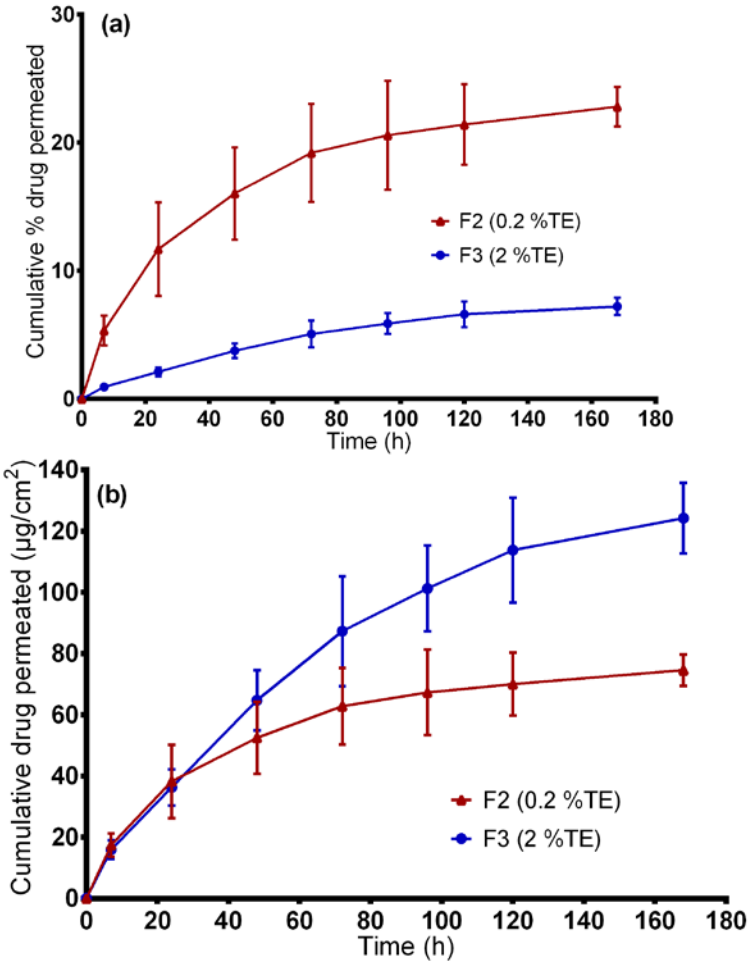

Figure 6. Ex vivo drug permeation studies. (**a**) percentage of permeated betulin and (**b**) amount of betulin permeated (µg/cm^2) from TE-loaded wound dressings.

4.4.6 Ex Vivo Wound Healing Model

The healing performance of the wound dressings was microscopically evaluated in an ex vivo experiments. As shown in Figure 7, all the tested formulations favored wound closure in comparison to control, but the greatest wound area reduction was observed in the group treated with the F2 fiber mats. This is clearly reflected by the corresponding histological micrographs (Figure 8) where the F2 fiber mat (Figure 8 (e)) showed a complete reepithelialization and proved to enhance wound healing more efficiently than all other tested samples. Statistical evaluation revealed that the differences with the rest of the groups were statistically significant (***$p < 0.001$). Among the rest of the groups, the electrospun wound dressings performed much better than the TE-oleogel. Moreover, given that F2 fiber mats presented a significantly higher wound closure, it can be observed that low concentrations of TE are more favorable to wound healing than higher amounts of TE (F3 fiber mats, *$p < 0.05$). Perhaps higher concentrations of TE inside the fiber mats had some impairing effects on the cells, which slowed wound closure. In addition, the two placebos, F1 fiber mats (**$p < 0.01$) and pure PVA fiber mats (***$p < 0.001$), also showed a significant improvement of

reepithelialization in comparison to the control, but the formulation containing PL90H without TE was slightly better than pure PVA scaffolds. However, it would be interesting to assess the effects of PL90H on the wound healing process in a further study. Other researchers have shown that electrospun scaffolds in wound healing promote cell proliferation, cell support, and enhanced tissue regeneration [21,24].

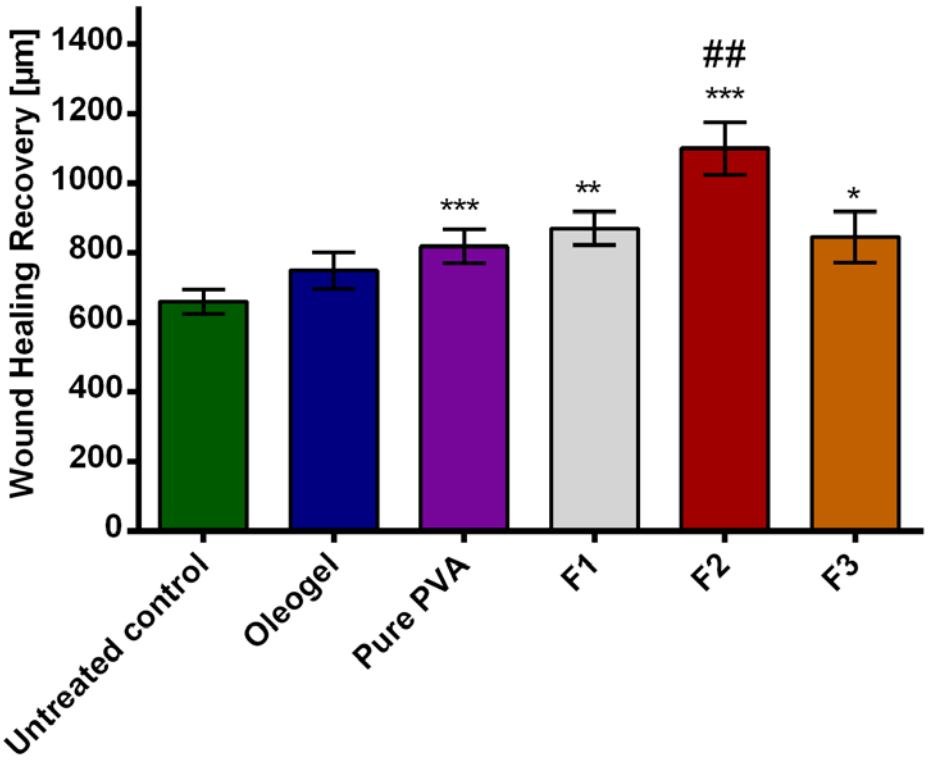

Figure 7. Wound healing recovery. * statistically significant, * $p < 0.05$; ** $p < 0.01$; *** $p < 0.001$ vs untreated control and ## compared to TE-oleogel.

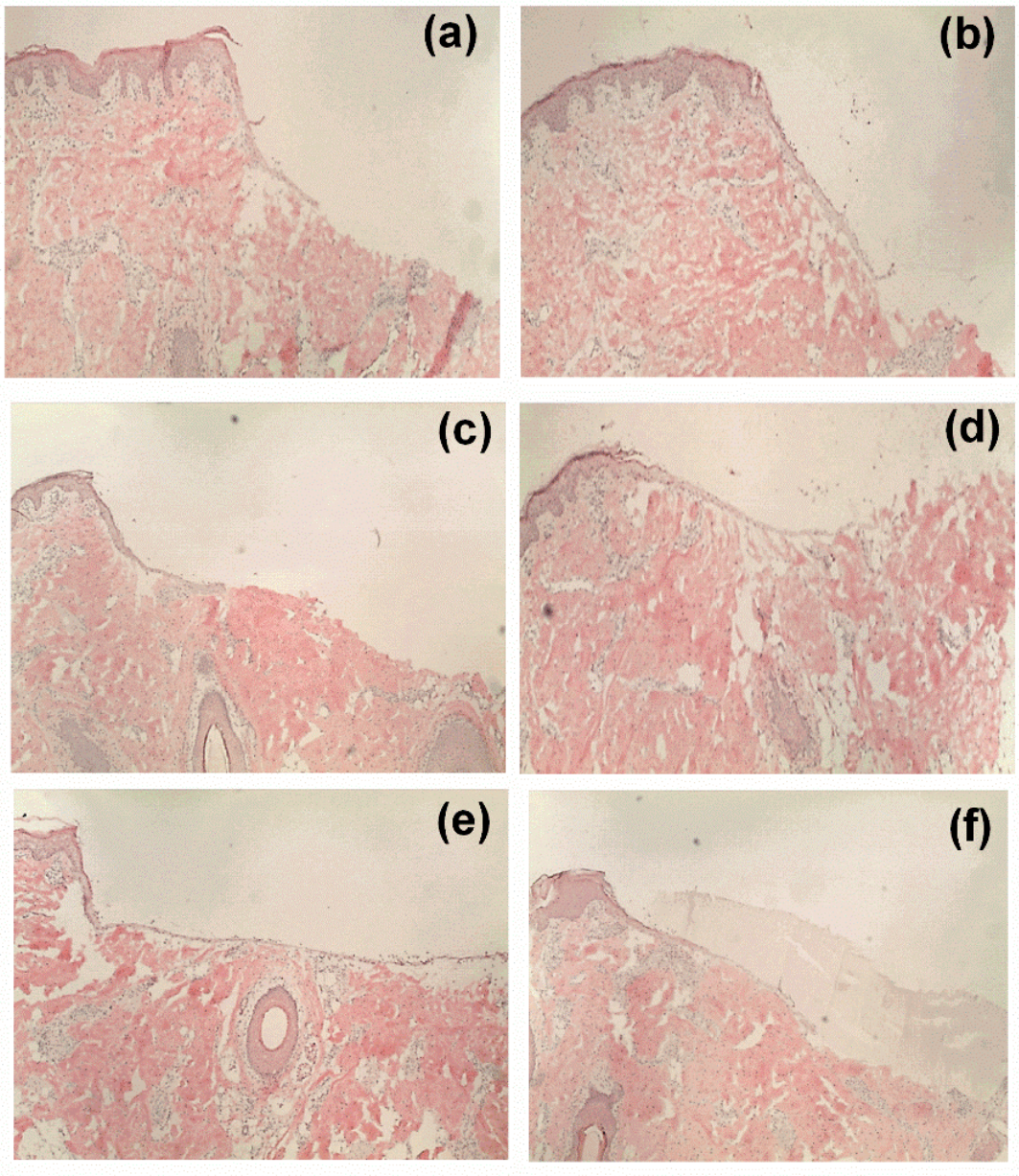

Figure 8. Microscopic observation: histological evaluations of wounds treated with TE-oleogel (**b**), pure PVA fiber mat (**c**), F1 (**d**), F2 (**e**), and F3 (**f**). (a) is the untreated control.

4.5 Conclusions

In conclusion, for the first time, we have successfully developed a bioactive PVA-based wound dressing containing colloidal dispersions of birch bark extract through emulsion-electrospinning. The betulin was released from the electrospun fiber mats in a diffusion-controlled manner. Scanning electron microscopy showed that fiber characteristics and morphology can be influenced by just adjusting compositions in the colloidal dispersions. The electrospun fiber mats varied from smooth to rough surfaces with average fiber diameters between 300 and 1586 nm. Confocal Raman spectral imaging confirmed that TE and other substances were indeed part of the electrospun fiber structures. The ex vivo wound healing assay carried out in porcine ears showed an improvement in wound healing in terms of wound closure and reepithelialization when PVA-TE fiber mats were applied on the wound. Accordingly, these results demonstrated that the developed wound dressings ideally suited for the treatment of wounds. The proven sustained release enables less frequent changing of the wound dressing. Due to the extended TE release, application to chronic wounds seems also to be conceivable. Such a TE-PVA hybrid system comes with tremendous effects not only for covering wounds, but also essential in accelerating the wound healing process due to the positive effects of TE. In addition, the wound healing study showed that wound healing is a complex process and that the performance of a wound dressing can be not estimated neither from the physicochemical characterization nor from ex vivo permeation studies. Selection must be done on a case-by-case approach. However, it can be concluded that such a composite scaffold fabricated through emulsion electrospinning would be an appropriate candidate for wound healing applications.

Author Contributions: Conceptualization, F.K.M. and R.D.; Data curation, F.K.M and J.M.B.; Funding acquisition, F.K.M. and R.D..; Investigation, F.K.M and J.M.B.; Methodology, F.K.M., J.M.B and R.D.; Project administration, R.D.; Supervision R.D.; Writing—original draft, F.K.M.; Writing—review & editing, R.D and J.M.B. The authors have read and agreed to the published version of the manuscript.

Funding: This research was funded (PRC20170703) by the Phospholipid Research Center in Heidelberg, Germany.

Acknowledgments: The authors would like to thank Lipoid GmbH for the kind donation of the phospholipids.

Conflicts of Interest: The authors declare no conflict of interest.

4.6 References

1. Agra, L.C.; Ferro, J.N.S.; Barbosa, F.T.; Barreto, E. Triterpenes with healing activity: A systematic review. Journal of Dermatological Treatment**2015**, *26*, 465–470, doi:10.3109/09546634.2015.1021663.
2. Aiken, C.; Chen, C. Betulinic acid derivatives as HIV-1 antivirals. Trends in Molecular Medicine, **2005**, *11*, 31–36, doi:10.1016/j.molmed.2004.11.001.
3. Haque, S.; Nawrot, D.A.; Alakurtti, S.; Ghemtio, L.; Yli-Kauhaluoma, J.; Tammela, P. Screening and Characterisation of Antimicrobial Properties of Semisynthetic Betulin Derivatives. *PLOS ONE* **2014**, *9*, e102696, doi:10.1371/journal.pone.0102696.
4. Dehelean, C. A., C. M. Soica, C.-C. Toma, S. Feflea, A. T. Gruia, and P. Kasa Jr, Antitumoral activity of betulin, a compound present in birch tree, in formulations with cyclodextrin. *Studia Universitas. VG, Seria St. Vietii*, **2010,** *20*, 5558.
5. Dehelean, C.A.; Soica, C.; Ledeţi, I.; Aluaş, M.; Zupkó, I.; Găluşcan, A.; Pinzaru, S.C.; Munteanu, M. Study of the betulin enriched birch bark extracts effects on human carcinoma cells and ear inflammation. Chemistry Central Journal *.* **2012**, *6*, 137, doi:10.1186/1752-153x-6-137.
6. Ebeling, S.; Naumann, K.; Pollok, S.; Wardecki, T.; Vidal-Y-Sy, S.; Nascimento, J.M.; Boerries, M.; Schmidt, G.; Brandner, J.M.; Merfort, I. From a Traditional Medicinal Plant to a Rational Drug: Understanding the Clinically Proven Wound Healing Efficacy of Birch Bark Extract. *PLOS ONE* **2014**, *9*, e86147, doi:10.1371/journal.pone.0086147.
7. Metelmann, H.-R.; Podmelle, F.; Waite, P.D. Long-Term Cosmetic Benefit of Wound Healing by Betuline. The American Journal of Cosmetic Surgery *.* **2012**, *29*, 19–24, doi:10.5992/AJCS-D-11-00046.1.
8. Steinbrenner, I.; Houdek, P.; Pollok, S.; Brandner, J.M.; Daniels, R. Influence of the Oil Phase and Topical Formulation on the Wound Healing Ability of a Birch Bark Dry Extract. *PLOS ONE* **2016**, *11*, e0155582, doi:10.1371/journal.pone.0155582.
9. Färber, A.; Daniels, R. Ex vivo Skin Permeation of Betulin from Water-in-Oil Foams. *Skin Pharmacology and Physiology* **2016**, *29*, 250–256, doi:10.1159/000448689.
10. Hordyjewska, A.; Ostapiuk, A.; Horecka, A.; Kurzepa, J. Betulin and betulinic acid: Triterpenoids derivatives with a powerful biological potential. *Phytochemistry Reviews* **2019**, *18*, 929–951, doi:10.1007/s11101-019-09623-1.
11. Laszczyk, M.; Jäger, S.; Simon-Haarhaus, B.; Scheffler, A.; Schempp, C. Physical, Chemical and Pharmacological Characterization of a New Oleogel-Forming Triterpene Extract from the Outer Bark of Birch (Betulae Cortex). *Planta Medica* **2006**, *72*, 1389–1395, doi:10.1055/s-2006-951723.
12. Krasutsky, P.A. Birch bark research and development. *Natural product reports* **2006**, *23*, 919, doi:10.1039/b606816b.
13. Jäger, S.; Laszczyk, M.N.; Scheffler, A. A Preliminary Pharmacokinetic Study of Betulin, the Main Pentacyclic Triterpene from Extract of Outer Bark of Birch (Betulae alba cortex). *Molecules.* **2008**, *13*, 3224–3235, doi:10.3390/molecules13123224.

14. Reinke, J.; Sorg, H. Wound Repair and Regeneration. *European Surgical Research* **2012**, *49*, 35–43, doi:10.1159/000339613.
15. Weckesser, S.; Schumann, H.; Laszczyk, M.; Müller, M.; Schempp, C.M. Topical Treatment of Necrotising Herpes Zoster with Betulin from Birch Bark. *Complementary Medicine Research* **2010**, *17*, 271–273, doi:10.1159/000320592.
16. Schwieger-Briel, A.; Kiritsi, D.; Schempp, C.; Has, C.; Schumann, H. Betulin-Based Oleogel to Improve Wound Healing in Dystrophic Epidermolysis Bullosa: A Prospective Controlled Proof-of-Concept Study. *Dermatology research and practice* **2017**, *2017*, 1–10, doi:10.1155/2017/5068969.
17. Frew, Q.; Rennekampff, H.-O.; Dziewulski, P.; Moiemen, N.; Zahn, T.R.; Hartmann, B.; BBW-11 Study Group Betulin wound gel accelerated healing of superficial partial thickness burns: Results of a randomized, intra-individually controlled, phase III trial with 12-months follow-up. *Burns.* **2019**, *45*, 876–890, doi:10.1016/j.burns.2018.10.019.
18. Metelmann, H.-R. Topisches Betulin-Gel zum beschleunigten Wundverschluss bei plastischen Operationen. *Zeitschrift für Phytotherapie* **2016**, *37*, 54–58, doi:10.1055/s-0042-104793.
19. El-Hadi, A.M.; Al-Jabri, F.Y. Influence of Electrospinning Parameters on Fiber Diameter and Mechanical Properties of Poly(3-Hydroxybutyrate) (PHB) and Polyanilines (PANI) Blends. *Polymers* **2016**, *8*, 97, doi:10.3390/polym8030097.
20. Reneker, D.H.; Chun, I. Nanometre diameter fibres of polymer, produced by electrospinning. *Nanotechnolology.* **1996**, *7*, 216–223, doi:10.1088/0957-4484/7/3/009.
21. Zahedi, P.; Rezaeian, I.; Ranaei-Siadat, S.-O.; Jafari, S.H.; Supaphol, P. A review on wound dressings with an emphasis on electrospun nanofibrous polymeric bandages. *Polymers Advanced Technologies* **2009**, *21*, 77–95, doi:10.1002/pat.1625.
22. Mwiiri, F.K.; Daniels, R. Chapter 3 - Electrospun nanofibers for biomedical applications. In *Delivery of Drugs*; Shegokar, R.,Editor. Elsevier: Tuebingen, Germany, 2020; Volume. pp. 53-74.
23. Kai, D.; Liow, S.S.; Loh, X.J. Biodegradable polymers for electrospinning: Towards biomedical applications.*Materials Science and Engineering: C* **2014**, *45*, 659–670, doi:10.1016/j.msec.2014.04.051.
24. Zhong, S.P.; Zhang, Y.; Lim, C.T. Tissue scaffolds for skin wound healing and dermal reconstruction. *Wiley Interdiscip. Rev. Nanomed. Nanobiotechnology* **2010**, *2*, 510–525, doi:10.1002/wnan.100.
25. IgnatovaM.; Rashkov, I.; Manolova, N. Drug-loaded electrospun materials in wound-dressing applications and in local cancer treatment. *Materials Science and Engineering* **2013**, *10*, 469–483, doi:10.1517/17425247.2013.758103.
26. Jiang, T.; Carbone, E.J.; Lo, K.W.-H.; Laurencin, C.T. Electrospinning of polymer nanofibers for tissue regeneration. *Progress in Polymer Science* **2015**, *46*, 1–24, doi:10.1016/j.progpolymsci.2014.12.001.

27. Gajra*, B., S. S. Pandya, G. Vidyasagar, H. Rabari, R. R. Dedania, and S. J. I. J. o. P. R. Rao, Poly vinyl alcohol hydrogel and its pharmaceutical and biomedical applications: A review. **2012**, *4*, 2026.
28. Gaaz, T.S.; Sulong, A.; Akhtar, M.N.; Kadhum, A.A.H.; Mohamad, A.B.; Al-Amiery, A. Properties and Applications of Polyvinyl Alcohol, Halloysite Nanotubes and Their Nanocomposites. *Molecules (Basel, Switzerland).* **2015**, *20*, 22833–22847, doi:10.3390/molecules201219884.
29. Kamoun, E.A.; Chen, X.; Eldin, M.S.M.; Kenawy, E.-R. Crosslinked poly(vinyl alcohol) hydrogels for wound dressing applications: A review of remarkably blended polymers. *Arabian Journal of Chemistry* **2015**, *8*, 1–14, doi:10.1016/j.arabjc.2014.07.005.
30. Augustine, R.; Hasan, A.; Nath, V.K.Y.; Thomas, J.; Augustine, A.; Kalarikkal, N.; Al Moustafa, A.-E.; Thomas, S. Electrospun polyvinyl alcohol membranes incorporated with green synthesized silver nanoparticles for wound dressing applications. *Journal of Materials Science: Materials in Medicine* **2018**, *29*, 163, doi:10.1007/s10856-018-6169-7.
31. Saeed, S.M.; Mirzadeh, H.; Zandi, M.; Barzin, J. Designing and fabrication of curcumin loaded PCL/PVA multi-layer nanofibrous electrospun structures as active wound dressing. *Progress in Biomaterials.* **2017**, *6*, 39–48, doi:10.1007/s40204-017-0062-1.
32. Alavi, A.; Sibbald, R.G.; Ladizinski, B.; Saraiya, A.; Lee, K.C.; Skotnicki-Grant, S.; Maibach, H. Wound-Related Allergic/Irritant Contact Dermatitis. *Advances in skin & wound care* **2016**, *29*, 278–286, doi:10.1097/01.asw.0000482834.94375.1e.
33. Boateng, J.S.; Catanzano, O. Advanced Therapeutic Dressings for Effective Wound Healing—A Review. *Journal of Pharmaceutical Sciences* **2015**, *104*, 3653–3680, doi:10.1002/jps.24610.
34. Rott, C. Herstellung und Charakterisierung betulinhaltiger Zubereitungen für berührungsempfindliche Haut (PhD thesis), University of Tuebingen: Tuebingen, Germany, 2016.
35. Zhang, Z.; Lunter, D.J. Confocal Raman microspectroscopy as an alternative method to investigate the extraction of lipids from stratum corneum by emulsifiers and formulations. *European Journal of Pharmaceutics and Biopharmaceutics* **2018**, *127*, 61–71, doi:10.1016/j.ejpb.2018.02.006.
36. Heck, R.; Hermann, S.; Lunter, D.J.; Daniels, R. Film-forming formulations containing porous silica for the sustained delivery of actives to the skin. *European Journal of Pharmaceutics and Biopharmaceutics* **2016**, *108*, 1–8, doi:10.1016/j.ejpb.2016.08.010.
37. Lunter, D.J.; Rottke, M.; Daniels, R. Oil-in-Oil-Emulsions with Enhanced Substantivity for the Treatment of Chronic Skin Diseases. Journal of Pharmaceutical Sciences **2014**, *103*, 1515–1519, doi:10.1002/jps.23944.
38. Dash, S.; Murthy, P.N.; Nath, L.; Chowdhury, P. Kinetic modeling on drug release from controlled drug delivery systems. Acta Poloniae Pharmaceutica*.* **2010**, *67*, 217–23.

39. Ritger, P.L.; Peppas, N.A. A simple equation for description of solute release I. Fickian and non-fickian release from non-swellable devices in the form of slabs, spheres, cylinders or discs. *Journal of Controlled Release* **1987**, *5*, 23–36, doi:10.1016/0168-3659(87)90034-4.
40. Armbruster, M.; Mönckedieck, M.; Scherließ, R.; Daniels, R.; Wahl, M. Birch Bark Dry Extract by Supercritical Fluid Technology: Extract Characterisation and Use for Stabilisation of Semisolid Systems. Applied Sciences . **2017**, *7*, 292, doi:10.3390/app7030292.
41. He, M.; Zhang, B.; Dou, Y.; Yin, G.; Cui, Y.; Chen, X.-J. Fabrication and characterization of electrospun feather keratin/poly(vinyl alcohol) composite nanofibers. RSC Advances **2017**, *7*, 9854–9861, doi:10.1039/C6RA25009B.
42. Cho, D.; Netravali, A.N.; Joo, Y.L. Mechanical properties and biodegradability of electrospun soy protein Isolate/PVA hybrid nanofibers. *Polymer Degradation andStability* **2012**, *97*, 747–754, doi:10.1016/j.polymdegradstab.2012.02.007.
43. Grysko, M.; Daniels, R. Evaluation of the mechanism of gelation of an oleogel based on a triterpene extract from the outer bark of birch. *Die Pharmazie-An International Journal of Pharmaceutical Sciences***2013**, *68*, 572–577.
44. Kolbina, M.; Schulte, A.; Van Hoogevest, P.; Körber, M.; Bodmeier, R. Evaluation of Hydrogenated Soybean Phosphatidylcholine Matrices Prepared by Hot Melt Extrusion for Oral Controlled Delivery of Water-Soluble Drugs. *AAPS PharmSciTech* **2019**, *20*, 159, doi:10.1208/s12249-019-1366-3.
45. Koosha, M.; Mirzadeh, H. Electrospinning, mechanical properties, and cell behavior study of chitosan/PVA nanofibers. *Journal of Biomedical Materials Research Part A* **2015**, *103*, 3081–3093, doi:10.1002/jbm.a.35443.
46. Gordon, V.; Marom, G.; Magdassi, S. Formation of hydrophilic nanofibers from nanoemulsions through electrospinning. *International Journal of Pharmaceutics* **2015**, *478*, 172–179, doi:10.1016/j.ijpharm.2014.11.038.
47. Ritger, P.L.; Peppas, N.A. A simple equation for description of solute release II. Fickian and anomalous release from swellable devices. *Journal of Controlled Release* **1987**, *5*, 37–42, doi:10.1016/0168-3659(87)90035-6.
48. Han, X.; Huo, P.; Ding, Z.; Kumar, P.; Liu, B. Preparation of Lutein-Loaded PVA/Sodium Alginate Nanofibers and Investigation of Its Release Behavior. *Pharmaceutics.* **2019**, *11*, 449, doi:10.3390/pharmaceutics11090449.
49. Abboud, R.; Charcosset, C.; Greige-Gerges, H. Tetra- and Penta-Cyclic Triterpenes Interaction with Lipid Bilayer Membrane: A Structural Comparative Study. *The Journal of Membrane Biology* **2016**, *249*, 327–338, doi:10.1007/s00232-016-9871-8.
50. Akhgari, A.; Dezfuli, A.G.; Rezaei, M.; Kiarsi, M.; Abbaspour, M. The Design and Evaluation of a Fast-Dissolving Drug Delivery System for Loratadine Using the Electrospinning Method. *Jundishapur Journal of Natural Pharmaceutical Products.* **2016**, *11*, doi:10.17795/jjnpp-33613.
51. Nikmaram, N.; Roohinejad, S.; Hashemi, S.; Koubaa, M.; Barba, F.J.; Abbaspourrad, A.; Greiner, R. Emulsion-based systems for fabrication of electrospun nanofibers: food, pharmaceutical and biomedical applications. *Royal*

Society of Chemistry Advances. **2017**, *7*, 28951–28964, doi:10.1039/C7RA00179G.
52. Chou, S.-F.; Carson, D.; Woodrow, K.A. Current strategies for sustaining drug release from electrospun nanofibers. *Journal of Control. Release* **2015**, *220*, 584–591, doi:10.1016/j.jconrel.2015.09.008.
53. Kajdič, S.; Planinšek, O.; Gašperlin, M.; Kocbek, P. Electrospun nanofibers for customized drug-delivery systems. *Journal of Drug Delivery Science and Technology* **2019**, *51*, 672–681, doi:10.1016/j.jddst.2019.03.038.

5 Chapter 5: Influence of PVA Molecular Weight and Concentration on Electrospinnability of Birch Bark Extract Loaded Nanofibrous Scaffolds Intended for Enhanced Wound Healing.

Francis Kamau Mwiiri, Rolf Daniels

Department of Pharmaceutical Technology, Eberhard Karls University,

Tuebingen, Germany

Reprinted from Molecules 2020, 25(20), 4799; Special Issue: Polymer Scaffolds for Biomedical Applications 2020

DOI: 10.3390/molecules25204799

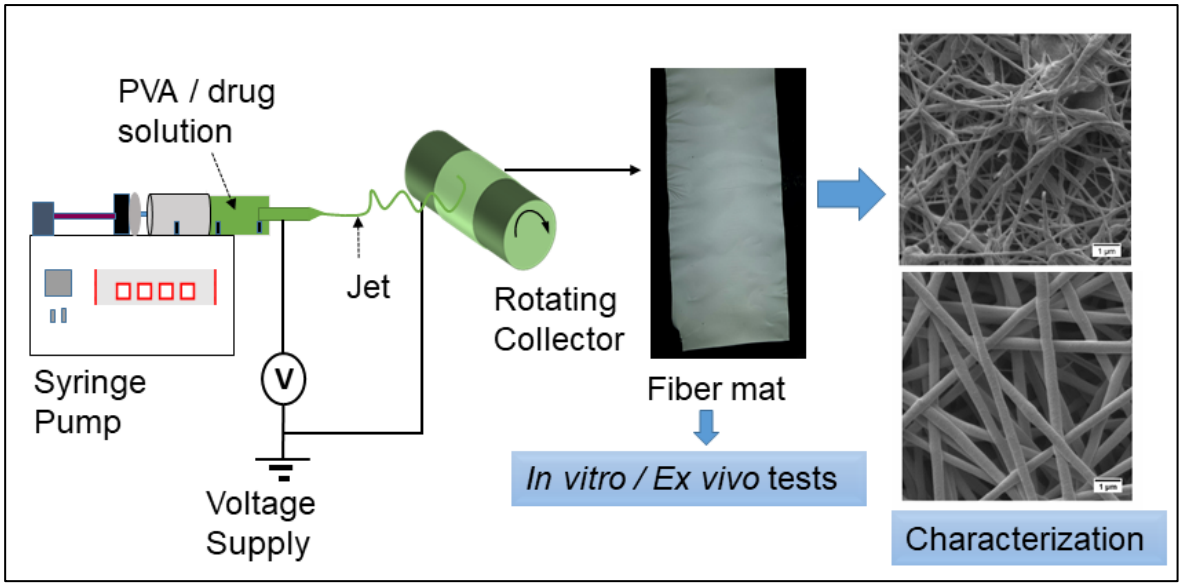

Graphical Abstract

5.1 Abstract

Triterpenes from the outer bark of birch (TE) are known for various pharmacological effects including enhanced wound healing. Apart from an already authorized oleogel, electrospun nanofiber mats containing these triterpenes in a polyvinyl alcohol (PVA) matrix appear to be an advantageous application form. The effects of PVA molecular weight and concentration on the fiber morphology have been investigated. Three different molecular weights of PVA ranging from 67 to 186 kDa were used. The concentration of PVA was varied from 5 to 20 wt%. Polymer solutions were blended with colloidal dispersions of birch bark extract at a weight ratio of 60:40 (wt.%). The estimated viscosity of polymer solutions was directly linked to their concentration and molecular weight. In addition, both pure and blended solutions showed viscoelastic properties with a dominant viscous response in the bulk. Fiber morphology was confirmed using scanning electron microscopy (SEM). Both polymer concentration and molecular weight were found to be significant factors affecting the diameter of the fibers. Fiber diameter increased with a higher molecular weight and polymer concentration as more uniform fibers were obtained using PVA of higher molecular weight (146–186 kDa). In vitro drug release and ex vivo permeation studies indicated a faster drug release of betulin from electrospun scaffolds with lower PVA molecular weight. Our research suggests that the fabricated TE-loaded PVA electrospun dressings represent potential delivery systems of TE for wound care applications.

Keywords: Electrospinning, PVA, Molecular weight, Birch bark extract, Wound dressing

5.2 Introduction

Once the skin is damaged, very important skin functions such as physical protection and thermoregulation are lost which can result in either acute or chronic wounds. Most of the wound dressings in the market have their basic functions to provide a protective barrier against bacterial contamination and absorb exudate [1]. Thus, developing wound dressings for not only covering wounds but with loaded active ingredients to improve the wound healing process would be greatly beneficial. The pentacyclic triterpenes from outer birch bark extract are known for their pharmacological effects such as anti-inflammatory, antimicrobial, anti-viral, anti-cancer activity and wound healing effects [2–9]. A suitable triterpene dry extract (TE) from the outer bark of birch contains > 80% (*w/w*) betulin as the main component and is obtained by accelerated solvent extraction with n-heptane [10]. Other disclosed triterpenes of this dry extract include lupeol (LU), erythrodiol (ER), betulinic acid (BA) and oleanolic acid (OA) (Table 1) [11]. However, TE exhibits low solubility in polar and non-polar solvents that may lead to a poor bioavailability which might limit its therapeutic application [8,12]. Currently, topical formulations containing TE include water-in-oil foams [9], cosmetic water-in-oil creams (Imlan Creme pur, Birken AG) and a TE oleogel based on sunflower oil received from the European marketing authorization in January 2016 [13]. Notably, TE together with sunflower oil supports more wound healing than in combination with other oils as examined by Steinbrenner et al [8]. The efficacy of TE-based formulations has been well investigated in vivo on different types of wounds including dystrophic epidermolysis bullosa, where treatments promoted wound healing [14–16]. A study conducted by Ebeling et al. showed the molecular mechanism of the effects of birch bark extract on wound healing properties in human primary keratinocytes and porcine ex vivo wound healing models. They showed that TE and betulin mainly accelerated re-epithelialization by enhancing migration of keratinocytes and their differentiation. Beyond that, they found that TE led to upregulation of proinflammatory mediators such as COX-2 and IL-6 which play a key role in wound healing and epidermal barrier repair [6]. In addition, TE positive effects have been observed in all three phases of wound healing [13].

Table 1 Physical-chemical characteristics of the dry birch bark extract used [9].

TE Composition	Specific surface area	Particle size D50%
Betulin 81.60%, lupeol 2.08%, betulinic acid 3.84%, erythrodiol 1.05%, oleanolic acid 0.97%, Betulinic acid methyl ester 0.52%, undisclosed substances 9.94%	42 ± 0.4 m^2/g	5.8 µm

By use of the electrospinning technique, it is possible to prepare fibers with a diameter from a few micrometers down to several nanometers [17,18]. These nanofibers have interesting characteristics, e.g., high surface area to volume ratio, and can form mats/fleeces with high porosity which makes them attractive materials for wound

dressing [19]. Additionally, electrospun nanofibrous scaffolds tend to mimic the structure of the native extracellular matrix (ECM), hence they facilitate cell proliferation, improve gaseous exchange, assist in the removal of exudate and act as a physical barrier against entry of microorganisms during wound healing with eventual tissue repair of damaged tissues [19–23].

PVA is a water-soluble, non-toxic, biocompatible and biodegradable hydrophilic polymer with good chemical and mechanical properties, and has been approved by the U.S. Food and Drug Administration (FDA) for both biomedical and pharmaceutical applications [24,25]. Many researchers have investigated the influence of various parameters on fiber morphology and diameters of electrospun PVA fibers. Some of these parameters include polymer molecular weight and solution concentration [26,27]. PVA polymer has either been used alone or combined with other biodegradable polymers and electrospun to form scaffolds for various applications. Furthermore, PVA has also been blended and electrospun with active ingredients such as hyaluronic acid/L-arginine, soursop leaves extract, silver nanoparticles and curcumin for wound healing [28–31]. Recently, we have developed, for the first time, a PVA bioactive wound dressing containing TE which showed accelerated wound healing [32]. In this present work, we investigated the influence of PVA molecular weight on TE-loaded electrospun nanofibers.

The purpose of this work was to (1) assess the effect of PVA molecular weight, blend composition and solution concentrations on rheological properties and the resulting fiber morphology, and (2) investigate the relationship of rheological properties and electrospinnability of polymer solutions. Rotational and amplitude sweep tests of the prepared solutions were performed. The surface properties of electrospun fiber mats were characterized by SEM. We also conducted ex vivo permeation and in vitro release studies using Franz diffusion cells to test the biopharmaceutical characteristics of betulin containing electrospun nanofiber mats.

5.3 Results and Discussion

The electrospinnability of polymer solutions is known to depend strongly on their viscosity, surface tension and electrical conductivity. This might be affected further by the properties of an active compound which is added to the matrix forming polymer. In this study, the active compound is added as a colloidal dispersion consisting of TE, Phospholipon 90H (PL90H) and sunflower oil (SO) dispersed in water [33]. Therefore, the properties of PVA solutions and blended dispersions were assessed and related to their ability to form electrospun fibers.

5.3.1 Rheological Characterization of the Electrospinning Solutions

Rotational and amplitude sweep tests were performed on all PVA/TE blended solutions as well as on plain polymer solutions. Figure 1 (a) shows the results obtained from rotational tests, where changes in viscosity as a function of concentrations for pure polymer solutions with different molecular weights are presented. As expected, solution viscosity clearly increases significantly ($p < 0.05$) with increasing polymer concentration and molecular weight. For example, the viscosity of the pure PVA solutions (5–20 wt.%) varied from 0.012 to 2.43 Pa × s (low molecular weight (LMW)), 0.035 to 17.9 Pa × s (medium molecular weight (MMW)) and 0.09 to 40.2 Pa × s (high molecular weight (HMW)). The results presented in Figure 2 show the viscoelastic properties of the pure polymer solutions (5–20 wt.%) with their molecular weights. It can be observed that the loss modulus (G″) and storage modulus (G′) increase consistently with an increase in PVA concentration and molecular weight. Additionally, solutions with low PVA concentrations (< 10 wt.%) showed a steep decline in their storage modulus (G′) already at weak deformation. Notably, G″ dominates always over G′, indicating that PVA forms predominantly viscous liquids. Similar observations were also made elsewhere [26,34,35].

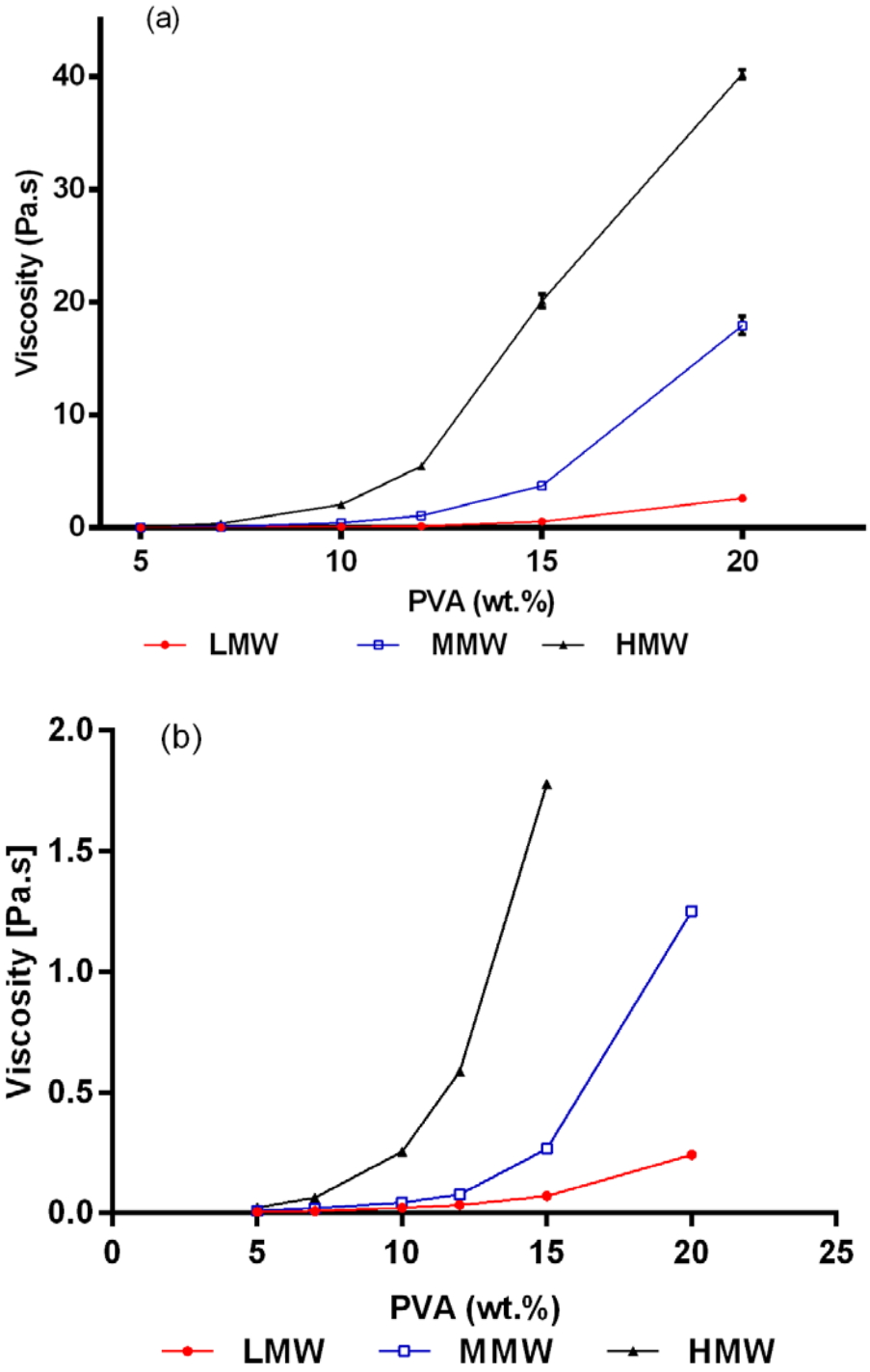

Figure 1. (**a**) Influence of molecular weight and PVA concentration on viscosity. (**b**) Viscosity of blended PVA/TE dispersions solutions in the ratio of 60:40 (error bars are smaller than the symbol size).

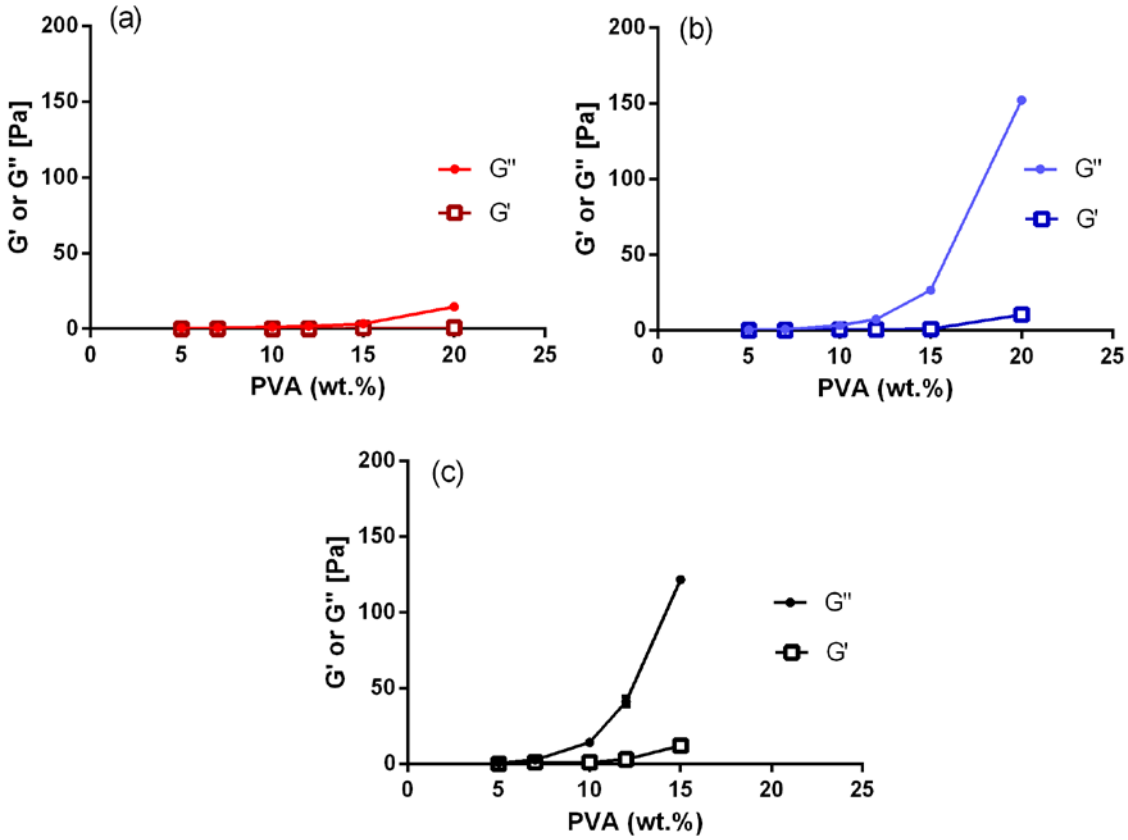

Figure 2. Storage (G′) and loss (G″) moduli as a function of PVA concentration (wt.%). (**a**) Low molecular weight (LMW), (**b**) medium molecular weight (MMW) and (**c**) high molecular weight (HMW) (error bars are smaller than the symbol size).

As expected, blending of pure polymer solutions with colloidal dispersions (60:40) resulted in a reduction in the viscosity (Figure 1 (b)). The viscosity is almost the same as for plain PVA solutions with the respective lower concentration indicating that there is no specific interaction of PVA and the colloidal dispersion. A similar reduction in viscosity has been reported after blending PVA with other agents [36–38]. Figure 3 shows the results from rotational tests when 12 wt.% of all molecular weights was blended with the colloidal dispersion in different compositions (20:80, 40:60, 50:50, 60:40, 70:30, 80:20). It can be clearly seen that the viscosity increased significantly ($p < 0.05$) as the amount of PVA increased in the blend. Again, there are no hints that the colloidal TE dispersions interact specifically with PVA. PVA/TE dispersion blended solutions maintained their viscoelastic characteristic, with the loss modulus (G″) always being greater than the storage modulus (G′). Further, both G″ and G′ values increase as the molecular weight increases in the blend composition.

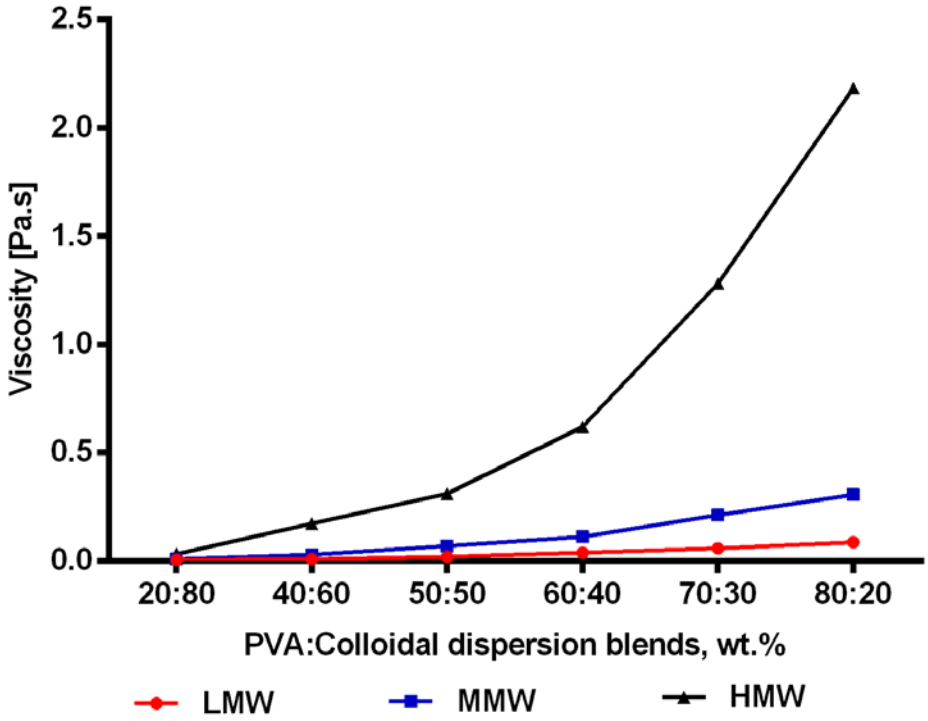

Figure 3. Viscosity as a function of PVA/colloidal dispersion aqueous blends (error bars are smaller than the symbol size).

Not surprisingly, polymer concentration, molecular weight and viscosity are correlated with each other. An increase in polymer solution concentration will result in greater polymer chain entanglement since polymer chain length or molecular weight is directly proportional to the number of entanglements [26,27,39].

5.3.2 Surface Tension and Conductivity of Polymer Solutions

Electrospinning only occurs when the charges applied on the polymer solution are high enough to overcome the surface tension. Therefore, a low surface tension is favorable in electrospinning as this minimizes the amount of critical voltage needed for the jet formation from the Taylor cone. The results in Figure 4 (a) clearly show that the used PVA solutions are surface-active being related to H-bonding between hydroxyl groups on PVA chains and water [40]. The surface tension of the polymer solutions remained nearly unchanged regardless of the polymer concentration and molecular weight used, indicating that the surface is completely saturated with the polymer in the whole relevant concentration range. The conductivity values in Figure 4 (c) increased gradually as the amount of PVA concentration and molecular weight increased. This can be attributed to the fact that sodium acetate is a major impurity during production of PVA, dissociating into sodium and acetate ions in water, and therefore conductivity increases as a higher amount of PVA is added [41,42]. As expected, the addition of the colloidal TE dispersion which comprised only substances which are practically insoluble in water did neither affect the surface tension nor the electrical conductivity (Figure 4 (b) and (d)), the latter being only reduced according to the reduced fraction

of PVA in the blend. With respect to electrospinnability, it is known that both a too low or a conductivity beyond a critical value, for example, through addition of salts, e.g., NaCI, will hinder Taylor cone formation and the electrospinning process [43,44]. The measured values (0.34–0.96 mS/cm) are within a range that are reported to be suitable for electrospinning [45,46].

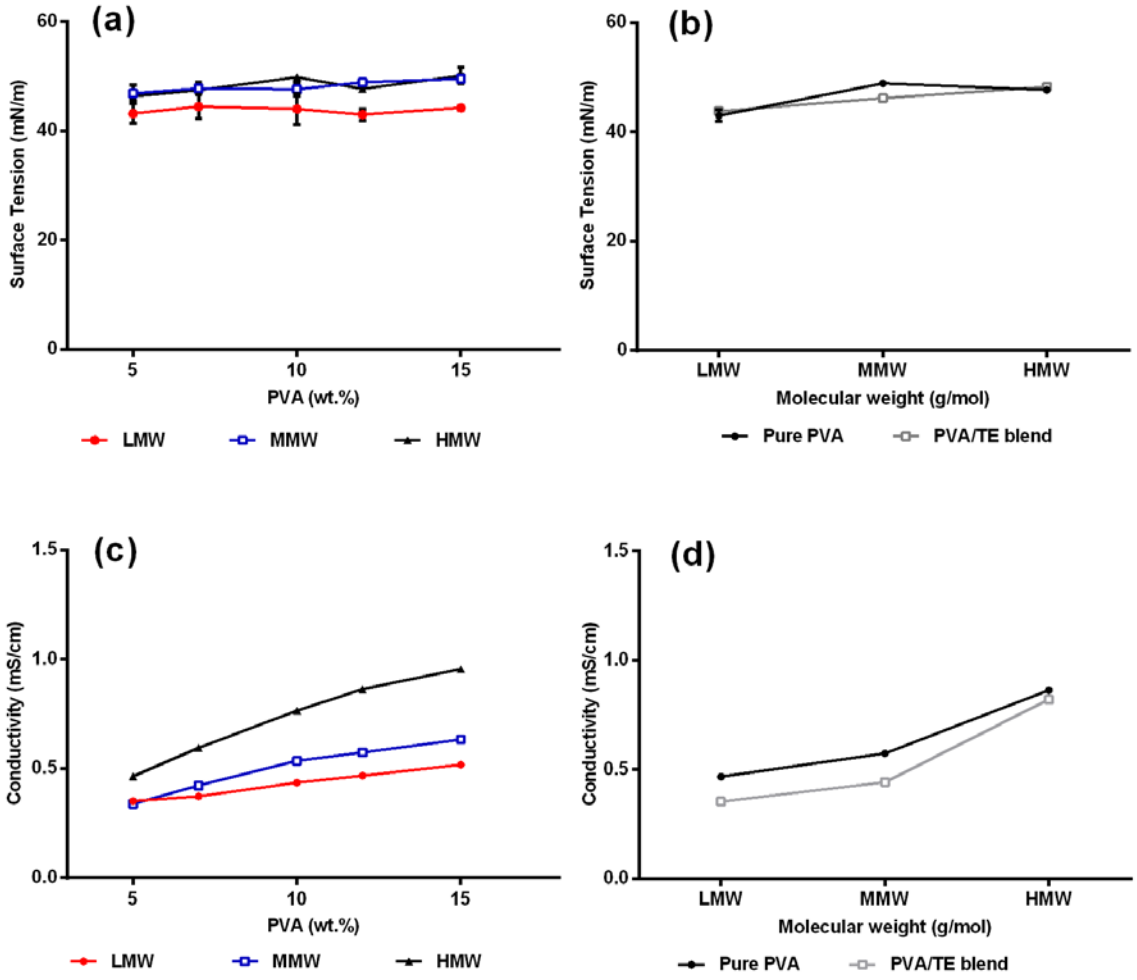

Figure 4. (**a**) Surface tension and (**c**) conductivity as a function of PVA concentration and molecular weight. (**b**) Surface tension and (**d**) conductivity of blended PVA/TE solution (60:40) at different molecular weights (error bars are smaller than the symbol size).

5.3.3 Qualitative Analysis of Electrospinning Process and Nanofiber Formation

Pure polymer solutions at lower concentrations < 10 wt.% of LMW showed unstable Taylor cone and discontinuous jet during electrospinning. Only at 12 wt.%, a stable jet was observed. Beyond this concentration, Taylor cone and jet instability occurs. The same phenomena were observed with MMW, where below 7 wt.% PVA polymer solution, an unstable jet and Taylor cone were formed. Between 10 and 12 wt.%, the jet stability improved. Beyond 15 wt.%, unstable jet formation can be observed. Pure polymer solutions of HMW between 5 and 7 wt.% exhibited stable continuous jet, whereas they destabilized between 10 and 15 wt.% and became discontinuous. After a prolonged electrospinning process with polymer solutions of high concentrations, the Taylor cone dries out and clogging of the needle tip was observed. With the polymer solution at 20 wt.% of HMW, the solution did not flow through the needle tip, while jet formation only occurred for a few seconds and the electrospinning process stopped. No jet formation with PVA/TE blends of LMW at low concentrations (< 12 wt.%), < 10 wt.% of MMW and < 7 wt.% of HMW was observed. Blends of 20 wt.% in LMW, 12–15 wt.% in MMW and 10–12 wt.% in HMW had good performance in the formation of a continuous jet during the electrospinning process even after a long duration (4 h).

The success of the electrospinning process is strongly correlated with the characteristics of the polymer solutions from which the fibers were produced. Hence, with the change in molecular weight and concentration, a difference in the electrospinnability and morphology of the obtained fibers was expected. For instance, in the case of pure PVA solutions (Figure 5), bead-free fibers were obtained with solutions at lower concentrations (5–7 wt.%) of HMW and 7–15 wt.% for MMW, while for LMW in the range of 12–20 wt.%. While electrospinning pure polymer solutions at high concentrations of 10–20 wt.%, particularly of HMW, the high viscosity prohibits the continuous flow of the polymer solution jet towards the collector. Even practical handling of such a kind of solution was difficult. At 5–7 wt.% of HMW blended solutions (Figure 6), due to low viscoelasticity, only beaded fibers were formed. Once the PVA solution concentration was increased to 10–15 wt.%, the bead defect was completely removed and smooth fibers were formed. The solutions with low viscosity (< 0.09 Pa × s), mainly those of LMW or low amounts of PVA in blend composition, produced a mixture of fibers and beads. Only droplets were produced instead of jet formation, due to the jet breaking up into droplets similar to electrospraying. This indicated that by increasing the polymer concentration of the solution, chain entanglement increases among polymer chains which overcome the surface tension and bead-free fibers can be produced [26,43,47]. We hereby conclude that polymer solutions or blends should show greater viscous properties over elastic behavior in the bulk, but only a proper relation between these two characteristics enables jet and fiber formation during the electrospinning process.

5.3.4 Effect of Concentration and Molecular Weight on Fiber Morphology

Figure 5 shows electrospun fibers produced from pure PVA polymer solutions. SEM analysis showed drastic changes in terms of fiber morphology when the molecular weight and concentration of polymer solutions were changed. In LMW, no fibers were formed over the collector with the polymer solution of 5 wt.% due to the low viscosity. With higher concentrations of 7 wt.% and 10 wt.%, a mixture of fibers with beads was formed. From 12 wt.% PVA, uniformity of fibers increased, where at 20 wt.% PVA, smooth uniform thicker fibers were observed instead of beaded fibers. For MMW, the formation of beaded fibers was only observed at 5 wt.% PVA. With 7 to 15 wt.% polymer solutions, smooth, uniform and bead-free fibers were produced. Flat and thicker fibers were observed with the polymer solution of 20 wt.% due to its high concentration.

In the case of HMW, a different pattern was observed, where only between 5 and 7 wt.% PVA, smooth, uniform fibers were produced. Besides that, between 10 and 20 wt.% PVA, fiber uniformity decreased and resulted in flat non-uniform thicker fibers with a few interconnected web-like structures in several points. Further, the observed poor fiber morphology of unloaded electrospun fibers (Figure 5) especially with HMW at high concentrations (10 to 20 wt.%) was due to the high viscosity which caused resistance to jet stretching during the electrospinning process.

The measured fiber diameter indicated that the fiber diameter not only increased across polymer concentrations but also with the increase to the higher molecular weight. Pure electrospun fibers produced with LMW had average diameters between 147 (10 wt.%) and 390 nm (20 wt.%), MMW ranged between 183 (5 wt.%) and 1357 (20 wt.%) nm and HMW ranged between 269 (5 wt.%) and 2204 nm (20 wt.%) (Table 2). In accordance with Koski et al. [26], this finding shows that polymer concentration and molecular weight are influential in determining whether fibers or beads are produced.

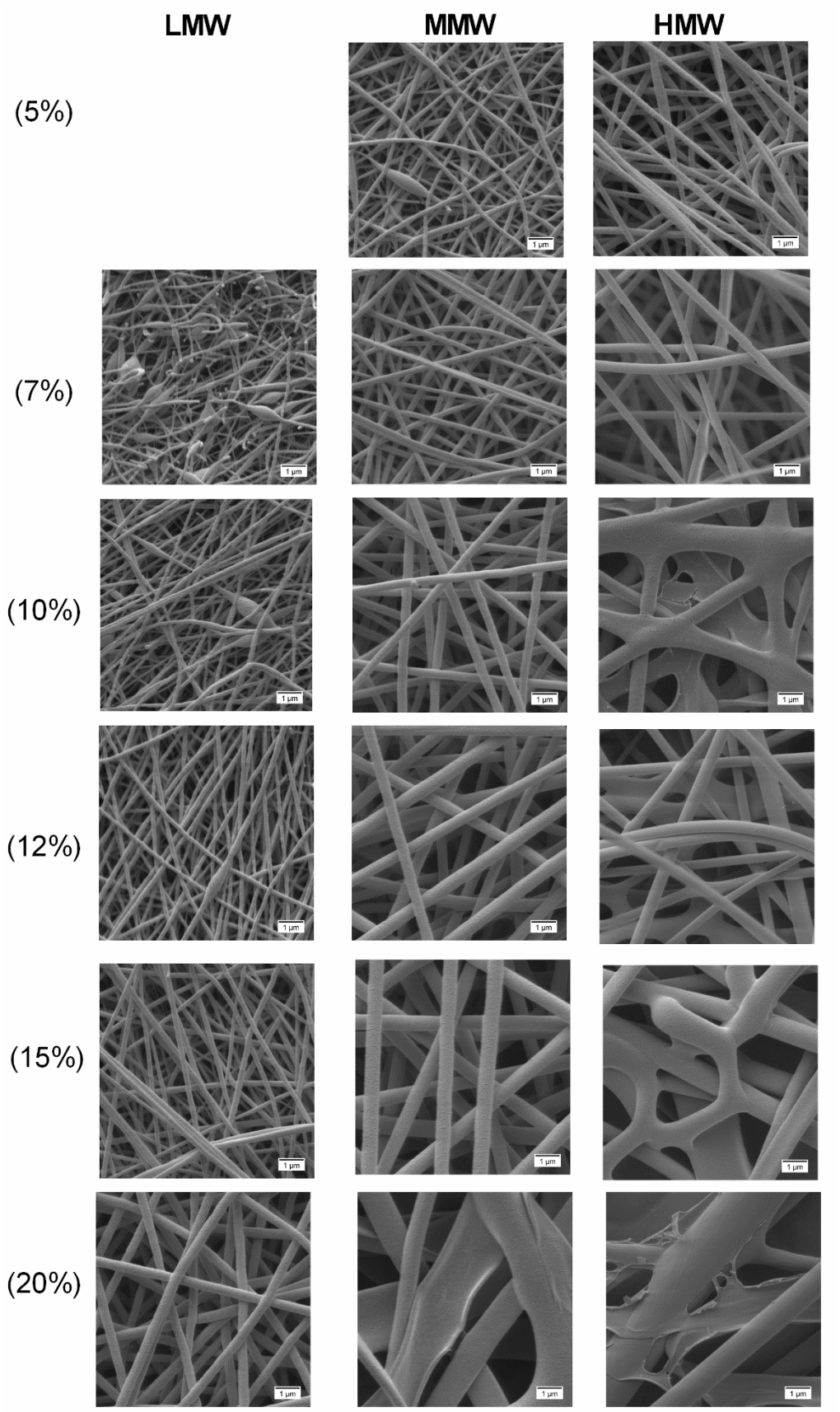

Figure 5. SEM images at 10,000× showing the obtained electrospun fibers from pure PVA polymer solutions. All scale bars represent 1 µm.

Table 2. Fiber diameters of the obtained electrospun fibers from pure PVA solutions

Molecular weight	PVA (wt.%)	Average diameter (nm) ± SD	Minimum diameter (nm)	Maximum diameter (nm)
LMW	5%	-	-	-
	7%	-	-	-
	10%	147 ± 24	91	202
	12%	174 ± 25	113	228
	15%	224 ± 22	178	271
	20%	390 ± 36	304	466
MMW	5%	183 ± 46	108	307
	7%	224 ± 35	162	276
	10%	372 ± 26	288	418
	12%	543 ± 70	437	670
	15%	655 ± 46	589	759
	20%	1357± 450	742	2333
HMW	5%	269 ± 24	226	311
	7%	358 ± 38	305	443
	10%	688 ± 94	482	863
	12%	975 ± 170	768	1364
	15%	1135 ± 405	762	2337
	20%	2204 ± 151	1500	2397

5.3.5 Incorporation of TE Colloidal Dispersions into Nanofibers

Figure 6 shows the examined SEM morphologies after blending of differently concentrated pure PVA solutions with colloidal dispersions (60:40), where different structures with varied molecular weight and concentration were observed. The results clearly show that not only the morphology of electrospun fibers but also the resulting fiber diameter was changed after PVA was blended with the aqueous colloidal dispersions. As can be seen, with blends of LMW at 5 and 7 wt.%, no fibers were formed due to the low viscosity. By increasing the concentration from 10 to 20 wt.%, fiber uniformity increased gradually as the blend at 20 wt.% produced more uniform fibers. In the case of MMW, blends at 5 and 7 wt.% produced a mixture of fibers and beads, whereas at 10 to 12 wt.%, uniformity increased with the presence of a few beads. Blends at 15 and 20 wt.% produced smooth, uniform fibers without beads.

Similar observations were made with blends of HMW at 5 to 7 wt.%, where a mixture of beads and fibers was formed. In contrary, smooth, uniform homogenous fibers were already achieved at 10 to 15 wt.%. Blends of electrospun fibers produced with LMW had average diameters between 143 (12 wt.%) and 241 nm (20 wt.%), MMW ranged between 174 (10 wt.%) and 424 nm (20 wt.%) and HMW ranged between 319 (10 wt.%) and 605 nm (15 wt.%) (Table 3). Overall, the addition of colloidal dispersions resulted in a decrease in the average fiber diameter to submicron range < 1 µm due to the viscosity reduction of polymeric solutions. Moreover, and as also reputed by other groups, the reduced viscosity contributed to better stretching of the jet and improved fiber morphology with smooth, thinner fibers [36,48,49]. Furthermore, formation of smooth, uniform fibers without beads indicated that colloidal dispersions were entrapped in the fibers and were within the range of the carrying capacity of the fibers [32].

Table 3. Diameters of the obtained electrospun fibers from PVA/colloidal dispersions blends (60:40).

Molecular weight	PVA (wt.%)	Average diameter (nm) ± SD	Minimum diameter (nm)	Maximum diameter (nm)
LMW	12%	143 ± 29	88	225
	15%	187 ± 31	152	272
	20%	241 ± 28	191	298
MMW	10%	174 ± 22	129	225
	12%	241 ± 32	178	317
	15%	308 ± 29	263	373
	20%	424 ± 33	355	497
HMW	10%	319 ± 56	267	503
	12%	392 ± 41	341	499
	15%	605 ± 55	509	689

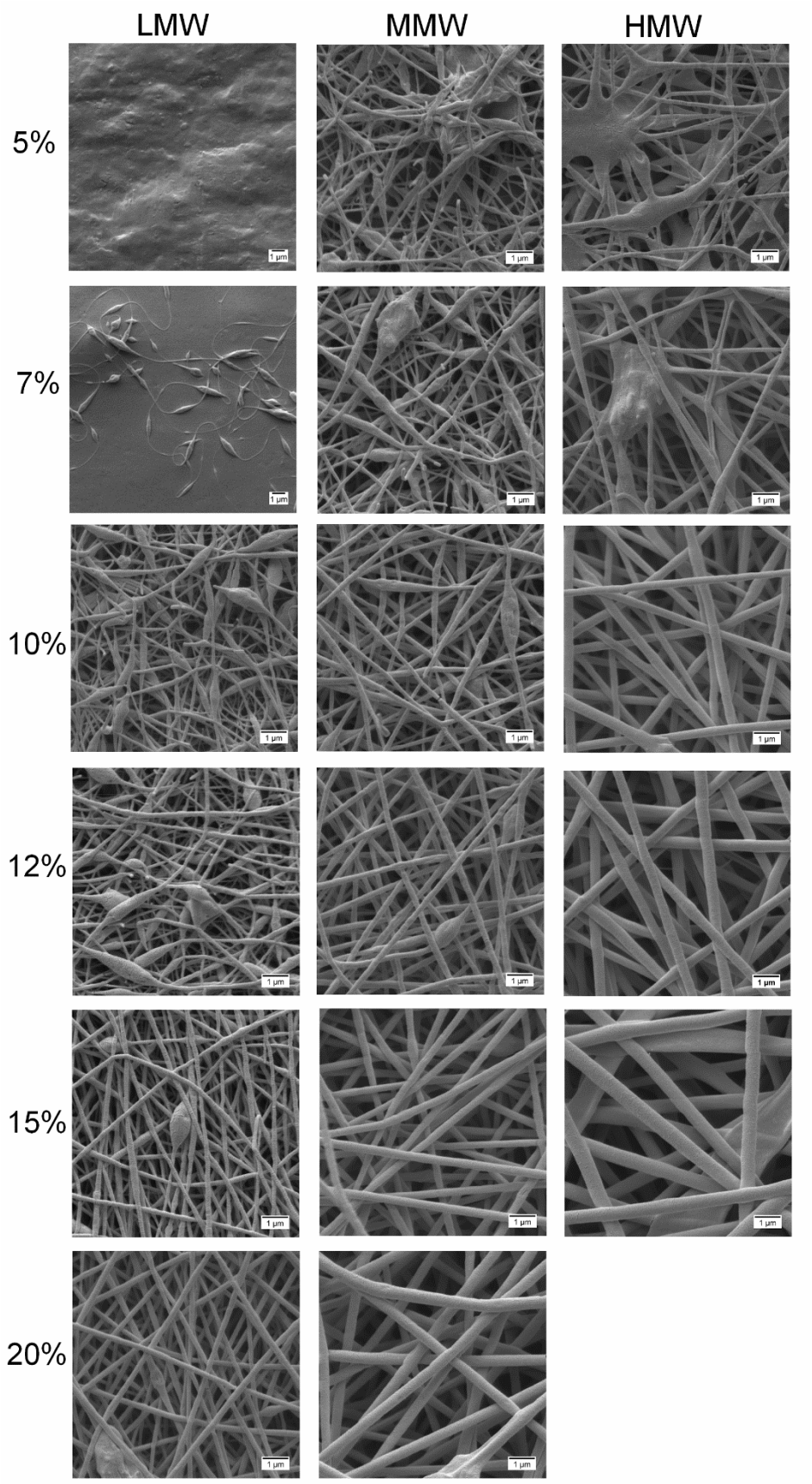

Figure 6. SEM morphologies at 10,000× of loaded electrospun PVA/TE blend (60:40) fibers at different concentrations and molecular weights. All scale bars represent 1 µm.

5.3.6 Fiber Morphology in Different Compositions

The polymer solutions with 12 wt.% PVA of all molecular weights blended with the colloidal dispersion in different compositions (20:80, 40:60, 50:50, 60:40, 70:30, 80:20) were electrospun and the obtained fiber morphologies are shown in Figure 7. It is evident that the composition of the spinning solutions had a significant impact on the morphology of the nanofibers. In all cases, improved morphological changes are observed with increasing amounts of PVA in the blend, resulting in an increase in the values of their rheological properties. However, at very high amounts of PVA (70:30 and 80:20) in the blends of HMW, the uniformity decreases. Therefore, we conclude that if the PVA fraction is less than 40% in the blend, beaded fibers are formed, while fiber uniformity improves from the ratio of 50:50 with the best uniformity being achieved at 60:40 of HMW.

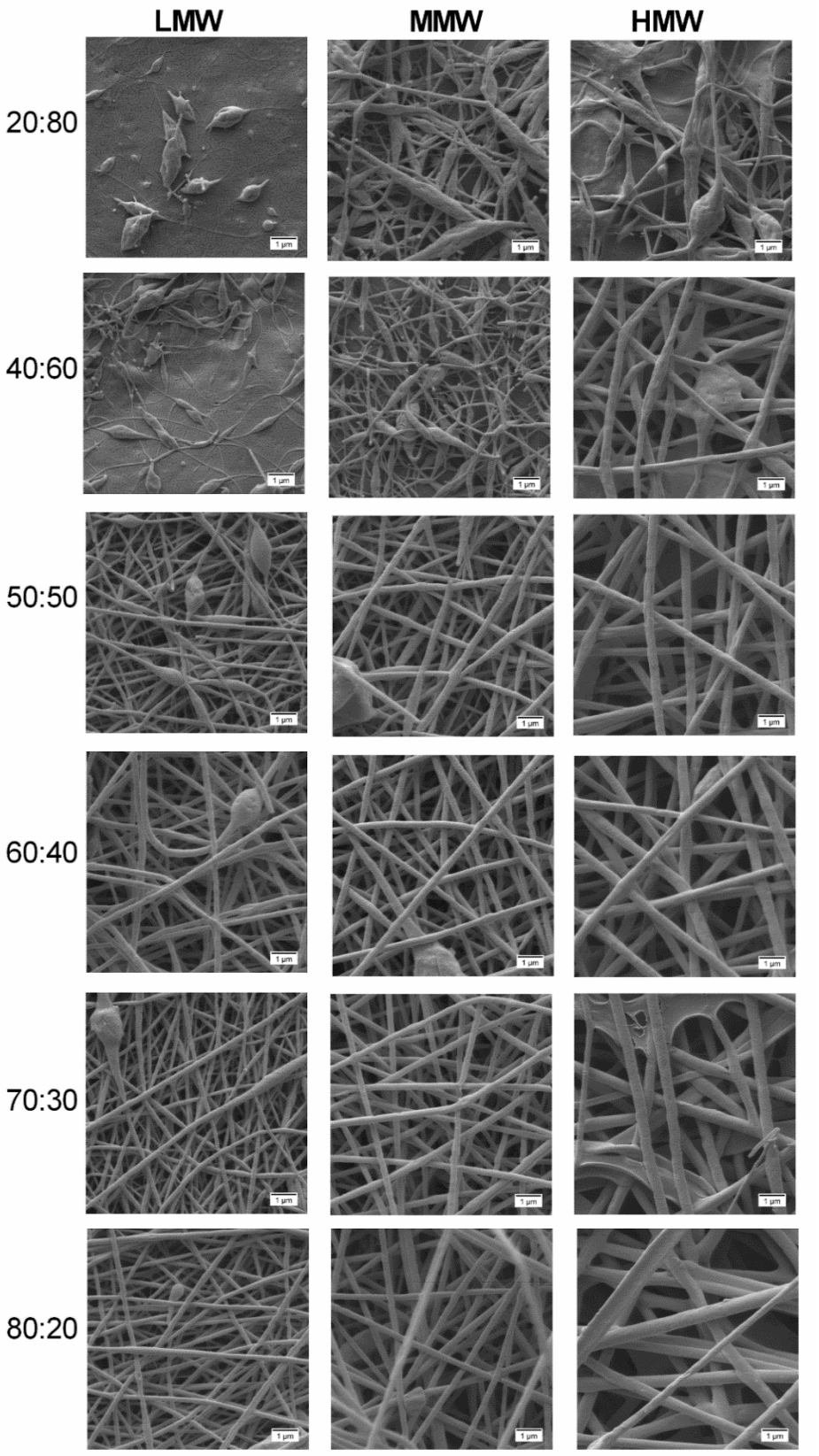

Figure 7. SEM morphologies at 10,000× of electrospun 12 wt.% PVA/colloidal dispersion fibers at different compositions and molecular weights. All scale bars represent 1 µm.

5.3.7 In Vitro Release Studies

Electrospun fiber mats prepared from blends with 12 wt.% PVA solutions of different molecular weights and colloidal TE dispersions (60:40) were subjected to release studies using modified Franz diffusion cells. Figure 8 depicts the cumulative amount of betulin released within 72 h. As can be seen, nanofibers from LMW showed higher and quicker release of betulin (194.46 ± 35.1 µg/cm^2), followed by MMW (182.67 ± 5.2 µg/cm^2) and HMW (165.13 ± 11.2 µg/cm^2) electrospun fibers. This effect was attributed to the fiber morphologies and diameters. Blends from both molecular weights, LMW and MMW, exhibited a mat of thinner fibers making it easier for the drug to diffuse through. Between LMW and MMW, no significant differences were observed. On the other hand, the blend of HMW showed thicker fibers and drug molecules have to travel a longer distance through the polymeric matrix leading to a slower release [50]. Release profiles between LMW and HMW differed significantly ($p < 0.05$) on the release of betulin from electrospun fibers.

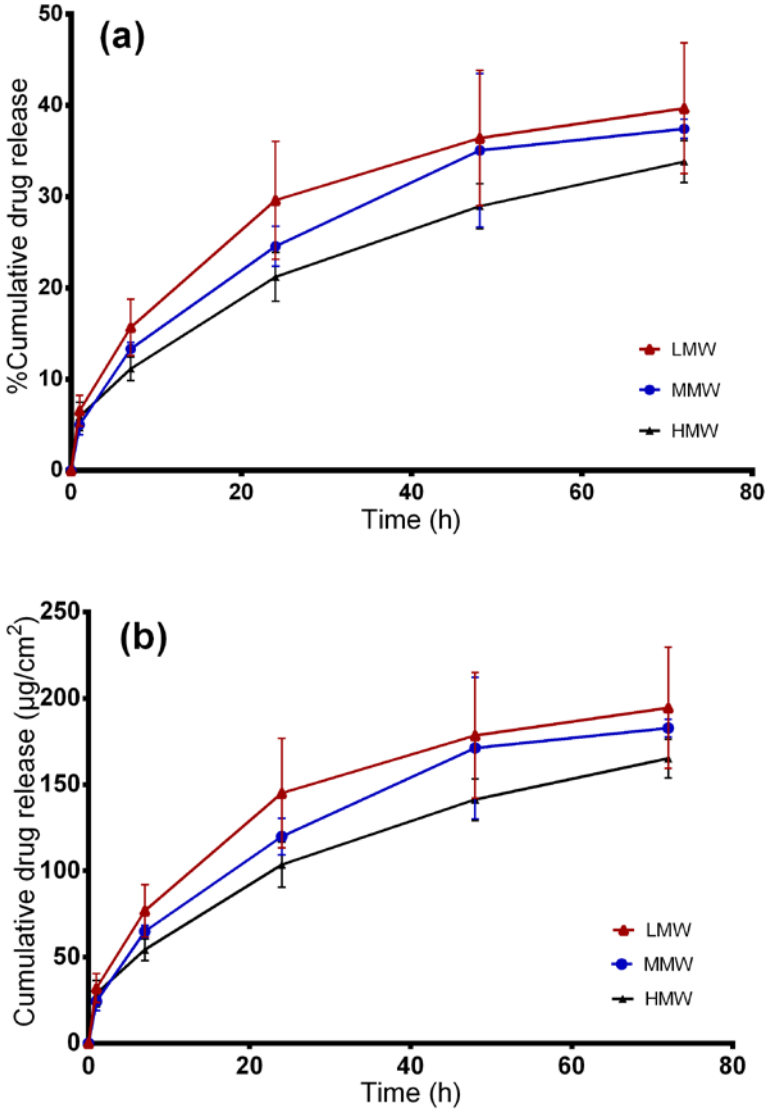

Figure 8. In vitro drug release studies. (**a**) Percentage of released betulin and (**b**) amount of betulin released from TE-loaded wound dressings.

Table 4 shows the modeling results obtained from the four kinetic models. On comparing the R^2 values of the formulations, it was found that betulin release from the electrospun PVA could be best fitted by the Korsmeyer–Peppas model as this model showed higher R^2 values than all the other models. From the Korsmeyer–Peppas model, n values were found to be between 0.41 and 0.48 for all dressings, indicating that betulin release from PVA/TE fiber mats can be largely described as matrix diffusion [51,52]. This is in perfect agreement with the spatial distribution of the colloidal TE dispersion within PVA found by confocal Raman micro-spectroscopy, indicating that a hydrocolloid matrix is formed [32]. A fiber mat can be assumed to be a multiparticulate matrix system where the overall TE release is largely affected by the size of the individual fibers which form a diffusion barrier [50,53].

Table 4. In vitro release kinetics data of the TE-loaded electrospun fiber mats fitted to mathematical models.

Sample	Zero-order	First-order	Higuchi	Korsmeyer-Peppas model	
	R^2	**R^2**	**R^2**	**R^2**	**n**
LMW	0.8674	0.8955	0.9518	0.9727	0.41
MMW	0.9062	0.9233	0.9705	0.9875	0.46
HMW	0.9504	0.9670	0.9947	0.9967	0.48

5.3.8 Ex vivo Permeation Through Wounded Skin

The developed wound dressings are intended to be applied on wounded skin. Figure 9 shows the cumulative permeated amount of betulin from PVA/TE blend electrospun fiber mats in different molecular weights after 120 h. The cumulative amount of drug permeated from LMW was 146.81 ± 35.6, 95 ± 8.8 for MMW and 92 ± 1.8 µg/cm^2 from the HMW/TE blend at 120 h. Again here, a higher and faster cumulative amount of drug permeated from the LMW formulation (permeation coefficient: 8.3 × 10^{-2} mg/cm^2.h, $p < 0.05$), whereas no substantial differences were observed between MMW (permeation coefficient: 4.8 × 10^{-2} mg/cm^2.h) and HMW (permeation coefficient: 5.4 × 10^{-2} mg/cm^2.h) nanofibers. Electrospun fibers from MMW (241 nm) and HMW (392 nm), being thicker in diameter, demonstrated lower drug permeation in comparison to LMW (143 nm) where the fibers are thinner.

Analysis of the permeation data showed that the kinetic can be fitted best to the Korsmeyer–Peppas model (R^2: 0.9938 for LMW, 0.9997 for MMW and 0.9912 for HMW). From the Korsmeyer–Peppas model, n values were found to be between 0.74 and 0.77 for all the dressings, showing that betulin permeation from PVA/TE fiber mats is largely influenced by the diffusion through the skin even though the barrier had been removed.

Drug release from the electrospun fibers and transport through the synthetic membrane is markedly faster ($p < 0.05$) in comparison to diffusion through the dermatomed skin. For instance, only 22% (108 ± 19.5 µg/cm^2) of betulin from LMW/TE fibers permeated through the skin, whereas about 40% (194.46 ± 35 µg/cm^2) was released through the synthetic membrane after 72 h. However, an influence of the kind of electrospun fibers is still visible. To put this in the context of wound healing, a controlled release from the PVA matrix is achievable in the very early phase of the treatment, whereas with increasing closure of the wound, the skin itself contributes to a sustained release stopping the permeation almost completely when the barrier function of the skin is restored [9].

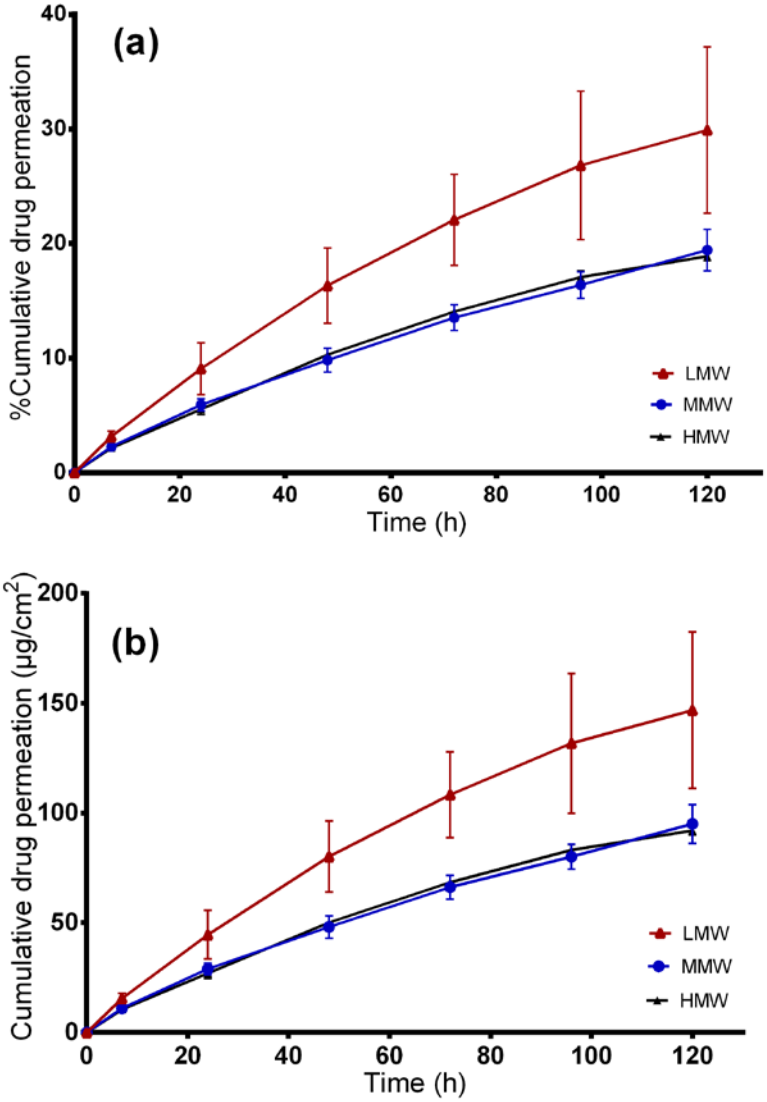

Figure 9. Ex vivo drug permeation studies. (**a**) Percentage of permeated betulin and (**b**) amount of betulin permeated from TE-loaded wound dressings.

5.4 Materials and Methods

5.4.1 Materials

PVA with molecular weights of 67 (low molecular weight, (LMW)), 130 (medium molecular weight (MMW)) and 146–186 kDa (high molecular weight, (HMW)) (87–89% hydrolyzed) was purchased from Sigma Aldrich (Steinheim, Germany). All other materials were obtained from the named supplier. Hydrogenated phospholipids, Lipoid GmbH (PL90 H, Ludwigshafen, Germany), Sunflower oil, Caesar & Loretz GmbH (Hilden, Germany), Birch bark extract, (Amryt AG, Niefern-Öschelbronn, Germany), Parafilm®, Bemis Company Inc., (Oshkosh, WI, USA), Whatman Nuclepore polycarbonate membrane filters, Sigma-Aldrich ,(Steinheim, Germany). Ultra-pure water (ELGA Labwater, Celle, Germany) was used as a solvent to prepare the aqueous solutions. Pig ears for ex vivo permeation studies were provided by the Department of Experimental Medicine, University of Tuebingen [54].

5.4.2 Preparing the Colloidal Dispersions

The colloidal dispersion with particle sizes of 400 ± 49 nm which was utilized in this work consisted of 2.5% PL90H, 1.0% SO and 0.5% TE as the dispersed phase and water as the continuous phase optimized from our previous study. Briefly, the dispersion was prepared using a two-stage homogenization process where a pre-dispersion is first formed using a rotor-stator system (Ultra Turrax T25, IKA, Staufen, Germany), at 9500 rpm with eventual homogenization using a high-pressure homogenizer (Emulsiflex C-3, Avestin, Mannheim, Germany) for 8 cycles at a pressure of 100 MPa [33].

5.4.3 Preparation of Solutions and Electrospinning of Nanofibers

From all molecular weights, PVA polymer solutions were prepared with varying concentrations (5, 7, 10, 12, 15 and 20 wt.%) by dissolving PVA in water at 90 °C under magnetic stirring. After PVA was completely dissolved, the solution was cooled to room temperature and used the following day. Subsequently, for electrospinning experiments, the colloidal TE dispersions were blended with the prepared PVA solutions in the ratio of 60:40 using a magnetic stirrer at 40 °C for 2 h to form a homogeneous solution. Besides, blends of colloidal dispersions/12 wt.% PVA solutions with different mass ratios (20:80, 40:60, 50:50, 60:40, 70:30 and 80:20) were prepared to test the influence of blend compositions on fiber morphology. Samples were then cooled down to room temperature prior to electrospinning.

5.4.4 Electrospinning of nanofibers

Electrospinning was performed using a conventional unit, Nanolab Instruments Sdn. Bhd. (Subang Jaya, Malaysia). Figure 10 shows a scheme of the electrospinning setup used to perform the experiments. A blunt-end needle (18-gauge) attached to a 5 mL plastic syringe was used, while the electrospinning conditions were a needle to

collector distance = 10 cm, voltage = 15 kV and flow rate = 0.5 mL/h. A drum rotating collector covered with non-sticky aluminium foil and a speed fixed at 1000 rpm was used to collect the fibers. All electrospinning studies were carried out at ambient temperature (23 ± 2 °C) and a relative humidity of 45%.

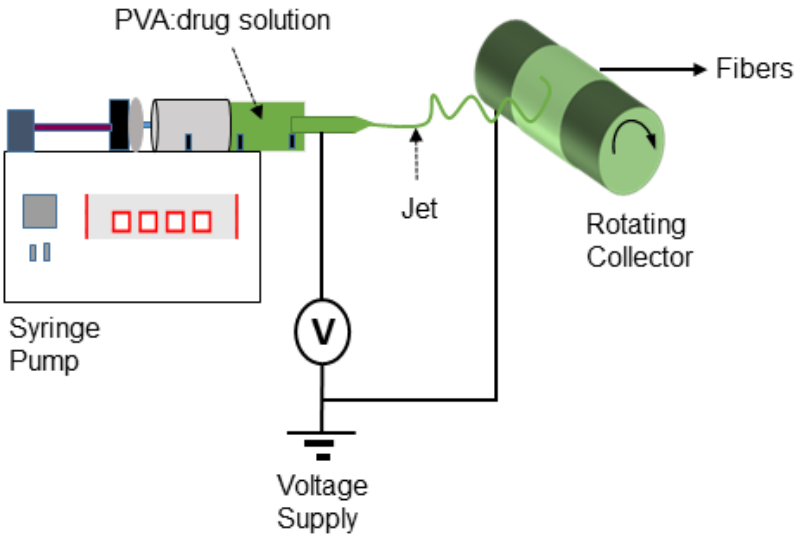

Figure 10. Schematic representation of the electrospinning set up used to fabricate nanofibers.

5.4.5 Rheological Characterization of the Spinning Solutions

Rheological properties in the bulk were determined for all polymer solutions using a Physica MCR 501 rheometer (Anton Paar, Graz, Austria) with the cone-plate measuring system CP25-1 at a constant temperature of 25 °C. Rotational tests were performed in order to determine the viscosity of the solutions at a shear rate of 100 s^{-1}.The amplitude sweep tests were performed to estimate the viscoelastic properties expressed as storage modulus G′ and loss modulus G″. The frequency was set at 1 Hz and the deformation was in the range of 0.01 to 1000 %. Both the storage modulus G′ and loss modulus G″ were determined in the linear viscoelastic range (LVE).

5.4.6 Surface Tension and Conductivity

Surface tension was measured at room temperature by the Du Noüy ring method with a TD1C LAUDA tensiometer (Lauda-Königshofen, Germany). For each solution, average values of parameters from at least three measurements are reported. Conductivity of solutions was also measured at 25 °C using a WTW Conductivity meter 340i (Weilheim, Germany).

5.4.7 Qualitative Analysis of Electrospinning Process and Nanofiber Formation

A qualitative evaluation was done on the performance of polymer solutions during electrospinning using a plugged digital camera (Digimicro Profi, DNT, Dietzenbach, Germany). The camera was attached to the electrospinning process and so it was possible to visualize what was happening at the tip of the needle, like the formation of jet or droplets and Taylor cone behavior.

5.4.8 Characterization of Nanofibrous Scaffolds

The fiber morphology of both the blank and the TE-loaded fibers was observed by SEM, using a Zeiss DSM 940 A, Carl Zeiss GmbH (Oberkochen, Germany). Prior to SEM observation, each of the fiber mats (0.5 × 0.5 cm) was placed on a conductive double-sided tape and sputtered with gold using Biorad E 5100 Sputter Coater (Bio-Rad GmbH, Munich, Germany) at 2.1 kV and 20 mA for 240 s. Based on these SEM images, the average fiber diameters were determined from at least 30 measurements using ImageJ software (National Institute of Health, Bethesda, MD, USA).

5.4.9 Ex vivo Skin Permeation and In vitro Drug Diffusion Studies

Modified vertical Franz diffusion cells with a reservoir capacity of 12 mL (Gauer Glas, Püttlingen, Germany) were used to conduct ex vivo permeation and in vitro release studies. In the case of in vitro release studies, synthetic polycarbonate membranes (pore size diameter of 0.4 µm) were used. For ex vivo permeation studies, pig ears were received from the Department of Experimental Medicine, University Hospital of Tuebingen right after the death of the animals. *The Department of Pharmaceutical Technology is registered for the use of animal products at the District Office of Tuebingen (registration number: DE 08 416 1052 21).* In ex vivo permeation studies, the skin was prepared according to previous studies [55,56]. Briefly, fresh pig ears were washed with isotonic saline using cotton balls and after postauricular skin excision, wrapped in aluminium foil and stored at −30 °C until further use. On the day of experiment, the skin samples were thawed at room temperature, cut into skin strips of 3 cm width and pinned to a block of Styrofoam pre-covered with aluminium foil. Thereafter, “wounded” skin samples were prepared by a skin grafting method using a Dermatom (Dermatom GA 630, Aesculap AG & Co. KG, Tuttlingen, Germany). Here, the skin was “wounded” through initial removal of the 0.2 mm outermost layers of the skin using Dermatom. Subsequently, the remaining skin was dermatomed to a thickness of 0.4 mm, and punched to obtain discs of 25 mm in diameter using a circular hole punch (Eduard Gottfried Ferne, Remscheid, Germany) [9].

Afterwards, the Franz diffusion cells equipped with synthetic membrane/porcine skin were filled with a mixture of ethanol and water, 50:50 (*v/v*), as the receptor medium. The diffusion area was 1.77 cm^2. In all molecular weights, the final composition (wt.%) of PVA/colloidal dispersions (60:40) blends consisted of 7.2 wt.% PVA, 1 wt.% PL90H, 0.4 wt.% SO and 0.2 wt.% TE. In both experiments, samples of 30.50 mg fiber mats,

exactly weighed, were loaded in the donor compartments and covered with parafilm to avoid solvent evaporation. The experiments were performed at 32 °C with continuous stirring at 500× *g*.

The amount of betulin diffused through the membrane/skin was determined by withdrawing samples of 1 mL from the receptor chamber at a predetermined time interval and replacing them with an equal volume of fresh prewarmed receptor medium to keep the sink condition. The samples were analyzed directly for betulin content using high-performance liquid chromatography with ultraviolet detection (HPLC-UV). The experiments were conducted in triplicate.

5.4.10 Betulin Permeation/Release Kinetics Assessment

The release/permeation kinetic of betulin from TE/PVA scaffolds was fitted by zero-order (Equation 1), first-order (Equation 2), Korsmeyer–Peppas (Equation 3) and Higuchi (Equation 4 [57]. After evaluating the regression coefficient (R^2), the best mathematical kinetic model was obtained. In all cases, M_t is the amount of betulin determined in the receptor medium at the fixed times, and t is the time intervals.

Zero−order model, where k_0 is the zero-order release constant:

$$M_t = k_0 t \quad (1)$$

First-order model, where K_1 is the first-order release rate constant:

$$\ln (1 - M_t) = -K_1 t \quad (2)$$

Korsmeyer−Peppas model: $Mt = kt^n$, where K is the Korsmeyer–Peppas constant which is related to the characteristics of the delivery system and the encapsulated drug. The n is the diffusional exponent that shows the betulin release mechanism, where n = 0.45, a Fickian diffusion mechanism; 0.45 < n < 1, a non-Fickian diffusion mechanism (anomalous transport), in which both Fickian diffusion and Case-II transport occurs [58]. (3)

Higuchi model, where k is the Higuchi constant:

$$Mt = kt^{0.5} \quad (4)$$

5.4.11 HPLC Analysis

The LC-20A prominence HPLC system (Shimadzu, Kyoto, Japan) was used for betulin analysis. The mobile phase was composed of acetonitrile and water with the addition of 0.1% (*v/v*) phosphoric acid. For efficient betulin quantification, gradient conditions were used according to the isocratic/gradient modes developed by Armbruster et al. [59]. The flow rate was set to 1.2 mL/min, the injection volume was 100 µL and the oven temperature was 40 °C. For HPLC separation, a Nucleosil 100-5 C18 EC 125/4 column together with a precolumn Universal RP EC 4/3 (Macherey-Nagel, Düren, Germany) was used. The retention time of betulin was approximately 7.5 min and the detection wavelength was set at 210 nm.

5.4.12 Statistical Analysis

The obtained data were acquired from repeated experiments, at least three times, and statistically evaluated in terms of the mean and its standard deviation (mean ± SD). Statistical differences were determined by one-way or two-way analysis of variance (ANOVA) using GraphPad Prism 6.0 (GraphPad Software Inc., La Jolla, CA, USA). Results were considered to be statistically significant at the level of *p*-value less than 0.05.

5.5 Conclusions

This study broadens the knowledge on PVA-based electrospun fibers with a colloidal dispersion of a birch bark extract as the active principle for enhanced wound healing. The concentration and molecular weight of the polymer as the most decisive parameters have a significant effect on the rheological properties of the polymer solution and affect directly the resulting fiber properties. Overall, the viscosity of the prepared polymer solutions increased as the molecular weight and solution concentration increased. Incorporation of colloidal TE dispersions resulted in electrospun fibers of thinner diameters. The average fiber diameters in the whole studied design space varied between 143 and 2204 nm. It was also possible to control the release rate of betulin by just adjusting mainly the thickness of the electrospun fibers which can be adjusted by either, or both, the polymer concentration and molecular weight. TE was released much faster from fibers of LMW, while MMW and HMW performed better in terms of electrospinnability with more uniform fiber morphologies. We conclude that such developed scaffolds together with the positive benefits of birch bark extract present excellent dressing materials which can be tailored to the specific needs of enhanced healing of various types of wounds.

Author Contributions: Conceptualization, F.K.M. and R.D.; data curation, F.K.M.; funding acquisition, F.K.M. and R.D..; investigation, F.K.M.; methodology, F.K.M. and R.D.; project administration, R.D.; supervision R.D.; writing—original draft, F.K.M.; writing—review and editing, R.D. Both authors have read and agreed to the published version of the manuscript.

Funding: This research was funded (PRC20170703) by the Phospholipid Research Center in Heidelberg, Germany.

Acknowledgments: We would like to thank Lipoid GmbH for supplying us with phospholipids and Amryt AG for the kind donation of birch bark extract.

Conflicts of Interest: The authors declare no conflict of interest.

5.6 References

1. Boateng, J.S.; Matthews, K.H.; Stevens, H.N.; Eccleston, G.M. Wound Healing Dressings and Drug Delivery Systems: A Review. *J. Pharm. Sci.* **2008**, *97*, 2892–2923, doi:10.1002/jps.21210.
2. Aiken, C.; Chen, C.H.; Betulinic acid derivatives as HIV-1 antivirals. *Trends Mol. Med.* **2005**, *11*, 31–36, doi:10.1016/j.molmed.2004.11.001.
3. Haque, S.; Nawrot, D.A.; Alakurtti, S.; Ghemtio, L.; Yli-Kauhaluoma, J.; Tammela, P. Screening and Characterisation of Antimicrobial Properties of Semisynthetic Betulin Derivatives. *PLoS ONE* **2014**, *9*, e102696, doi:10.1371/journal.pone.0102696.
4. Dehelean, C.A., Soica, C.M.; Toma, C.-C.; Feflea, S.; Gruia, A.T. and Kasa Jr., P. Antitumoral activity of betulin, a compound present in birch tree, in formulations with cyclodextrin. *Studia Univ. VG, Seria St. Vietii* **2010**, *20*, 55–58.
5. Dehelean, C.; Şoica, C.; Ledeţi, I.; Aluaş, M.; Zupkó, I.; Găluşcan, A.; Pinzaru, S.C.; Munteanu, M. Study of the betulin enriched birch bark extracts effects on human carcinoma cells and ear inflammation. *Chem. Central J.* **2012**, *6*, 137, doi:10.1186/1752-153x-6-137.
6. Ebeling, S.; Naumann, K.; Pollok, S.; Wardecki, T.; Vidal-Y-Sy, S.; Nascimento, J.M.; Boerries, M.; Schmidt, G.; Brandner, J.M.; Merfort, I. From a Traditional Medicinal Plant to a Rational Drug: Understanding the Clinically Proven Wound Healing Efficacy of Birch Bark Extract. *PLoS ONE* **2014**, *9*, e86147, doi:10.1371/journal.pone.0086147.
7. Metelmann, H.-R.; Podmelle, F.; Waite, P.D. Long-Term Cosmetic Benefit of Wound Healing by Betuline. *Am. J. Cosmet. Surg.* **2012**, *29*, 19–24, doi:10.5992/ajcs-d-11-00046.1.
8. Steinbrenner, I.; Houdek, P.; Pollok, S.; Brandner, J.M.; Daniels, R. Influence of the Oil Phase and Topical Formulation on the Wound Healing Ability of a Birch Bark Dry Extract. *PLoS ONE* **2016**, *11*, e0155582, doi:10.1371/journal.pone.0155582.
9. Färber, A.; Daniels, R. Ex vivo Skin Permeation of Betulin from Water-in-Oil Foams. *Ski. Pharmacol. Physiol.* **2016**, *29*, 250–256, doi:10.1159/000448689.
10. Laszczyk, M.; Jäger, S.; Simon-Haarhaus, B.; Scheffler, A.; Schempp, C.M. Physical, Chemical and Pharmacological Characterization of a New Oleogel-Forming Triterpene Extract from the Outer Bark of Birch (Betulae Cortex). *Planta Medica* **2006**, *72*, 1389–1395, doi:10.1055/s-2006-951723.
11. Krasutsky, P.A. Birch bark research and development. *Nat. Prod. Rep.* **2006**, *23*, 919–942, doi:10.1039/b606816b.
12. Jäger, S.; Laszczyk, M.N.; Scheffler, A. A Preliminary Pharmacokinetic Study of Betulin, the Main Pentacyclic Triterpene from Extract of Outer Bark of Birch (Betulae alba cortex). *Mol.* **2008**, *13*, 3224–3235, doi:10.3390/molecules13123224.
13. Scheffler, A. The Wound Healing Properties of Betulin from Birch Bark from Bench to Bedside. *Planta Medica* **2019**, *85*, 524–527, doi:10.1055/a-0850-0224.
14. Weckesser, S.; Schumann, H.; Laszczyk, M.; Müller, M.; Schempp, C.M. Topical Treatment of Necrotising Herpes Zoster with Betulin from Birch Bark. *Forschende Komplementärmedizin / Research in Complementary Medicine* **2010**, *17*, 271–273, doi:10.1159/000320592.
15. Schwieger-Briel, A.; Kiritsi, D.; Schempp, C.; Has, C.; Schumann, H. Betulin-Based Oleogel to Improve Wound Healing in Dystrophic Epidermolysis Bullosa: A Prospective Controlled Proof-of-Concept Study. *Dermatol. Res. Pr.* **2017**, *2017*, 1–10, doi:10.1155/2017/5068969.

16. Frew, Q.; Rennekampff, H.-O.; Dziewulski, P.; Moiemen, N.; Zahn, T.; Hartmann, B. Betulin wound gel accelerated healing of superficial partial thickness burns: Results of a randomized, intra-individually controlled, phase III trial with 12-months follow-up. *Burn.* **2019**, *45*, 876–890, doi:10.1016/j.burns.2018.10.019.
17. El-Hadi, A.M.; Al-Jabri, F.Y. Influence of Electrospinning Parameters on Fiber Diameter and Mechanical Properties of Poly(3-Hydroxybutyrate) (PHB) and Polyanilines (PANI) Blends. *Polym.* **2016**, *8*, 97, doi:10.3390/polym8030097.
18. Reneker, D.H.; Chun, I. Nanometre diameter fibres of polymer, produced by electrospinning. *Nanotechnol.* **1996**, *7*, 216–223, doi:10.1088/0957-4484/7/3/009.
19. Zahedi, P.; Rezaeian, I.; Siadat, S.O.R.; Jafari, S.-H.; Supaphol, P. A review on wound dressings with an emphasis on electrospun nanofibrous polymeric bandages. *Polym. Adv. Technol.* **2009**, *21*, 77–95, doi:10.1002/pat.1625.
20. Kai, D.; Liow, S.S.; Loh, X.J. Biodegradable polymers for electrospinning: Towards biomedical applications. *Mater. Sci. Eng. C* **2014**, *45*, 659–670, doi:10.1016/j.msec.2014.04.051.
21. Zhong, S.P.; Zhang, Y.Z.; Lim, C.T. Tissue scaffolds for skin wound healing and dermal reconstruction. *Wiley Interdiscip. Rev. Nanomed. Nanobiotechnol.* **2010**, *2*, 510–525, doi:10.1002/wnan.100.
22. IgnatovaM.; Rashkov, I.; Manolova, N. Drug-loaded electrospun materials in wound-dressing applications and in local cancer treatment. *Expert Opin. Drug Deliv.* **2013**, *10*, 469–483, doi:10.1517/17425247.2013.758103.
23. Jiang, T.; Carbone, E.J.; Lo, K.W.-H.; Laurencin, C.T. Electrospinning of polymer nanofibers for tissue regeneration. *Prog. Polym. Sci.* **2015**, *46*, 1–24, doi:10.1016/j.progpolymsci.2014.12.001.
24. Gajra*, B., Pandya, S. S., G. Vidyasagar, H. Rabari, R.R. Dedania, and S.J.I.J.o.P.R. Rao, Poly vinyl alcohol hydrogel and its pharmaceutical and biomedical applications: A review. *Int. J. Pharm. Res.* **2012**, *4*, 20–26.
25. Gaaz, T.S.; Sulong, A.B.; Akhtar, M.N.; Kadhum, A.A.H.; Mohamad, A.B.; Al-Amiery, A.A. Properties and Applications of Polyvinyl Alcohol, Halloysite Nanotubes and Their Nanocomposites. *Molecules* **2015**, *20*, 22833–22847, doi:10.3390/molecules201219884.
26. Koski, A.; Yim, K.; Shivkumar, S. Effect of molecular weight on fibrous PVA produced by electrospinning. *Mater. Lett.* **2004**, *58*, 493–497, doi:10.1016/s0167-577x(03)00532-9.
27. Ngadiman, N.H.A.; Noordin, M.; Idris, A.; Shakir, A.S.A.; Kurniawan, D. Influence of Polyvinyl Alcohol Molecular Weight on the Electrospun Nanofiber Mechanical Properties. *Procedia Manuf.* **2015**, *2*, 568–572, doi:10.1016/j.promfg.2015.07.098.
28. Augustine, R.; Hasan, A.; Nath, V.K.Y.; Thomas, J.; Augustine, A.; Kalarikkal, N.; Al Moustafa, A.-E.; Thomas, S. Electrospun polyvinyl alcohol membranes incorporated with green synthesized silver nanoparticles for wound dressing applications. *J. Mater. Sci. Mater. Med.* **2018**, *29*, 163, doi:10.1007/s10856-018-6169-7.
29. Saeed, S.M.; Mirzadeh, H.; Zandi, M.; Barzin, J. Designing and fabrication of curcumin loaded PCL/PVA multi-layer nanofibrous electrospun structures as active wound dressing. *Prog. Biomater.* **2017**, *6*, 39–48, doi:10.1007/s40204-017-0062-1.
30. Aruan, N.M.; Sriyanti, I.; Edikresnha, D.; Suciati, T.; Munir, M.M.; Khairurrijal, K. Polyvinyl Alcohol/Soursop Leaves Extract Composite Nanofibers Synthesized Using Electrospinning Technique and their Potential as Antibacterial Wound Dressing. *Procedia Eng.* **2017**, *170*, 31–35, doi:10.1016/j.proeng.2017.03.006.

31. Hussein, Y.; El-Fakharany, E.M.; Kamoun, E.A.; Loutfy, S.A.; Amin, R.; Taha, T.H.; Salim, S.A.; Amer, M. Electrospun PVA/hyaluronic acid/L-arginine nanofibers for wound healing applications: Nanofibers optimization and in vitro bioevaluation. *Int. J. Biol. Macromol.* **2020**, *164*, 667–676, doi:10.1016/j.ijbiomac.2020.07.126.
32. Mwiiri, F.K.; Brandner, J.M.; Daniels, R. Electrospun Bioactive Wound Dressing Containing Colloidal Dispersions of Birch Bark Dry Extract. *Pharm.* **2020**, *12*, 770, doi:10.3390/pharmaceutics12080770.
33. Mwiiri, F.K.; Daniels, R. Optimized Birch Bark Extract-Loaded Colloidal Dispersion Using Hydrogenated Phospholipids as Stabilizer. *Pharm.* **2020**, *12*, 832, doi:10.3390/pharmaceutics12090832.
34. Gao, H.-W.; Yang, R.-J.; He, J.-Y.; Yang, L. Rheological behaviors of PVA/H2O solutions of high-polymer concentration. *J. Appl. Polym. Sci.* **2009**, *116*, 1459–1466, doi:10.1002/app.31677.
35. Gao, H.; He, J.; Yang, R.; Yang, L. Characteristic rheological features of high concentration PVA solutions in water with different degrees of polymerization. *J. Appl. Polym. Sci.* **2010**, *116*, 2734–2741, doi:10.1002/app.31900.
36. Esparza, Y., A. Ullah, Y. Boluk, and J. Wu, Preparation and characterization of thermally crosslinked poly(vinyl alcohol)/feather keratin nanofiber scaffolds. *Materials & Design* **2017**, *133*, 1–9.
37. Hay, W.T.; Byars, J.A.; Fanta, G.F.; Selling, G.W. Rheological characterization of solutions and thin films made from amylose-hexadecylammonium chloride inclusion complexes and polyvinyl alcohol. *Carbohydr. Polym.* **2017**, *161*, 140–148, doi:10.1016/j.carbpol.2017.01.011.
38. Sousa, A.M.; Souza, H.K.; Uknalis, J.; Liu, S.-C.; Gonçalves, M.; Liu, L. Electrospinning of agar/PVA aqueous solutions and its relation with rheological properties. *Carbohydr. Polym.* **2015**, *115*, 348–355, doi:10.1016/j.carbpol.2014.08.074.
39. Rwei, S.-P.; Huang, C.-C. Electrospinning PVA solution-rheology and morphology analyses. *Fibers Polym.* **2012**, *13*, 44–50, doi:10.1007/s12221-012-0044-9.
40. Bhattacharya, A.; Ray, P. Studies on surface tension of poly(vinyl alcohol): Effect of concentration, temperature, and addition of chaotropic agents. *J. Appl. Polym. Sci.* **2004**, *93*, 122–130, doi:10.1002/app.20436.
41. Le Corre Bordes, D., Hofman, K., Bordes, N., Tucker, N., Huber, T.; Staiger, M. P. Electrospinning window: Solution properties for uniform fibres from electrospinnable biopolymers. In International Conference on Processing and Fabrication of Advanced Materials, Auckland, New Zealand, January 2017; pp.22–25.
42. Shin, J.; Kim, Y.; Lim, Y.M.; Nho, Y.C. Removal of sodium acetate in poly(vinyl alcohol) and its quantification by1H NMR spectroscopy. *J. Appl. Polym. Sci.* **2007**, *107*, 3179–3183, doi:10.1002/app.27453.
43. Haider, A.; Haider, S.; Kang, I.-K. A comprehensive review summarizing the effect of electrospinning parameters and potential applications of nanofibers in biomedical and biotechnology. *Arab. J. Chem.* **2018**, *11*, 1165–1188, doi:10.1016/j.arabjc.2015.11.015.
44. Angammana, C.J.; Jayaram, S.H. Analysis of the Effects of Solution Conductivity on Electrospinning Process and Fiber Morphology. *IEEE Trans. Ind. Appl.* **2011**, *47*, 1109–1117, doi:10.1109/tia.2011.2127431.
45. Zhang, C.; Yuan, X.; Wu, L.; Han, Y.; Sheng, J. Study on morphology of electrospun poly(vinyl alcohol) mats. *Eur. Polym. J.* **2005**, *41*, 423–432, doi:10.1016/j.eurpolymj.2004.10.027.

46. Supaphol, P.; Chuangchote, S. On the electrospinning of poly(vinyl alcohol) nanofiber mats: A revisit. *J. Appl. Polym. Sci.* **2008**, *108*, 969–978, doi:10.1002/app.27664.
47. Ramakrishna, S. An introduction to electrospinning and nanofibers. World Scientific: Toh Tuck Link, Singapore, 2005.
48. He, M.; Zhang, B.; Dou, Y.; Yin, G.; Cui, Y.; Chen, X. Fabrication and characterization of electrospun feather keratin/poly(vinyl alcohol) composite nanofibers. *RSC Adv.* **2017**, *7*, 9854–9861, doi:10.1039/C6RA25009B.
49. Cho, D.; Netravali, A.N.; Joo, Y.L. Mechanical properties and biodegradability of electrospun soy protein Isolate/PVA hybrid nanofibers. *Polym. Degrad. Stab.* **2012**, *97*, 747–754, doi:10.1016/j.polymdegradstab.2012.02.007.
50. Imani, R.; Yousefzadeh, M.; Nour, S. Functional Nanofiber for Drug Delivery Applications. In *Handbook of Nanofibers*; Springer Nature Switzerland AG, Cham, Switzerland,, 2018; pp. 1–55.
51. Ritger, P.L.; Peppas, N.A. A simple equation for description of solute release II. Fickian and anomalous release from swellable devices. *J. Control. Release* **1987**, *5*, 37–42, doi:10.1016/0168-3659(87)90035-6.
52. Han, X.; Huo, P.; Ding, Z.; Kumar, P.; Liu, B. Preparation of Lutein-Loaded PVA/Sodium Alginate Nanofibers and Investigation of Its Release Behavior. *Pharmaceutics* **2019**, *11*, 449, doi:10.3390/pharmaceutics11090449.
53. Nikmaram, N.; Roohinejad, S.; Hashemi, S.; Koubaa, M.; Barba, F.J.; Abbaspourrad, A.; Greiner, R. Emulsion-based systems for fabrication of electrospun nanofibers: Food, pharmaceutical and biomedical applications. *RSC Adv.* **2017**, *7*, 28951–28964, doi:10.1039/c7ra00179g.
54. Zhang, Z.; Lunter, D.J. Confocal Raman microspectroscopy as an alternative method to investigate the extraction of lipids from stratum corneum by emulsifiers and formulations. *Eur. J. Pharm. Biopharm.* **2018**, *127*, 61–71, doi:10.1016/j.ejpb.2018.02.006.
55. Lunter, D.J.; Rottke, M.; Daniels, R. Oil-in-Oil-Emulsions with Enhanced Substantivity for the Treatment of Chronic Skin Diseases. *J. Pharm. Sci.* **2014**, *103*, 1515–1519, doi:10.1002/jps.23944.
56. Lunter, D.; Daniels, R. In vitro Skin Permeation and Penetration of Nonivamide from Novel Film-Forming Emulsions. *Ski. Pharmacol. Physiol.* **2013**, *26*, 139–146, doi:10.1159/000348464.
57. Suvakanta, D.; Murthy, P.N.; Nath, L.; Chowdhury, P. Kinetic modeling on drug release from controlled drug delivery systems. *Acta Pol. Pharm.-Drug Res.* **2010**, *67*, 217–223.
58. Ritger, P.L.; Peppas, N.A. A simple equation for description of solute release I. Fickian and non-fickian release from non-swellable devices in the form of slabs, spheres, cylinders or discs. *J. Control. Release* **1987**, *5*, 23–36, doi:10.1016/0168-3659(87)90034-4.
59. Armbruster, M.; Mönckedieck, M.; Scherließ, R.; Daniels, R.; Wahl, M.A. Birch Bark Dry Extract by Supercritical Fluid Technology: Extract Characterisation and Use for Stabilisation of Semisolid Systems. *Appl. Sci.* **2017**, *7*, 292, doi:10.3390/app7030292.

6 Supplementary data

6.1 Influence of PL90H and oil content on drug release/Permeation

In order to evaluate the influence of PL90H and SO on drug release or permeation through the skin, colloidal dispersions containing different compositions of these two components were produced. The PL90H content used was 1 wt.% and 3.2 wt.% while sunflower oil was 0.4 wt.% and 4 wt.%. TE was kept constant at 0.2 wt.%. The colloidal dispersions were prepared according to our previous study through high pressure homogenization process. Henceforth, the colloidal dispersions were blended with 12 wt.% PVA solution from molecular weight of 146-186,000 in the ratio of 60:40 and electrospun into nanofibers.

Table 1. Final composition (wt.%) of formulation blends for electrospinning.

Component	Sample 1 (S1) [%]	Sample 2 (S2) [%]	Sample 3 (S3) [%]
PVA	7.2	7.2	7.2
PL90H	1	3.2	3.2
Sunflower oil	0.4	0.4	4
TE	0.2	0.2	0.2
Purified water	ad 100	ad 100	ad 100

The release and permeation profiles of different formulations composed of various amounts of PL90H and sunflower oil are presented in Figure 1 and 2. Betulin gradually released or permeated from all scaffolds. The S1 scaffolds incorporated with 1 wt.% PL90H released betulin at the significantly higher extent than those incorporated with 3.2 wt.% PL90H (S2) and 4 wt.% sunflower oil (S3). The S3 showed the slowest release. For example, release rate of betulin from S1 scaffolds was about 44 %, 34 % from S2 and 28% from S3 after 72 h. At the same period, about 21% of the drug permeated from S1 scaffolds, followed by fiber mats of S2 with 14% and S3 scaffolds exhibited the slowest permeation of 8%.

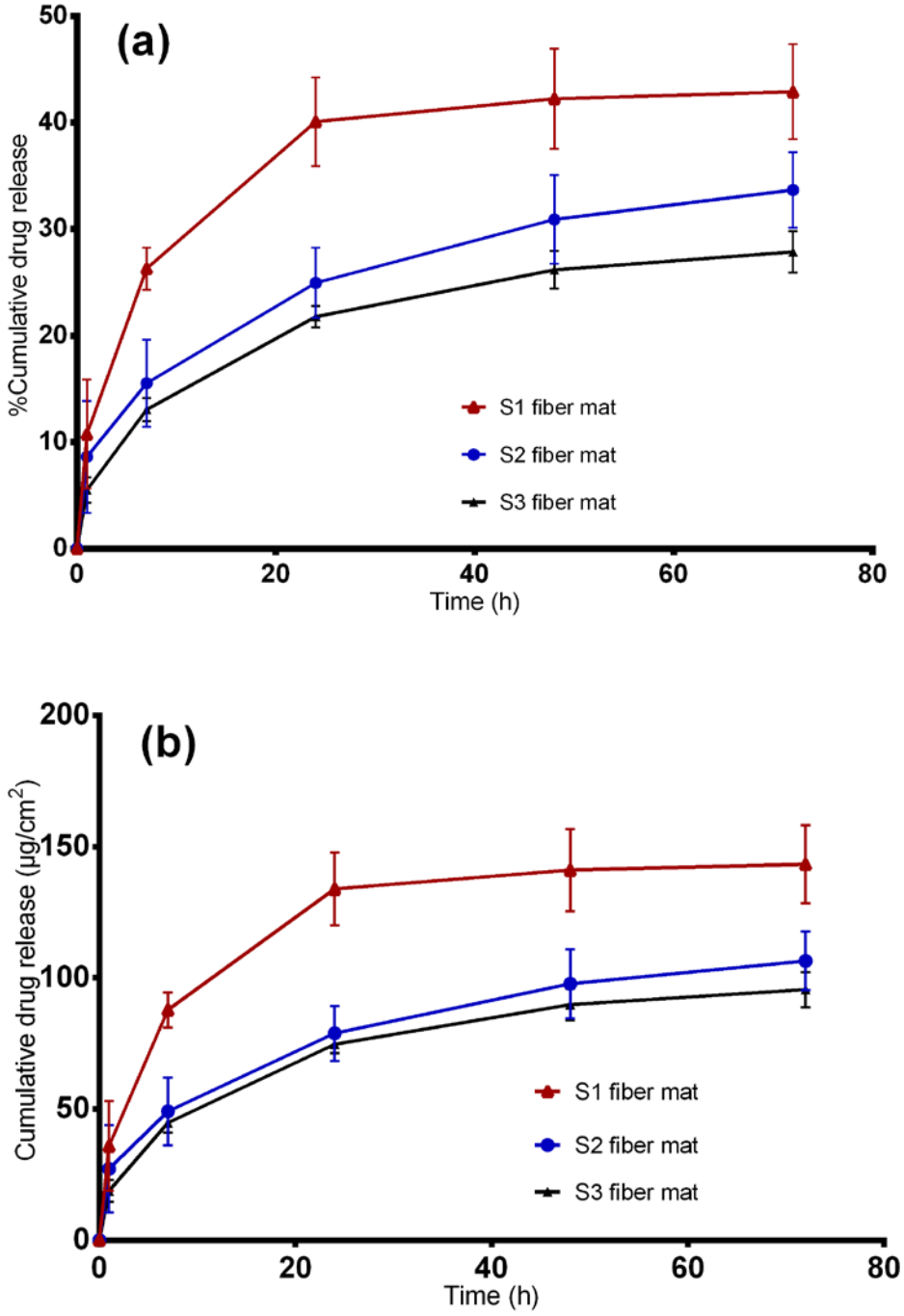

Figure 1. In vitro drug release studies. (a) percentage of released betulin and (b) amount of betulin released (µg/cm^2) from TE-loaded wound dressings.

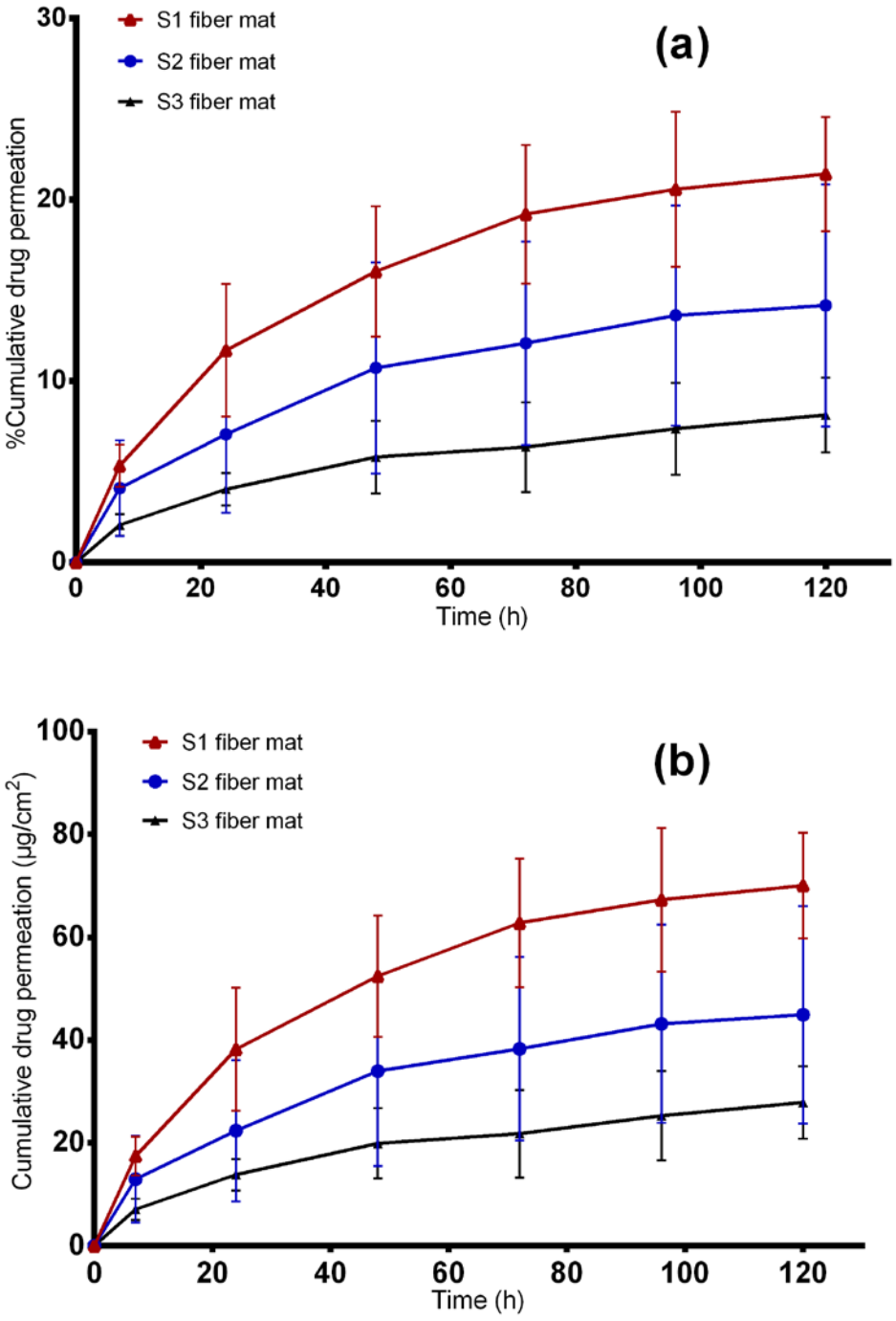

Figure 2. Ex vivo drug permeation studies. (a) percentage of permeated betulin and (b) amount of betulin permeated (µg/cm2) from TE-loaded wound dressings.

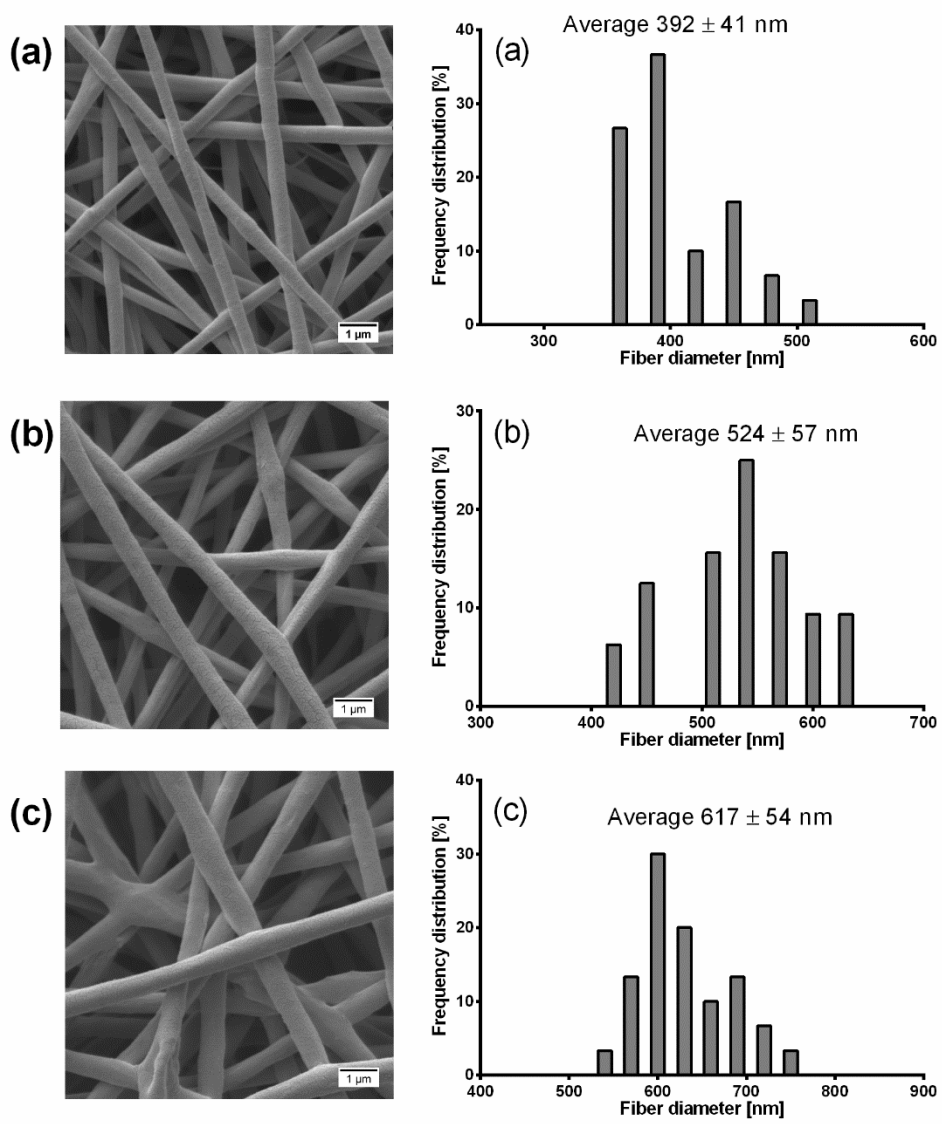

Figure 3. SEM morphologies of (a) S1, (b) S2 and (c) S3 electrospun fibers with their diameter distributions. All scale bars represent 1µm.

Clearly, the release and permeation of betulin depended mainly on the amount of PL90H / sunflower oil incorporated in the blend and a controlled release of betulin can be achieved by adjusting PL90H and sunflower oil content. The S1 blend had a permeation coefficient of 5 x 10^{-2} mg/cm^2.h, S2 (2 x 10^{-2} mg/cm^2.h) and S3 (1 x 10^{-2} mg/cm^2.h) which explains further slower betulin release with higher amounts of PL90H and sunflower oil. Notably, the S1 scaffolds incorporated with 1 wt.% PL90H had the thinnest average fiber diameters of 392 nm, followed by S2 with 524 nm and scaffolds with S3 had the thickest fibers of 617 nm (Figure 3) where betulin might have longer distance through which to diffuse from the polymeric matrix leading to a slower release [1]. It is also known that through emulsion electrospinning, core-shell nanofibers can be produced while designing controlled release drug delivery systems in that the drug

release rate can be modulated, for example, by just adjusting the oil phase and the water phase of the emulsions [2].

6.2 Solvent-Cast Films

The 12% wt.% PVA solution was prepared from molecular weight of Mw 146-186,000 by dissolving PVA in water at 90 °C under magnetic stirring for 5 h. The solution cooled to room temperature and used the following day. Subsequently, the polymer solution was blended with colloidal dispersions containing 2.5% Phospholipon 90H, 1% sunflower oil and 0.5% TE in the ratio of 60:40 using a magnetic stirrer for 2 h at 40 °C to form a homogeneous solution. The sample was then cooled down to room temperature prior to film casting. A modified film casting machine (Figure 4) was used to prepare the films. To fabricate the cast films with uniform thickness, the prepared solutions were cast onto a Teflon-coated glass plate (pre-heated at 32 °C, skin surface temperature) using a film applicator with a clearance gap thickness of 0.2 mm. The cast films were left to dry for 1 h before stored at 32 °C in a drying chamber (Heraeus Holding GmbH, Hanau, Germany) for 24 h [3, 4].

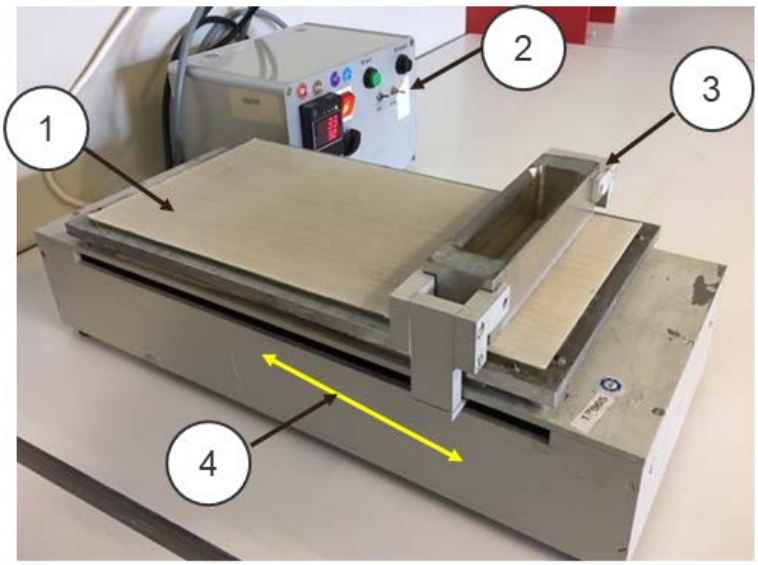

Figure 4. Photograph of the modified film casting machine. 1. Teflon-coated plate, 2. Temperature and speed control unit, 3. Applicator and 4. Processing directions.

The same characterization methods of electrospun fibers were also used for the cast films. Hence, produced films were evaluated with respect to morphology, drug release, wound healing, and compared to electrospun fiber mats. As can be observed from the scanning electron microscope (SEM) images in Figure 5, the electrospun fiber mat appeared white in colour compared to colourless cast film which could be attributed to

the incorporation of colloidal dispersions and an interaction favoured by the electrospinng process might have occurred. We also found that electrospun fiber mats had a porous structure and were more flexible than cast films.

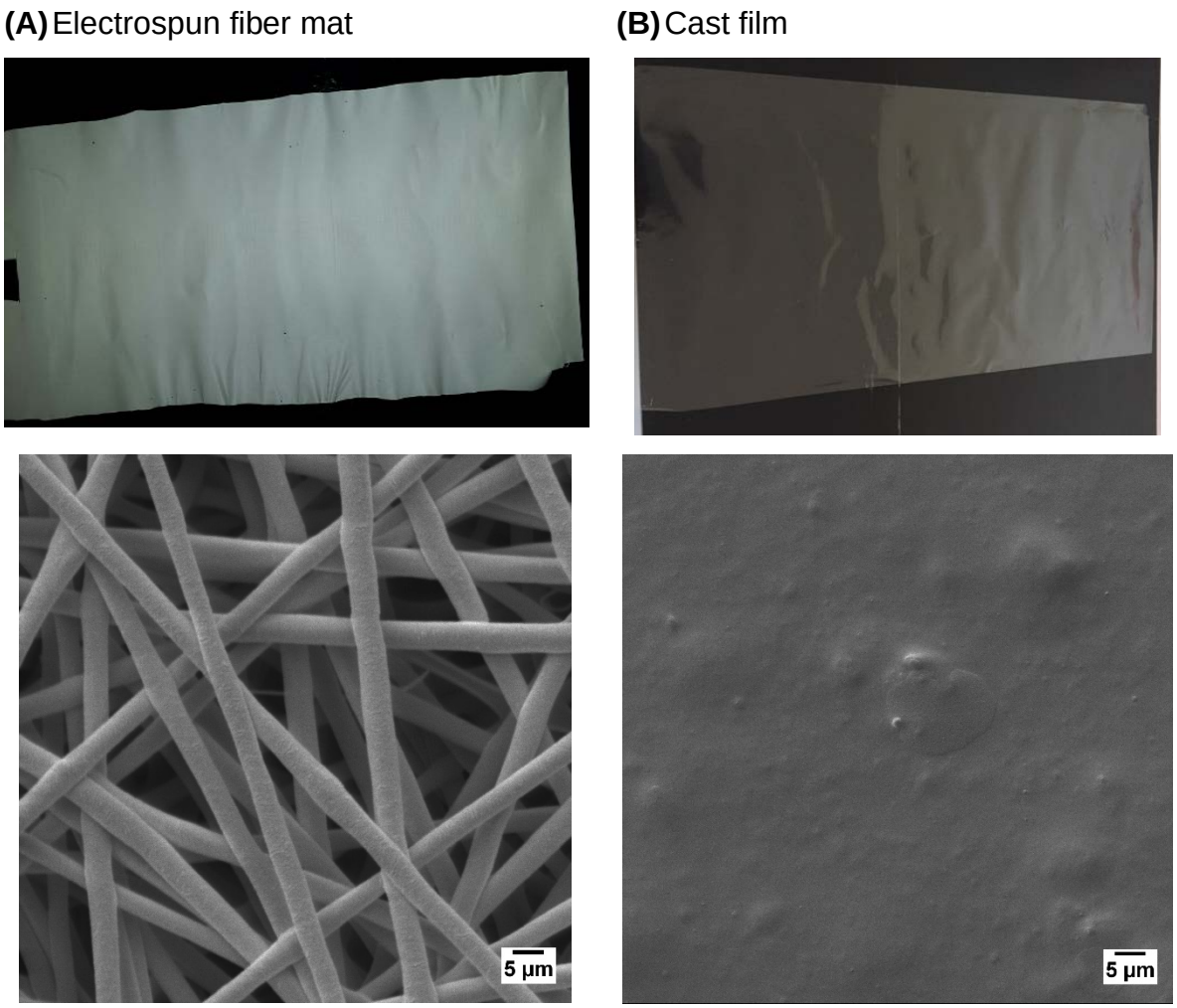

Figure 5. (A) Photographs of electrospun nanofibers (392 nm) and (B) cast film, 12%PVA:2.5% PL90H:1% Sunflower oil:0.5%TE (60:40).

The release characteristics of Betulin from the TE-loaded electrospun PVA fiber mats and films were carried out using Franz diffusion cells. Comparing drug release profiles in Figure 6, the cumulative amount of Betulin released from electrospun fibers was 34 % whereas from cast films was 41% after 72 h. The drug release from cast film was much faster than electrospun fiber mats. This could be contributed by the features of the nanofibers such as the core-sheath structures and fiber thickness which slowed the release of Betulin. Besides, drug in cast films is just entrapped in the PVA matrix rather than inside the fibers hence faster release.

From the *ex-vivo* wound healing assays (Figure 7), TE-loaded cast films and electrospun fibe rmats significantly accelerated the wound healing process more than a TE-oleogel. However, electrospun fiber mats were superior to cast films in wound healing which could be attributed to the key role played by nanofibers such as favouring cell proliferation, mimicking the ECM etc. [5].

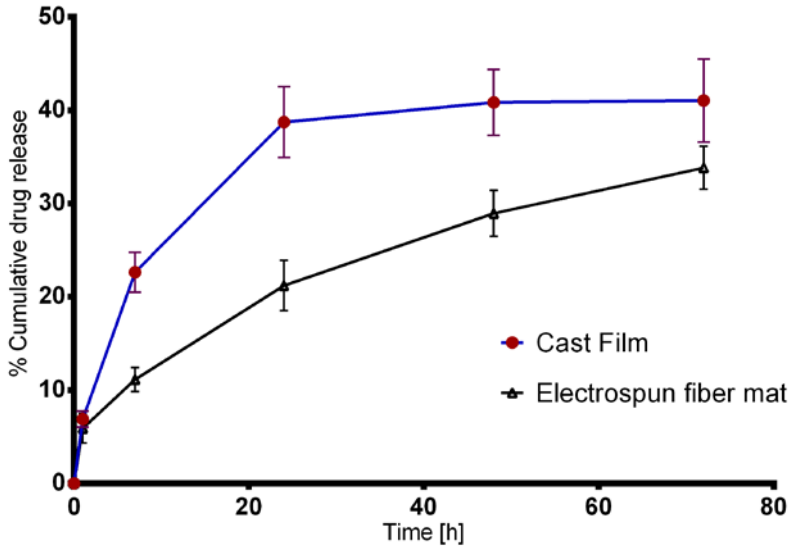

Figure 6. In vitro drug release studies of cast film and electrospun fiber mat (7.2%PVA:1%PL90H:0.4%Sunflower oil:0.2%TE in both formulations).

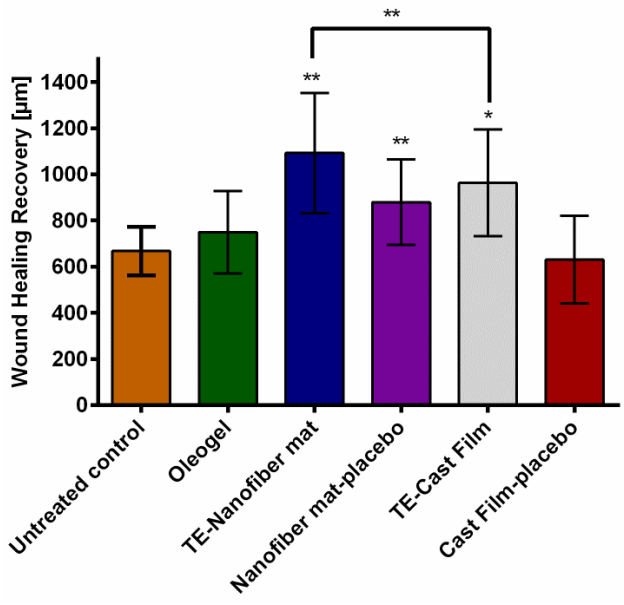

Figure 7. Wound healing recovery from oleogel, electrospun fiber mats and solvent-cast films. (TE-formulation:7.2%PVA:1%PL90H:0.4%SO:0.2%TE and Cast film-placebo: 7.2%PVA:1%PL90H:0.4%SO). statistically significant, * $p < 0.05$; ** $p < 0.01$ vs untreated control

6.3 References

1. Akhgari, A., et al., *The design and evaluation of a fast-dissolving drug delivery system for loratadine using the electrospinning method.* 2016. **11**(2).
2. Nikmaram, N., et al., *Emulsion-based systems for fabrication of electrospun nanofibers: food, pharmaceutical and biomedical applications.* RSC Advances, 2017. **7**(46): p. 28951-28964.
3. Gruetzmann, R. and K.G. Wagner, *Quantification of the leaching of triethyl citrate/polysorbate 80 mixtures from Eudragit® RS films by differential scanning calorimetry.* European Journal of Pharmaceutics and Biopharmaceutics, 2005. **60**(1): p. 159-162.
4. Heck, R., et al., *Film-forming formulations containing porous silica for the sustained delivery of actives to the skin.* European Journal of Pharmaceutics and Biopharmaceutics, 2016. **108**: p. 1-8.
5. Zahedi, P., et al., *A review on wound dressings with an emphasis on electrospun nanofibrous polymeric bandages.* Polymers for Advanced Technologies, 2010. **21**(2): p. 77-95.